



January 2015

Developing Novel 3D Antennas Using Advanced Additive Manufacturing Technology

Milad Mirzaee

Follow this and additional works at: <https://commons.und.edu/theses>

Recommended Citation

Mirzaee, Milad, "Developing Novel 3D Antennas Using Advanced Additive Manufacturing Technology" (2015). *Theses and Dissertations*. 1813.
<https://commons.und.edu/theses/1813>

This Thesis is brought to you for free and open access by the Theses, Dissertations, and Senior Projects at UND Scholarly Commons. It has been accepted for inclusion in Theses and Dissertations by an authorized administrator of UND Scholarly Commons. For more information, please contact zeinebyousif@library.und.edu.

DEVELOPING NOVEL 3D ANTENNAS USING ADVANCED ADDITIVE
MANUFACTURING TECHNOLOGY

By

Milad Mirzaee

A Thesis
Submitted to the Graduate Faculty

of the

University of North Dakota

In partial fulfillment of the requirements

for the degree of

Master of Science

Grand Forks, North Dakota

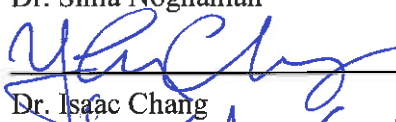
August
2015

Copyright 2015 Milad Mirzaee

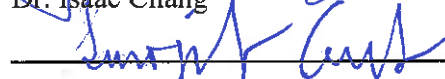
This thesis, submitted by Milad Mirzaee in partial fulfillment of the requirements for the Degree of Master of Science from the University of North Dakota, has been read by the Faculty Advisory Committee under whom the work has been done, and is hereby approved.



Dr. Sima Noghianian

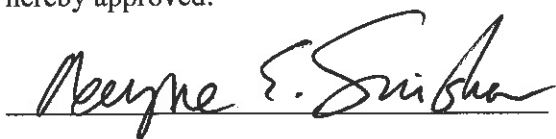


Dr. Isaac Chang

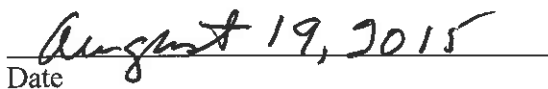


Dr. Surojit Gupta

This thesis is being submitted by the appointed advisory committee as having met all of the requirements of the Graduate School at the University of North Dakota and is hereby approved.



Dr. Wayne Swisher
Dean of the Graduate School



Date

PERMISSION

Title DEVELOPING NOVEL 3D ANTENNAS USING ADVANCED
 ADDITIVE MANUFACTURING TECHNOLOGY

Department Electrical Engineering

Degree Masters of Science

In presenting this thesis in partial fulfillment of the requirements for a graduate degree from the University of North Dakota, I agree that the library of this University shall make it freely available for inspection. I further agree that permission for extensive copying for scholarly purposes may be granted by the professor who supervised my thesis work or, in her absence, by the Chairperson of the department or the dean of the Graduate School. It is understood that any copying or publication or other use of this thesis or part thereof for financial gain shall not be allowed without my written permission. It is also understood that due recognition shall be given to me and to the University of North Dakota in any scholarly use which may be made of any material in my thesis.

Milad Mirzaee
DATE: August 2015

TABLE OF CONTENTS

LIST OF FIGURES	viii
LIST OF TABLES	xiii
ABBREVIATIONS	xiv
ACKNOWLEDGEMENTS	xv
ABSTRACT	xvii
CHAPTER	
1 INTRODUCTION	1
1.1 Motivation.....	1
1.2 Thesis Outline	5
2 LITERATURE REVIEW	7
2.1 Additive Manufacturing (AM).....	7
2.1.1 Background and Principle.....	7
2.1.2 AM Technologies.....	9
2.1.3 Application of AM for Fabrication of 3D Electronics.....	11
2.2 3D Antennas Manufacturing.....	14
2.2.1 3D Antennas Utilizing Traditional 2D Manufacturing Methods.....	14
2.2.2 Antennas Utilizing AM.....	14
2.3 A Brief Review on Antenna Tutorials	21
2.3.1 Electromagnetic Waves	22
2.3.2 Antenna Polarization.....	23

2.3.3	Antenna Radiation Patterns.....	24
2.3.4	Isotropic, Directional and Omnidirectional Antennas	26
2.3.5	Directivity	27
2.3.6	Efficiency	27
2.3.7	Gain.....	27
2.3.8	Voltage Standing Wave Ratio (VSWR)	27
2.3.9	Group Delay.....	28
3	HIGH FREQUENCY CHARACTERISATION OF NOVEL MATERIALS.....	29
3.1	Introduction.....	29
3.2	Dielectric Constant or Permittivity Theory.....	30
3.3	Dielectric Measurement Methods	32
3.4	Complex Permittivity Measurements	34
3.4.1	Probe Calibration	34
3.4.2	Error Sources	35
3.4.3	Measurements	35
4	DESIGN AND SIMULATION OF 3D ANTENNAS.....	38
4.1	Introduction.....	38
4.2	Design of Bowtie Antenna at the Center Frequency of 2.45 GHz.....	39
4.2.1	Parametric Study of the Proposed Bowtie Antenna.....	40
4.2.2	Far-field Study of the Proposed Antenna.....	44
4.2.3	Effects of Conductivity on the Performance.....	45
4.2.4	Effects of the Radiator Shape on the Performance of Bowtie Antenna	48
4.3	Design of 3D Bowtie Antenna for UWB Applications	51

4.3.1	Comparison of the UWB Bowtie Antennas.....	56
4.3.2	Optimizing Proposed Antenna for UWB Spectrum (3.1 to 10.6 GHz).....	58
4.4	Design of Embedded 3D Dipole Antenna	61
4.5	Design of 3D Microstrip Patch Antenna.....	67
5	FABRICATION PROCESS AND MEASUREMENT RESULTS.....	71
5.1	Fabrication of Bowtie Antenna using PLA and ABS Materials.....	71
5.2	Embedded Dipole Antenna Fabrication.....	80
5.3	3D Printed Antennas Fabrication using Sputtering Technology	84
6	FUTURE WORK AND CONCLUSION.....	89
6.1	High Frequency Materials Characterization.....	89
6.2	3D Antennas Fabrication	90
6.3	Attaching SMA Connector	91
6.4	Antennas Measurements.....	91
6.5	Conclusion	92
	REFERENCES	93

LIST OF FIGURES

Figure	Page
1 NSF AM awards [1].....	2
2 Timelines of AM developments and applications [2].....	3
3 AM process [8].	8
4 A waveguide antenna array and feed system made by SLA provides a compact device with improved gain and directionality [4].	12
5 Eight Vivaldi antennas placed vertically around a common central axis [14].	14
6 Antenna printed with Aerosol Jet direct write process [32].	16
7 Optical image of an antenna during the printing process [34].....	17
8 3D printed volcano smoke antenna [45].	18
9 Conical antenna printed utilizing IP [60].....	19
10 Schematic picture of the ultrasonic wire embedding technique [61].....	19
11 Antenna conductive part pattern [65].	20
12 Fabricated lens antenna using AM [73].....	21
13 Radiated region of antenna.	23
14 Polarization ellipse.....	24
15 3D radiation pattern of an antenna.....	25
16 Radiation patterns on E- and H-plane.	25
17 3D radiation pattern of an omnidirectional antenna	26
18 3D radiation pattern of a directional antenna.....	26

19	Parallel plate capacitor, DC case [87].	30
20	Parallel plate capacitor, AC case [87].	32
21	Coaxial probe method [87].	34
22	Fabricated samples for permittivity measurements.	36
23	85070E Agilent performance probe and a material under test.	36
24	Measured real (solid) and imaginary (dashed) parts of the complex permittivity of the utilized materials.	37
25	Configuration of the proposed antenna.	39
26	Top view of the proposed antenna with structural parameters.	39
27	Reflection coefficient of the proposed antenna.	40
28	Reflection coefficient for varying h.	41
29	Reflection coefficient for varying dielectric constant.	41
30	Reflection coefficient for varying feed lines gap a.	42
31	Reflection coefficient for varying feed lines width b.	42
32	Reflection coefficient for varying bowtie width W.	43
33	Reflection coefficient for varying bowtie length L.	43
34	Simulated radiation pattern of the proposed bowtie antenna.	44
35	Simulated surface current of the designed bowtie antenna at 2.45 GHz.	45
36	Effect of radiator conductivity on the reflection coefficient.	45
37	Surface current distribution for copper radiator and four lossy radiators with different conductivities in respect to copper at 2.45 GHz.	47
38	Proposed antenna with staircase shaped radiator.	48
39	Surface current distribution of the proposed antenna with staircase radiator at 1.64 GHz.	49
40	Surface current distribution of the proposed antenna at the radiator edges.	49

41	Simulated reflection coefficient of the staircase and planar radiator bowtie antenna.	50
42	Simulated E- and H- plane of the proposed bowtie antenna with staircase radiator configuration.....	50
43	Configuration of the proposed 3D UWB bowtie antenna.....	51
44	Reflection coefficient of the proposed 3D broad band antenna.....	51
45	VSWR of the proposed UWB antenna.	52
46	Input impedance of the proposed UWB antenna.	52
47	Group delay of the UWB antenna.....	53
48	Radiation patterns of the UWB antenna at 3 GHz, 6 GHz, and 9 GHz.	54
49	Current distribution of the UWB antenna at 3 GHz, 6 GHz, and 9 GHz.....	55
50	Efficiency of the proposed UWB antenna.	55
51	Surface current distribution for the UWB planar and 3D antennas.	56
52	Radiation pattern for the planar and 3D antennas.....	57
53	Configuration of the proposed antenna for UWB spectrum with optimized dimensions.	58
54	Reflection coefficient of the antenna.	58
55	Radiation patterns of the UWB antenna.	59
56	Input impedance of the UWB antenna.....	60
57	Group delay of the UWB antenna.....	61
58	Proposed substrate for dipole antenna.	62
59	Proposed dipole antenna.	62
60	Reflection coefficient of the proposed dipole antenna.	62
61	Radiation patterns of the designed antenna on E- and H-plane.	63
62	Configuration of the proposed Yagi-Uda antenna.	64
63	Reflection coefficient of the proposed Yagi-Uda antenna.....	64

64	Radiation patterns of the designed Yagi-Uda antenna on E- and H-plane.	65
65	Current distribution on the surface of the Yagi-Uda antenna at 3 GHz.....	65
66	3D Radiation patterns of the 3D dipole and 3D Yagi-Uda antenna at 3 GHz.....	66
67	Comparison of the 3D dipole and 3D Yagi-Uda H-planes.	66
68	Configuration of the pin-fed patch antenna.	67
69	Top view of the patch antenna.	68
70	Reflection coefficient of the patch antenna.	68
71	Radiation patterns of the patch antenna on E- and H-plane.....	69
72	Surface current distribution of the patch antenna at 5.8 GHz.....	69
73	3D radiation patterns of the patch antenna at 5.8 GHz.	70
74	The 3D model of the antenna created in SolidWorks.	71
75	A printed part between the extruder heads of MakerBot Dual and the heated build plate.....	72
76	Fabricated bowtie antenna.	74
77	Measured reflection coefficient of the bowtie antenna.....	74
78	Fabricated antenna under test.....	75
79	Measured E- and H-plane of the fabricated bowtie antenna.....	75
80	A photograph of fabricated bowtie with staircase radiator configuration.	77
81	Reflection coefficient of the fabricated bowtie with staircase radiator configuration.....	77
82	Radiation patterns of the fabricated bowtie antenna on E- and H-plane at 7.8 GHz..	78
83	Fabricated 3D antenna.	79
84	Reflection coefficient of the fabricated 3D antenna.	79
85	Radiation patterns of the fabricated UWB antenna on H- and E-plane at 3.5 GHz and 5.8 GHz.	80
86	ROBO 3D printer.....	81

87	Fabricated dipole antenna with ABS and carbon paste.	82
88	Fabricated dipole antenna with PLA and carbon paste.....	82
89	Measured reflection coefficient of the fabricated dipole antennas.	82
90	Measured reflection coefficient of the fabricated dipole antennas.	83
91	Fabricated bowtie substrate and its mask.....	84
92	Fabricated mask for the bowtie antenna.	85
93	DESK V HP sputtering system.	85
94	Antenna under sputtering process.	86
95	A photograph of the fabricated antenna.....	86
96	Measured reflection coefficient of fabricated bowtie antenna.....	87
97	Measured radiation patterns of fabricated bowtie antenna on E- and H-plane.....	87

LIST OF TABLES

Table	Page
1 AM and 3D printing industry (products and services) worldwide past and projected values [1, 2].....	2
2 Past, present and potential future AM developments and applications [2].....	4
3 Comparison between different measurement methods [87].	33
4 Specification of materials.	37
5 Physical dimension of the proposed bowtie antenna.	40
6 Effect of radiator conductivity on the directivity and gain.	46
7 Effect of radiator conductivity on the surface current.	47
8 Realized and IEEE gains of the antenna at different frequencies.	56
9 Comparison of planar and 3D antennas at 9 GHz.....	57
10 Realized and IEEE gains of the antenna at different frequencies.	60
11 Comparison of 3D dipole and 3D Yagi-Uda antenna.	67
12 Structural parameter of the patch antenna.	68
13 Material and temperature for different antennas.....	73
14 MakerBot Dual construction conditions for different antennas.....	73
15 Comparison of the E- and H-plane of the 3D antenna.....	79
16 Comparison of fabricated dipole antennas.....	84

ABBREVIATIONS

3D	Three Dimensional
PLA	Polylactic Acid
ABS	Acrylonitrile Butadiene Styrene
AM	Additive Manufacturing
FDM	Fuse Deposition Modeling
DP	Direct Print
CAD	Computer Aided Design
SLA	StereoLithography Apparatus
STL	STereoLithography
DLP	Digital Light Projection Technology
UV	UltraViolet
PC	PolyCarbonate
2D	Two Dimensional
FFF	Fused Filament Fabrication
PCB	Printed Circuit Board
ESAs	Electrically Small Antennas
LDS	Laser Direct Structuring
DTP	Direct Transfer Patterning
UE	Ultrasonic Embedding
PPT	Pad Printing Technology
UWB	Ultra WideBand
MMW	MilliMeter-Wave
VSWR	Voltage Standing Wave Ratio
WLAN	Wireless Local Area Network
RH	Right-Hand
LH	Left-Hand
MUT	Material Under Test
OLED	Organic Light Emitting Diode
AR	Axial Ratio
IP	Integrated Printing
NSF	National Science Foundation
RF	Radio Frequency
FCC	Federal Communications Commission

ACKNOWLEDGEMENTS

First of all, I wish to express my sincere gratitude to my advisor, Dr. Sima Noghanian, for her support and guidance during the course of this study. I would like also to thank Dr. Isaac Chang and Dr. Surojit Gupta, for serving on my advisory committee and their help in fabrications. I also want to thank Lindsey Wiest for her help in fabrications.

Additionally, I would like to express my appreciation to North Dakota Experiment Program to Stimulate Competitive Research (ND EPSCoR), University of North Dakota, National Science Foundation (NSF), and Rockwell Collins Inc., for the financial support of this project.

Last, but not the least, I wish to thank my family for their unconditional love and infinite support.

To my family...

ABSTRACT

In today's world of wireless communication systems, antenna engineering is rapidly advancing as the wireless services continue to expand in support of emerging commercial applications. Antennas play a key role in the performance of advanced transceiver systems where they serve to convert electric power to electromagnetic waves and vice versa. Researchers have held significant interest in developing this crucial component for wireless communication systems by employing a variety of design techniques. In the past few years, demands for electrically small antennas continues to increase, particularly among portable and mobile wireless devices, medical electronics and aerospace systems.

This trend toward smaller electronic devices makes the three dimensional (3D) antennas very appealing, since they can be designed in a way to use every available space inside the device. Additive Manufacturing (AM) method could help to find great solutions for the antennas design for next generation of wireless communication systems. In this thesis, the design and fabrication of 3D printed antennas using AM technology is studied. To demonstrate this application of AM, different types of antennas structures have been designed and fabricated using various manufacturing processes.

This thesis studies, for the first time, embedded conductive 3D printed antennas using PolyLactic Acid (PLA) and Acrylonitrile Butadiene Styrene (ABS) for substrate parts and high temperature carbon paste for conductive parts which can be a good

candidate to overcome the limitations of direct printing on 3D surfaces that is the most popular method to fabricate conductive parts of the antennas.

This thesis also studies, for the first time, the fabrication of antennas with 3D printed conductive parts which can contribute to the new generation of 3D printed antennas.

CHAPTER 1

INTRODUCTION

In the past few years the design of so-called 3D electromagnetics structures using AM method has been increasingly sought both in industry and academia, since it offers smaller form-factor, lighter-weight, lower cost, more time efficiency and more environmentally friendly option than conventional manufacturing methods. Advanced wireless communication applications impose unprecedented demands for antennas and electronic components capable of operating at wideband frequency ranges while maintaining smaller size and thinner form factor. Antennas suffer limitations in gain and bandwidth when their size is reduced less than quarter wavelength. The research efforts have been directed to the design of 3D antennas with smaller size, lighter weight and more design freedom while maintaining the same performance.

1.1 Motivation

AM, the technological innovation behind 3D printing, has revolutionized the way we conceive of, and build everything, from electronic devices to jewelry and artificial organs [1]. In 2009, the expiration of key 3D printing patents for Fuse Deposition Modeling (FDM) paved the way for today's thriving open source 3D printing movement [2]. The use of AM for the fabrication of parts for final products continues to grow. In ten years it has gone from almost nothing to 28.3% of the total product and services revenue from AM worldwide [2, 3]. Both public and private investments have contributed to the development of this technology. National Science Foundation (NSF) provided early

funding and continues to provide support for AM, totaling approximately \$200 million in 2005 adjusted dollars from more than 600 grants awarded from 1986-2012 [1].

3D printing contributed to more than \$2.2 billion in global industry in 2012 [1] and is poised to grow to more than \$10.8 billion in 2021 [2]. AM and 3D printing industry (products and services) worldwide past and projected values are given in Table 1.

Table 1: AM and 3D printing industry (products and services) worldwide past and projected values [1, 2].

Year	Past and projected values
2012	\$2.2 billion
2015	\$4 billion
2017	\$6 billion
2021	\$10.8 billion

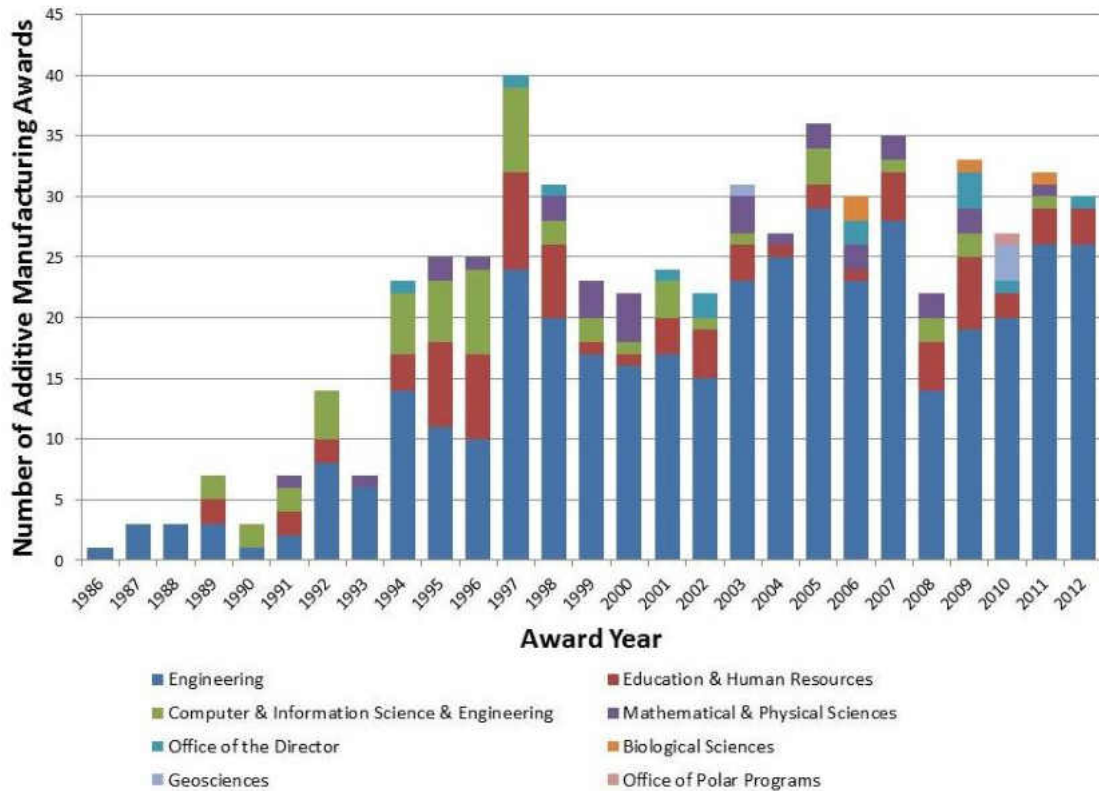


Figure 1. NSF AM awards [1].

Figure 1 shows the NSF additive manufacturing awards. Figure 2 lays out past, present and potential future AM developments and applications. The relevant information to Figure 2 are listed in Table 2.

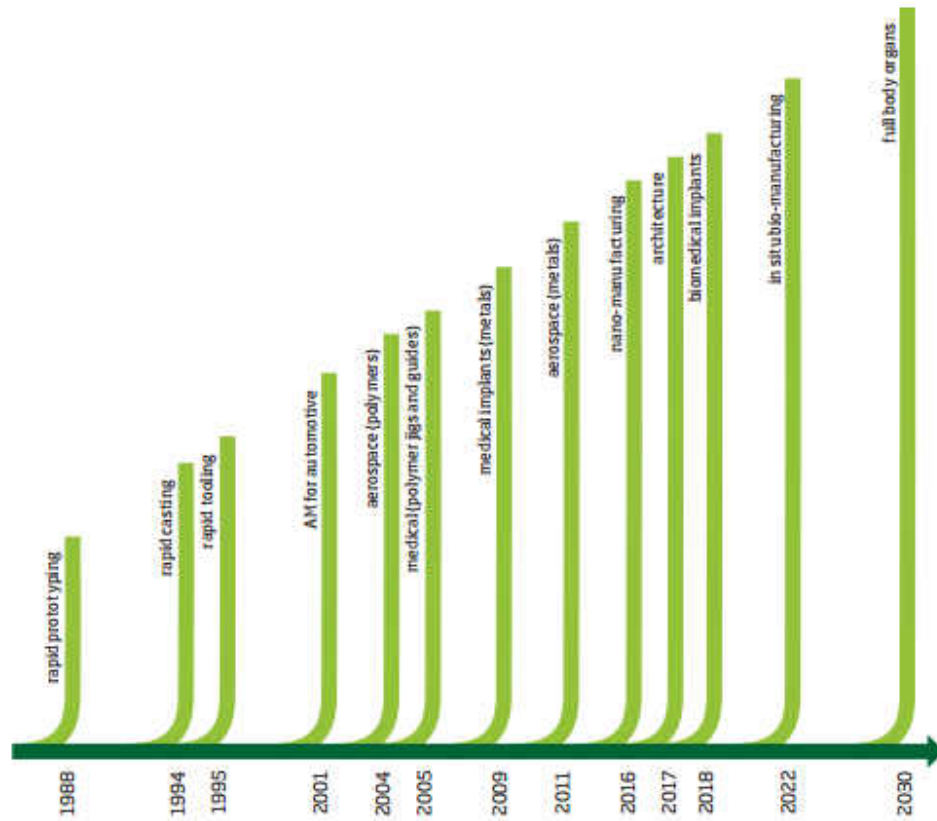


Figure 2. Timelines of AM developments and applications [2].

Additive manufacturing (AM) technologies are being applied across the entire spectrum of electronics from integrated circuits to discrete components and microwaves [4]. The integration of AM combined with Direct Print (DP) micro-dispensing can produce shapes of arbitrary and complex form that also allows for miniature cavities for inseting electronic components and conductive traces for electrical interconnect between components [5].

Table 2: Past, present and potential future AM developments and applications [2].

Year(s)	AM developments and applications
1988–1994	Rapid prototyping
1994	Rapid casting
1995	Rapid tooling
2001	AM for automotive
2004	Aerospace (polymers)
2005	Medical (polymer jigs and guides)
2009	Medical implants (metals)
2011	Aerospace (metals)
2013-2016	Nano-manufacturing
2013-2017	Architecture
2013-2018	Biomedical implants
2013-2022	In situ bio-manufacturing
2013-2030	Full body organs

In April 2013, Optomec Inc. announced that it is developing a new digital production solution that enables direct printing of antennas used in mobile device applications. The solution is based on Optomec’s patented Aerosol Jet printed electronics technology, an additive manufacturing process used to print electronics onto planar and 3D surfaces [6].

In September 2014, Optomec Inc. announced the availability of the Aerosol Jet 5X system for printing 3D electronics. The Aerosol Jet 5X platform was specifically developed to enable a new generation of lighter weight, high performance micro-electronic devices such as smart phones, tablets, and sensors [7].

The necessity for reliable antennas fabricated based on AM technology (which based on the above discussion is seen as a technology that can offer a great potential for providing 3D antennas) for next generation of wireless communication systems has motivated this research on the design of compact antennas using novel dielectric and conductive materials through advanced AM fabrication process.

This thesis investigates novel methods for developing of 3D printed electromagnetic structures with emphasis on the antenna as an essential component in Radio Frequency (RF) front-end modules utilizing AM technology. To demonstrate these methods, several antenna configurations including bowtie, dipole as well as patch antennas with different feed structures have been designed, simulated, and fabricated at different frequency bands for different applications. The dielectric substrates utilized for the fabrication of the antennas have been printed using different desktop and commercial 3D printers. A variety of dielectric materials including PLA and ABS have been used in the fabrication of the substrate parts of the proposed antennas. The complex permittivity of the utilized materials has been measured using 85070E Agilent performance probe. In addition this thesis studies the application of sputtering technology and conductive ABS materials in the fabrication of 3D printed antennas.

1.2 Thesis Outline

The thesis is organized into 6 chapters. Chapter one presents the introduction. Chapters two-five describe the main research that has been done for this thesis work. Chapter six is presenting the future work and conclusions.

Chapter two provides a literature review on the AM technologies utilized to make electronic devices and the previously published works and ideas to fabricate 3D antennas using AM. The measurement method for characterizing the complex permittivity of the utilized substrate and conductive materials for the design of proposed antennas is discussed in Chapter three. The complex permittivity measurement results using 85070E Agilent performance probe performance probe are also presented in this chapter.

Design, simulation and performance analysis of the proposed antennas are presented in Chapter four. Several antenna configurations for fabrication using 3D printing are discussed in this chapter. The simulation results of the proposed antennas for reflection coefficient, Voltage Standing Wave Ratio (VSWR), gain, directivity, efficiency, group delay are given in this chapter. In addition, the radiation patterns of the designed antennas are demonstrated.

Chapter five describes the fabrication process of the proposed antennas. Several fabrication methods using different materials for conductive and substrate parts of the antennas are considered in this chapter. The measurement results including reflection coefficient and radiation pattern for the fabricated antennas are demonstrated in this chapter.

CHAPTER 2

LITERATURE REVIEW

2.1 Additive Manufacturing (AM)

2.1.1 Background and Principle

3D printing or rapid prototyping is a process by which components are fabricated directly from computer models by selectively curing, depositing or consolidating materials in successive layers. These technologies have traditionally been limited to the fabrication of models suitable for product visualization, but over the past decade, they have quickly developed into a new paradigm called “additive manufacturing” [8].

Rapid prototyping first emerged as a means to accelerate the time consuming and costly iterative product design process, thereby, reducing time to market, improving product quality, and eventually decreasing the costs. By printing physical prototypes directly from 3D Computer Aided Design (CAD) data, rapid prototyping offered designers the opportunity to quickly run through many design iterations. This was essentially the impetus for the development of the first rapid prototyping systems, called StereoLithography Apparatus (SLA), patented by Charles Hull in 1986 and marketed by 3D systems [8].

SLA is based on the concept of photopolymerization by which monomers are linked into a polymer chain using photons [8]. A very detailed description of the SLA process is provided by Jacobs [9].

One of the key factors to unlocking the potential of layer based AM was the development of the standard STereoLithography (STL) file format. STL is currently used by most of the additive processes and is available as a standard format in most CAD systems. The STL format describes the external surface of the 3D CAD model with a series of triangular facets connected at the vertices. The size and number of the triangles can vary depending upon the accuracy of the process and the tolerances required [8].

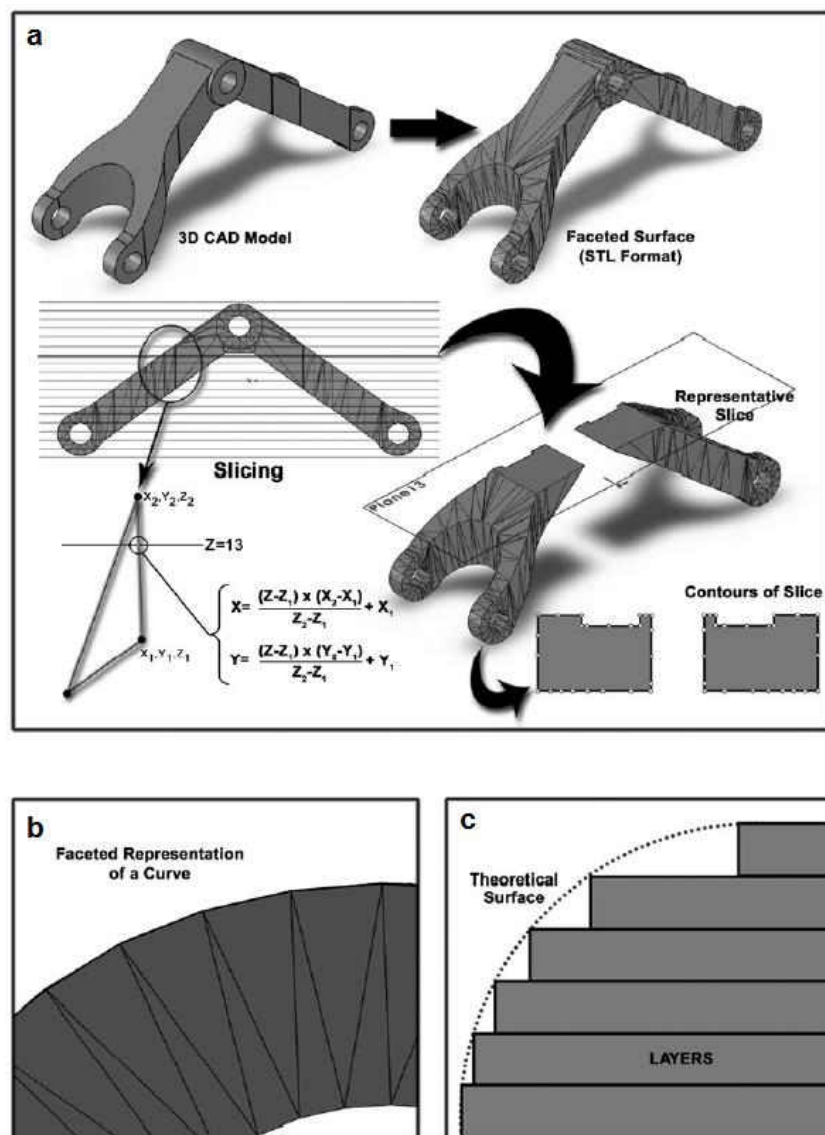


Figure 3. AM process [8].

The STL part model is oriented in Cartesian space and software is used to slice the model parallel to the X-Y plane in discrete increments equal to the layer's thickness. Because the vertices of each of the surface triangles are known, it is relatively simple to calculate the coordinates of the intersection between the triangles and the slicing plane. These intersection points are connected to form the contour of each layer that is then used to control the machine (Figure 3(a)). While approximating CAD surfaces with triangles is an effective and simple method for representing geometries and slicing models, it should be noted that it inherently builds geometric errors into the fabricated parts (Figure 3(b)). This can be partially offset by reducing the size (and increasing the number) of the facets, but only at the cost of increasing the data storage requirements. As one layer is stacked upon the next, a geometric stair-step error is introduced. This error is intrinsic to all additive processes (Figure 3(c)). As products produced with AM technologies are implemented in various industries and are incorporated into complex assemblies, tolerances to geometric errors such as these are likely to become more and more critical [8].

2.1.2 AM Technologies

Very soon after the development of the SLA technology many different types of rapid prototyping processes were developed and are still widely used today. However, there are a variety of additive manufacturing technologies [9-11], most of these operate on the same underlying principle that material is selectively cured, consolidated, or deposited layer upon layer [8].

2.1.2.1 Digital Light Projection Technology (DLP)

One of these technologies is Digital Light Projection Technology (DLP) which can reduce processing times and the high cost of components typically associated with SLA (specifically lasers) [8]. These systems typically have the build platform inverted so that the finished parts are upside down; this has the added benefit of minimizing the amount of material required in the build tank at any given time [8].

2.1.2.2 Inkjet Printing Technology

After the development of SLA, the use of inkjet printing technology to deposit a binder onto a powder bed in a layer wise fashion was developed by a research group at Massachusetts Institute of Technology (MIT) and marketed to numerous companies in the early 1990 [8, 11]. Other inkjet printing technologies have also been used to deposit photosensitive resins which are then subsequently cured by a UltraViolet (UV) light source. One benefit of this method is the ability to print multiple materials or colors within a single layer [8].

2.1.2.3 Deposition of Thermoplastics by Extrusion through a Heated Nozzle

Another technology that was developed relatively early on is the deposition of thermoplastics by extrusion through a heated nozzle. This typically involves feeding a filament of thermoplastic, such as PolyCarbonate (PC) or ABS, through an extrusion nozzle which is translated about a build platform using numerical control [8].

2.1.2.4 Laser Sintering Technology (LST)

This technology offers the potential to address the need of supporting more variety of materials for AM application [8]. The laser energy is used to heat and

consolidate layer upon layer of polymer powder. In theory, this suggests that any thermoplastic that can be rendered into a powder form of the appropriate size and morphology, can be processed using LST [8].

2.1.3 Application of AM for Fabrication of 3D Electronics

AM offers a great potential to overcome the limitations of conventional manufacturing approaches. It is beginning to be used in combination to solve complex problems such as fabricating electronics with mechanical parts and assemblies simultaneously. This may become quite common in the future since each technology has its particular and somewhat mutually-exclusive advantages [4].

2.1.3.1 Differences between 2D and 3D Printing of Electronics

Two dimensional (2D) circuit printing technologies include everything from screen printing, automatic conductive paste deposition systems on a flat surface, laser printing, thin film deposition, and solution coated Organic Light Emitting Diode (OLED) fabrication. All of these processes operate on flat surfaces for the most part, and cannot be applied to substrates with contours or multi-axis dimensions [12].

3D electronics printing can function much like 2D printing, with the advantage of being able to produce 3D objects with the wires and circuitry embedded within the structural material. 3D electronic printing allow designers to create products that are smaller, lighter, more efficient, and customized. Many 3D printed electronics are almost impossible to create with standard 2D electronic fabrication methods [12].

2.1.3.2 Trends in 3D Printing for Electronics

Broadly speaking, the 3D conductive and electrical printing technologies vying for commercial success, in no particular order are: filament base with inkjet applied conductive inks; filament base with syringe applied conductive gels; filament base with embedded copper conductors, a technology developed by the Keck Center of University of Texas at El Paso, a version of Fused Filament Fabrication (FFF); graphene substrate and conductor as demonstrated by Korea's KERI center; filament base with conductive aerogel applicator [12].

2.1.3.3 High Frequency and Microwave Electronics

High frequency component manufacturing is a strong application area for additive technologies. In some cases AM is permitting devices to be manufactured which can't be made any other way. In most cases, though, the geometric capability of additive technologies simply permits conventional components to be made at lower cost or even with better performance [4]. Figure 4 shows a waveguide antenna array and feed system with improved gain and directionality made by SLA [4].

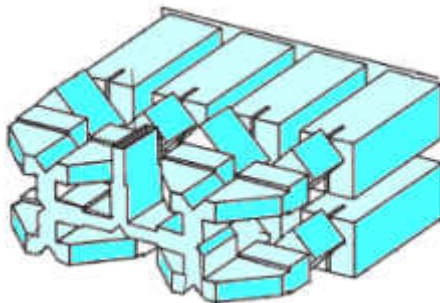


Figure 4. A waveguide antenna array and feed system made by SLA provides a compact device with improved gain and directionality [4].

2.1.3.4 Thermal Management

Electronic devices generate heat, and at whatever level that occurs, there are applications for AM to carry it away. One of the more interesting applications of AM is to make housings for electronic systems which guide cooling air to particular areas where it may be needed most. This may require complex geometries that can't be fabricated economically using any other manufacturing methods [4].

2.1.3.5 Challenges in Fabrication of Electronics Using AM

According to researchers including Dr. Elena Polyakova of Graphene 3D Lab, “The key challenge in 3D printing electronics is developing material suitable to be used in a desktop 3D printer. To do this, you must incorporate conductive material (such as graphene) with a standard 3D printing material, but not so much that the filament loses processability [12].”

In [13], the experiments showed that the mix of materials and the surface characteristics are the challenging application of the printed structures in high resolution and with very thin layers.

The researchers in the Keck Center-UTEP confronted many of the challenges mentioned above by Dr. Elena Polyakova. The team’s Research and Development has shifted from the prevalent silver paste injection method of 3D printing, to a new approach of embedding copper wire through unique processes. According to Professor Eric MacDonald, Associate Director of the Keck Center-UTEP, the future of additive manufacturing will include their copper embedding system [12].

2.2 3D Antennas Manufacturing

The tendency to have smaller size and thinner form factor in wireless devices makes the design of 3D antenna an important task to use every available space inside the device efficiently. A lot of research efforts have been put on the design of 3D antennas in the past few decades [14-75].

2.2.1 3D Antennas Utilizing Traditional 2D Manufacturing Methods

From the point of manufacturing method, the 3D antennas designed for wireless communication systems can be categorized in two major groups: i) antennas with 3D structures fabricated utilizing traditional methods, and ii) antennas fabricated based on AM methods. Most of the antennas in the first category are fabricated using 2D Printed Circuit Board (PCB) technology and put together in a way to create a compact 3D structure (Figure 5) [14-23].

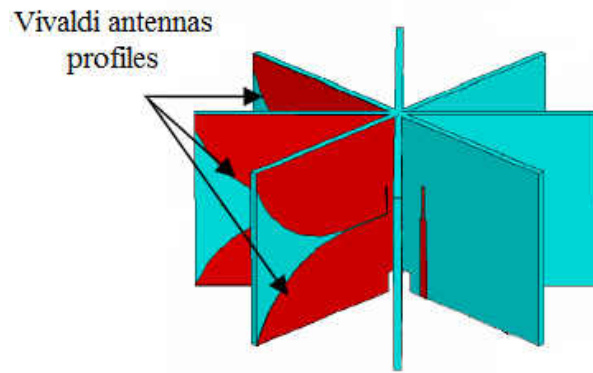


Figure 5. Eight Vivaldi antennas placed vertically around a common central axis [14].

2.2.2 Antennas Utilizing AM

Realizing electronic systems that are conformal with curved or complex surfaces is difficult, if not impossible, with conventional fabrication techniques discussed in 2.2.1, which require rigid 2D PCB [5].

Flexible copper based manufacturing is widely available commercially. These products provide conformity but not enough stiffness at the same time. As a result, these systems are susceptible to reliability problems if repeatedly bent or stretched [5].

The integration of AM with Direct Printing (DP) micro-dispensing can produce shapes of arbitrary and complex form that also allows for i) miniature cavities for inseting electronic components, and ii) conductive traces for electrical interconnect between components [5].

2.2.2.1 Antennas Utilizing DP on 3D Printed Substrates

In the past few years, DP has widely been used for the fabrication of 3D antennas for various applications. Antennas designed based on this method have taken different shapes and configurations. Sciperio has developed an advanced printing technology to conformally print “any” material on “any” surface [24]. 3D antennas have been designed and fabricated using the AM and micro-dispensing method [25-28]. Due to the lossy substrate materials used in the fabrication, the antenna gain was decreased by 2.5 dB relative to the PCB version of the antenna that was made using low loss microwave laminate [25]. In the other studies [26-28], the antenna substrate is built of ABS plus material using the fused deposition process and then metalized using the DP AM processed Dupont CB-028 silver ink [29]. A comparison with other designs from the literature fabricated with different processes shows that using FDM and conformal 3D printing is a promising manufacturing method and high performance antennas can be realized with the currently available materials using this method [26].

The direct write printing technique has been used to study the various parameters related to a handset antenna manufacturing on a 3D surface [30]. It has been demonstrated that there may be fine tuning required when the radiator of the antenna has very fine details and during the curing phase of the ink, the radiator dimensions may have been affected. Additionally, the lower conductivity of the ink is more dominant at lower band due to skin effect [30].

A cube-shaped antenna, which has been inkjet printed on a paper substrate and integrated with embedded electronics has been presented in [31]. Based on measured results, the performance of the antenna is not affected by the presence of embedded electronics inside the cube.

The capability of Aerosol Jet technology to print multi-layer and 3D antennas has been demonstrated in [32, 33]. It is shown that the Aerosol Jet technology is capable of printing both large scale features, such as phase-array antenna, as well as small scale features, such as 30 micron wide interconnects [33]. Figure 6 shows an antenna printed with Aerosol Jet direct write process [32].



Figure 6. Antenna printed with Aerosol Jet direct write process [32].

Researchers at the University of Illinois at Urbana-Champaign, IL, have proposed an omnidirectional printing of metallic nanoparticle inks to meet the demanding form factors of 3D Electrically Small Antennas (ESAs) [34-36]. These antennas are electrically small (Figure 7) relative to a wavelength (typically a twelfth of a wavelength or less) and exhibit performance metrics that are an order of magnitude better than those realized by monopole antenna designs [34]. Another study reveals that dome antenna with conformal menderlines can contribute to the developing of ESAs with dual and wideband performance [37].

As presented in [38, 39], Laser Direct Structuring (LDS) can be a good candidate to fabricate the conductive part of dome antennas. Direct Transfer Patterning (DTP) is another method that has been developed for printing ESAs [40]. However, none of the above mentioned contributions demonstrate a fully encapsulated device that would be suitable for a small wireless sensor node.

New 3D printing techniques using direct writing of a silver nanoparticle ink [41] onto the internal surfaces of glass hemisphere has been proposed in [42] which enables the integration of an antenna directly onto the package of a small wireless sensor node.

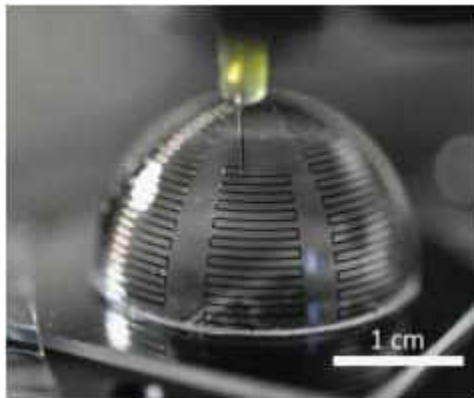


Figure 7. Optical image of an antenna during the printing process [34].

2.2.2.2 Antennas Utilizing Coating of Conductive Material on 3D Printed Substrate

Coating the 3D printed substrate structure with conductive materials has found a lot of applications in the fabrication of antennas and microwave components [43-57]. In these designs, firstly the prototype of the antenna is fabricated using available materials for 3D printing (ABS, PLA, etc.) and next it is covered by a conductive material to make the radiator part of the antenna. Figure 8 illustrates 3D printed volcano smoke antenna [45].



Figure 8. 3D printed volcano smoke antenna [45].

2.2.2.3 Antennas Utilizing Integrated Printing (IP)

In this manufacturing process, combination of printed electronics using conductive nanoparticle ink together with 3D printing of dielectric material is presented as one integrated process [58-60]. Measurement results demonstrate that this fabrication method is a promising method for the fabrication of complicated 3D EM structures such as wide range of different antennas and microwave devices to simultaneously include printing of conductive nanoparticle ink within 3D dielectric configurations [58]. Figure 9 shows a conical antenna printed using IP.

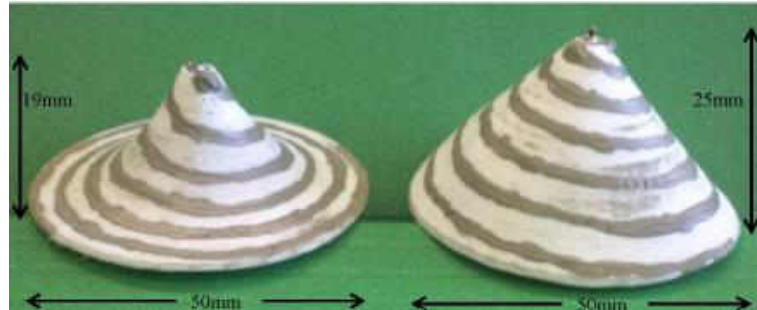


Figure 9. Conical antenna printed utilizing IP [60].

2.2.2.4 Antennas Utilizing Combination of FFF and Ultrasonic Embedding (UE)

Another interesting method for the fabrication of advanced antennas using AM is combination of FFF with UE [61, 62]. In this fabrication method, the antenna substrate structure is printed using FFF method and the wire mesh is submerged into the plastic dielectric substrate using UE as shown in Figure 10.

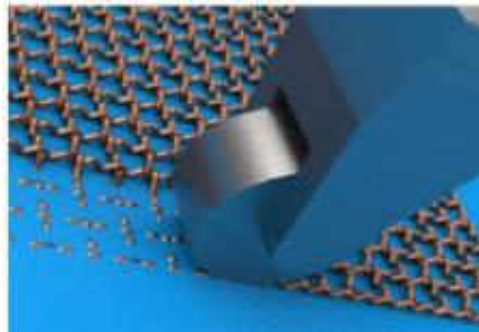


Figure 10. Schematic picture of the ultrasonic wire embedding technique [61].

This embedded wire-mesh method can be integrated into any surface regardless of curvature and is fully compatible with thermoplastic extrusion 3D printing technology [61].

2.2.2.5 Antennas Utilizing Pad Printing Technology (PPT)

New developments in the late 60s and early 70s, such as silicone pads and more advanced equipment, made the printing method far more practical. The unique properties

of the silicone pad enable it to pick the image up from a flat plane and transfer it to a variety of surfaces including flat, cylindrical, spherical, compound angles, textures, concave, and convex surfaces [65].

Nowadays, pad printing is a well-established technology covering a wide spectrum of industries and applications [63-66]. It has been demonstrated that that PPT can get the same RF performance as the common flex technology. In addition, it provides 3D design freedom with very good mechanical as well as environmental performance [65]. One interesting application of pad printing is fabricating radiator part of antenna for mobile phone applications (Figure 11).

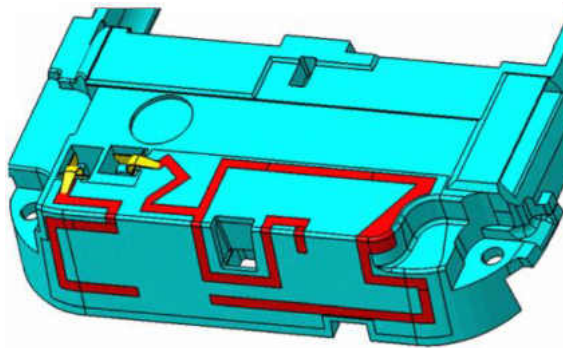


Figure 11. Antenna conductive part pattern [65].

2.2.2.6 Antennas Utilizing Fused Deposition and Micro-Dispensing

This manufacturing method is based on fused deposition of thermoplastic substrates with micro-dispensing for producing conductive traces which can be again considered as direct printing as discussed in 2.2.2.1. The obtained results demonstrate the strong potential of this method for fully-printed RF front-ends with light weight, low cost, conformal and readily customized applications [67-70].

2.2.2.7 Antennas Utilizing Flexible Materials

Generally 3D flexible antennas can be categorized in two main groups: i) the first group uses the AM to create the substrate of the antenna and then the substrate is metallized using conductive materials like conductive tape [71], and ii) the second group uses the AM for creating both substrate and radiator parts of the antenna at the same time [72].

2.2.2.8 Lens Antennas Utilizing AM

Another interesting application of AM technology as a possible low-loss and low-cost solution for high-gain MilliMeter-Wave (MMW) antennas is in the manufacturing dielectric lens antennas [73-75]. Achieved results show that available commercial plastic materials features suitable performances at MMW frequencies and designed lens are fully competitive with more expensive manufacturing technologies [75]. Figure 12 shows a lens antenna fabricated using AM [73].



Figure 12. Fabricated lens antenna using AM [73].

2.3 A Brief Review on Antenna Tutorials

Antennas as a crucial component in every successful wireless product are capable of converting the wireless power to electromagnetic waves that carry the data to be

transmitted and vice versa. As wireless devices continue to change in terms of size and performance, antenna designs to meet the new requirements, are gaining importance. Here, a brief review on the antennas tutorial will be presented. More information about the antenna parameters and different types of antennas can be found in [76, 77].

2.3.1 Electromagnetic Waves

The electromagnetic fields result from the acceleration of electric charges. The electric field due to accelerated charge (one at rest or in uniform motion in a straight line) is radially directed and decreased as the square of the distance from the charge. However, acceleration of the charges gives rise to the tangential component of the electric field, and this decreases linearly with distance [78]. This time-varying electric field is associated with the time-varying magnetic field. They comprise electromagnetic field together. An electromagnetic field that decreases linearly with distance represents an outward radiation [79].

In practice, one is almost concerned with macroscopic effects resulting from acceleration of a gross number of charges [79]. On the macroscopic scale, the interrelationship between electric and magnetic field is described mathematically by Maxwell's equations [80, 81]. An additional set of equations called "constitutive relationships" specifies the characteristics of the medium in which the field exist [81, 82].

The radiation field from a transmitting antenna is characterized by the complex Poynting vector $E \times H^*$ in which E is the electric field and H is the magnetic field. Close to the antenna the Poynting vector is imaginary (reactive) and (E, H) decay more rapidly than $1/r$, while further away it is real (radiating) and (E, H) decay as $1/r$. These two types of fields dominate in different regions in space around the antenna. Based on this

characterization of the Poynting vector, we can identify three major regions [83]: i) reactive field, ii) radiating near-field, and iii) radiating far-field (Figure 13) [83].

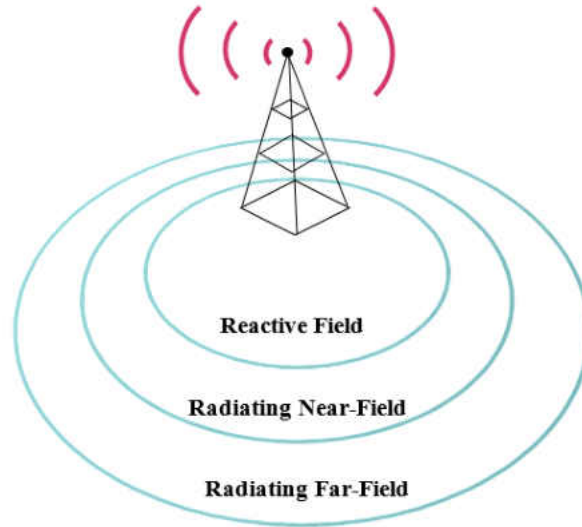


Figure 13. Radiated region of antenna.

2.3.2 Antenna Polarization

Polarization is the property of the electric field vector that defines the variation in direction and magnitude with time [83]. If the field is observed in a plane perpendicular to the direction of propagation at a fixed location in space, the end point of the vector representing the instantaneous electric field magnitude traces a curve. In general case, this curve is an ellipse, as shown in Figure 14. The ellipse is characterized by the Axial Ratio (AR), the ratio of the major to the minor axes, and the ellipse major axis tilt angle, τ [83].

The polarization may be classified as linear, circular or elliptical according to the shape of the curve. Linear and circular polarizations are special cases of elliptical polarization, when the ellipse becomes a straight line or a circle, respectively. Clockwise

rotation of the electric field vector is considered as Right-Hand (RH) polarization and counterclockwise rotation is Left-Hand (LH) polarization, for an observer looking in the direction of propagation [83].

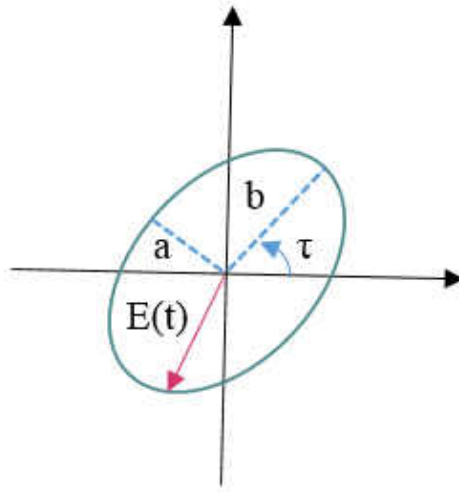


Figure 14. Polarization ellipse.

2.3.3 Antenna Radiation Patterns

The radiation pattern is the graphical representation of the radiation properties of the antenna as a function of space. The antenna's pattern describes how the antenna radiates or receives energy out into space. The antenna radiation pattern shape can be nearly spherical or all the energy can be directed in one direction, such as that generated by a large reflector antenna [79].

The energy radiated from the antenna is a three dimensional problem which is generally measured in the far field region. It is common to present radiation patterns with two planar planes, called E- and H-plane. The E-plane is any plane which includes the E-field and the direction of maximum propagation from the antenna, the H-plane, perpendicular to it, is any plane that contains the E-field and the direction of maximum

propagation. It is also common to show co-polarization (co-pol) and cross-polarization (x-pol) patterns for E- and H-plane. The co-pol is desired polarization component and x-pol is orthogonal to it and usually is not desired. Figures 15 and 16 show a 3D pattern and its E- and H-plane, respectively.

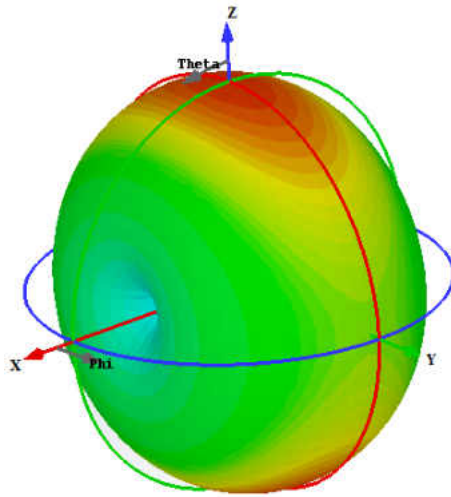


Figure 15. 3D radiation pattern of an antenna.

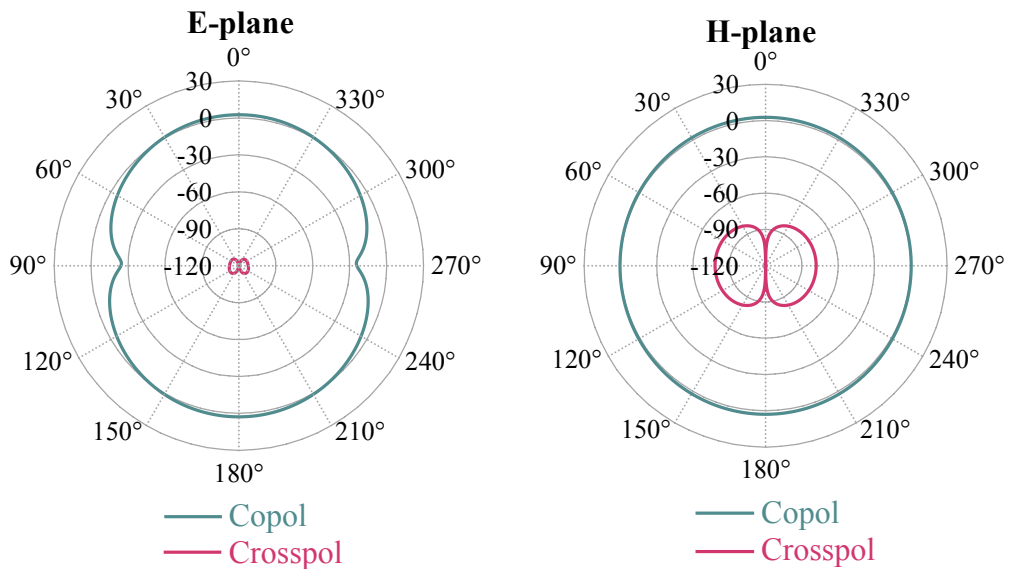


Figure 16. Radiation patterns on E- and H-plane.

2.3.4 *Isotropic, Directional and Omnidirectional Antennas*

An isotropic antenna is a hypothetical lossless antenna that radiates its energy equally in all directions. Omnidirectional antenna is an antenna that has a non-directional pattern (circular pattern) in a given plane with a directional pattern in any orthogonal plane [84] (Figure 17).

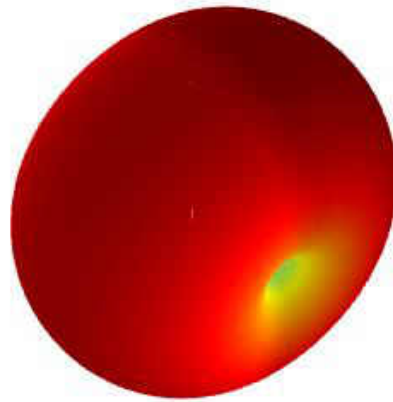


Figure 17. 3D radiation pattern of an omnidirectional antenna.

Directional antenna is an antenna that radiates its energy more effectively in one (or some) direction than others. Typically, these antennas have one main lobe (high radiation region) and several minor lobes. Examples of directional antennas are patch and dish antennas [84] (Figure 18).

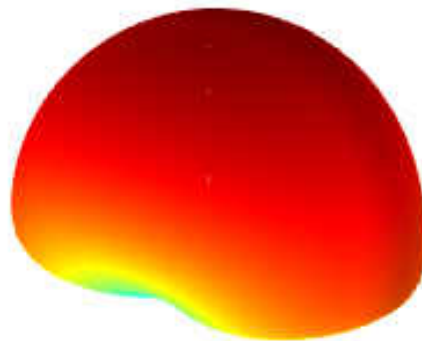


Figure 18. 3D radiation pattern of a directional antenna.

2.3.5 Directivity

The directivity is a measure that describes the directional transmitting properties of the antenna. It is defined as the ratio of the antenna radiation intensity in a specific direction in space over the radiation intensity of an isotropic source for the same radiated power [83].

2.3.6 Efficiency

The antenna efficiency accounts for all the losses in the antenna, prior to radiation. The losses may be due to mismatch at the input terminals, conduction losses, dielectric losses and aperture illumination losses [83].

2.3.7 Gain

The gain of the antenna is defined as the product of the directivity and the efficiency. It thus takes into account the directional and loss characteristics of the antenna [83].

The IEEE Test Procedure for antennas, Std-149 [85], defines the power gain of antenna in a specified direction as 4π times the ratio of the power radiated per unit solid angle (radiation intensity) in the direction to the net power accepted by the antenna from its generator. This is described mathematically by

$$G(\phi, \theta) = 4\pi\Phi(\phi, \theta)/P_o \quad (1)$$

where P_o is the power accepted by the antenna from its generator and $\Phi(\phi, \theta)$ is the radiation intensity (power radiated per solid angle).

2.3.8 Voltage Standing Wave Ratio (VSWR)

The Voltage Standing Wave Ratio (*VSWR*) is defined as the ratio of the maximum voltage to the minimum voltage in a standing wave pattern. A standing wave is

developed when power is reflected from a load. So the VSWR is a measure of how much power is delivered to a device as opposed to the amount of power that is reflected from the device. VSWR is also a measure of how closely the source and load impedance are matched. For most antennas in Wireless Local Area Network (WLAN), it is a measure of how close the antenna is to a perfect 50 Ohms [84].

2.3.9 Group Delay

Group delay is defined as the rate of change of transmission phase angle with respect to frequency. The units work out to time when the angle is in radians and frequency is in radians/time (seconds, nanosecond, picosecond or whatever is convenient, depending on the length of the path). When group delay is extracted from S-parameters, unless the network is a perfect measurement of a perfect transmission line, there will be variations over frequency. But within a small amount of bandwidth, group delay is usually nearly constant [86].

CHAPTER 3

HIGH FREQUENCY CHARACTERISATION OF NOVEL MATERIALS

3.1 Introduction

In a wide variety of industries there is a demand to better understand the materials in the design cycles, improve incoming inspection, process monitoring, and quality assurance. Every material has a unique set of electrical characteristics that are dependent on its dielectric properties. Accurate measurements of these properties can provide scientists and engineers with valuable information to properly incorporate the material into its intended application for more solid designs or to monitor a manufacturing process for improved quality control [87].

Dielectric materials measurement can provide critical design parameters information for many electronics applications. For example, the loss of a cable insulator, the impedance of a substrate, or the frequency of a dielectric resonator can be related to its dielectric properties. The information is also useful for improving ferrite, absorber and packaging designs. More recent applications in the area of aerospace, automotive, food and medical industries have also been found to benefit from knowledge of dielectric properties [87].

The application of additive manufacturing method for the fabrication of so-called 3D electromagnetics structures continues to soar. The advantage of state-of-the-art 3D printing offers smaller form factor, lighter weight, cost effective, time efficient and

environmentally friendly option in comparison with conventional manufacturing methods. Rapid expansion of the advanced wireless communication systems has encouraged the development of low profile antennas with reliable performance.

As the 3D printing for fabricating antennas and microwave components continues to expand, the broadband materials characterization are gaining importance. Materials from titanium to plastic and even sugars and proteins have been used in 3D printing [88]. To design and perform the simulations of the antenna using commercial simulation tools, dielectric constant and loss tangent or conductivity of the materials are needed.

3.2 Dielectric Constant or Permittivity Theory

A material is classified as “dielectric” if it has the ability to store energy when an external electric field is applied. The dielectric material increases the storage capacity of the capacitor by neutralizing charges at the electrodes, which ordinarily would contribute to the external field. The capacitance with the dielectric material is related to dielectric constant. If a DC voltage source “V” is placed across a parallel plate capacitor (Figure 19), more charge is stored when a dielectric material is between the plates than if no material (a vacuum) is between the plates [87].

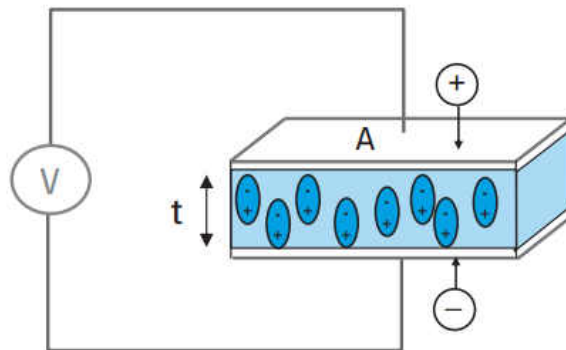


Figure 19. Parallel plate capacitor, DC case [87].

The capacitance with and without dielectric and dielectric constant are given by [87]:

$$C_0 = A/t \quad (2)$$

$$C = C_0 \varepsilon_r' \quad (3)$$

$$\varepsilon_r' = C/C_0 \quad (4)$$

where C and C_0 are capacitance with and without dielectric, ε_r' is the real dielectric constant or permittivity, and A and t are the area of the capacitor plates and the distance between them (Figure 19). The capacitance of the dielectric material is related to the dielectric constant as indicated in the above equations.

If an AC sinusoidal voltage source “V” is placed across the same capacitor (Figure 20), the resulting current will be made up of a charging current I_c and a loss current I_l that is again related to the dielectric constant. The losses in the material can be represented as a conductance (G) in parallel with a capacitor (C) as indicated in Figure 20. In this case, the permittivity consists of a real part (ε_r') and an imaginary part (ε_r''). The current is given by [87]

$$I = I_c + I_l = V(j\omega C_0 \varepsilon_r' + G) \quad (5)$$

where $G = \omega C_0 \varepsilon_r''$. Rewriting (5) in the form

$$I = I_c + I_l = V(j\omega C_0 \varepsilon_r' + \omega C_0 \varepsilon_r'') \quad (6)$$

shows that the complex permittivity can be calculated by

$$\varepsilon = \varepsilon_r' - j\varepsilon_r'' = I/V(j\omega C_0) \quad (7)$$

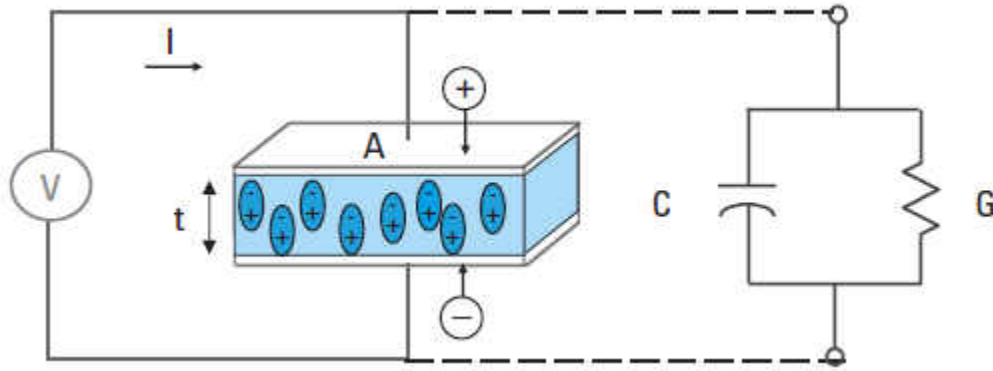


Figure 20. Parallel plate capacitor, AC case [87].

Dielectric constant is equivalent to relative permittivity (ϵ_r) or the absolute permittivity (ϵ) relative to the permittivity of free space (ϵ_0). The real part of permittivity (ϵ_r') is a measure of how much energy from an external electric field is stored in a material. The imaginary part of permittivity (ϵ_r'') is called the loss factor and is a measure of how dissipative or lossy a material is to an external electric field. The imaginary part of permittivity (ϵ_r'') is always greater than zero and is usually much smaller than (ϵ_r') [87]. The loss tangent ($\tan \delta$) is called dissipation factor and is given by [87]:

$$\tan \delta = \epsilon_r'' / \epsilon_r' \quad (8)$$


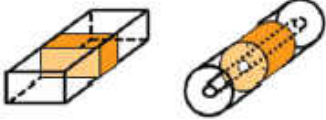
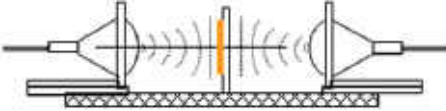
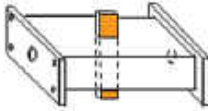
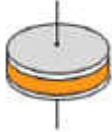
It should be noted that the loss factor includes the effects of both dielectric loss and conductivity [87].

3.3 Dielectric Measurement Methods

A measurement of the reflection from and/or transmission through a material along with knowledge of its physical dimensions provides the information to characterize the permittivity and permeability of the material [87]. In the past few years, a variety of techniques has been developed [87-90] to calculate the permittivity and permeability of

the materials. Many factors such as accuracy, convenience, and the material shape and form are important in selecting the most appropriate measurement technique. Some of the significant factors to consider includes frequency range, expected values of ϵ_r and μ_r , required measurement accuracy, material properties (i.e., homogeneous, isotropic), form of material (i.e., liquid, powder, solid, sheet), sample size restrictions, destructive or nondestructive, contacting or non-contacting, temperature, and cost [87]. Table 3 summarizes the specification of some of the measurement methods.

Table 3: Comparison between different measurement methods [87].

Method	Method image	Specification
Coaxial Probe		Broadband, convenient, non-destructive, best for lossy Material Under Test (MUT); liquids and semi-solids
Transmission line		Broadband, best for lossy to lowloss MUTs; machineable solids
Free space		Broadband; Non-contacting, best for flats sheets, powders, high temperatures
Resonant cavity		Single frequency; accurate, best for low loss MUTs; small samples
Parallel plate		Accurate, best for low frequencies; thin, flat sheets

3.4 Complex Permittivity Measurements

Taking into consideration the specification of the utilized materials for the fabrication of the proposed antennas using AM technology, the coaxial probe method was utilized to measure the complex permittivity of them. The open-ended coaxial probe is a cut-off section of transmission line. The material is measured by immersing the probe into a liquid or touching it to the flat face of a solid (or powder) material. The fields at the probe end “fringe” into the material and change as they come into contact with the MUT (Figure 21). The reflected signal [94] S_{11} can be measured and related to ϵ_r [87].

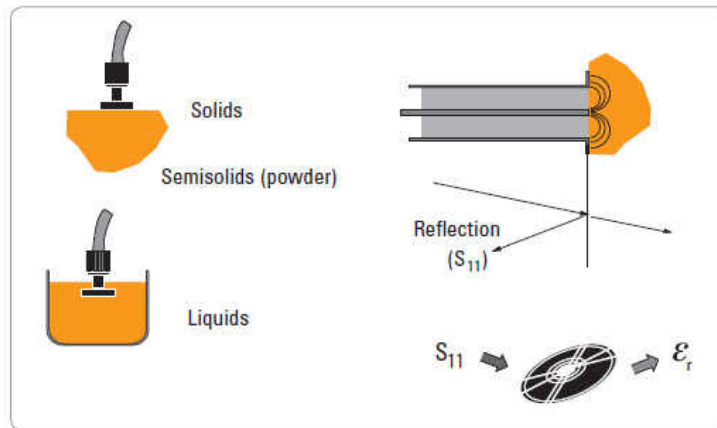


Figure 21. Coaxial probe method [87].

3.4.1 Probe Calibration

Before measurements, calibration at the tip of the probe must be performed. A three-term calibration corrects for the directivity, tracking, and source match errors that can be present in a reflection measurement. In order to solve for these three error terms, three well-known standards are measured. The difference between the predicted and actual values is used to remove the systematic (repeatable) errors from the measurement. The

three known standards are: i) air, ii) short circuit, and iii) distillate and de-ionized water [87].

3.4.2 Error Sources

Even after calibrating the probe, there are additional sources of error that can affect the accuracy of a measurement including cable stability, air gaps, and sample thickness [87]. It is important to allow enough time for the cable (that connects the probe to the network analyzer) to stabilize before making a measurement and to be sure that the cable is not flexed between calibration and measurement.

For solid materials, an air gap between the probe and sample can be a significant source of error unless the sample face is machined to be at least as flat as the probe face [87]. The sample must also be thick enough to appear “infinite” to the probe. A simple practical approach is to put a short behind the sample and check to see if it affects the measurement results [87].

3.4.3 Measurements

85070E Agilent performance probe was used to perform the complex permittivity measurements. At the first step, small cube shaped samples of the utilized materials with the dimensions of $2 \times 2 \times 1 \text{ cm}^3$ were fabricated using a desktop 3D printer. Figure 22 shows a photograph of the fabricated samples. Then fabricated samples were measured after three-term calibration of 85070E Agilent performance probe using E5071C network analyzer. Figure 23 shows the probe and a material under test.



Figure 22. Fabricated samples for permittivity measurements.



Figure 23. 85070E Agilent performance probe and a material under test.

Figure 24 illustrates the real and imaginary parts of the complex permittivity for the utilized materials in this thesis work. The loss tangent and conductivity (σ) can be calculated by [96]

$$\tan \delta = (\sigma + \omega \epsilon'') / \omega \epsilon' = \sigma_{\text{eff}} / \omega \epsilon' \quad (9)$$

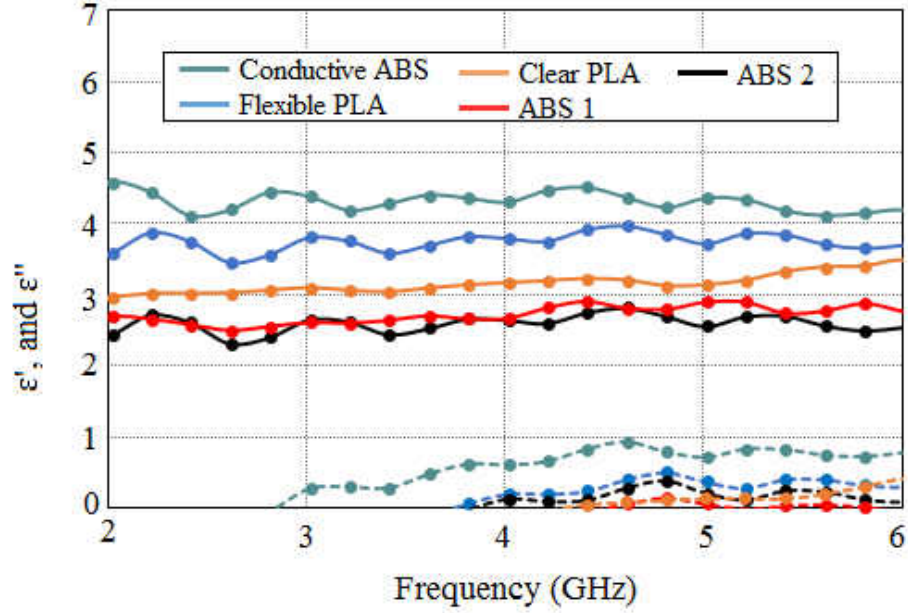


Figure 24. Measured real (solid) and imaginary (dashed) parts of the complex permittivity of the utilized materials.

Table 4 summaries the specifications of the utilized materials in terms of real and imaginary parts of complex permittivity, and loss tangent at the selected frequency of 5.8 GHz. It should be noted that the value of the loss tangent for the conductive ABS indicates that this material can be classified as a dielectric material, however, it offers much lower resistivity in comparison with the other utilized materials for fabrication of dielectric parts of the proposed antennas indicated in Table 4.

Table 4: Specification of materials.

Material	Specification at 5.8 GHz		
	ϵ'	ϵ''	$\tan \delta$
Conductive ABS	4.1133	0.7425	0.1805
Flexible PLA	3.6494	0.3199	0.0876
Clear PLA	3.3939	0.2889	0.0851
ABS 1	2.4990	0.1140	0.0456
ABS 2	2.8730	0.0090	0.0031

CHAPTER 4

DESIGN AND SIMULATION OF 3D ANTENNAS

4.1 Introduction

Antennas designed for use in wireless communications systems have taken on many forms and employed a variety of design techniques. Bowtie configuration has been widely used for the design of antennas for different applications [97-114]. In this thesis, at the first step a bowtie antenna with coplanar stripline feed structure is designed, simulated and optimized at the center frequency of 2.45 GHz. The optimized dimensions generate another operating frequency at around 6.67 GHz for the proposed antenna. In addition, the effect of structural parameters and radiator conductivity and configuration on the performance of the proposed antenna is studied.

In today's world of wireless communication systems, there is an increasing demand for electrically small Ultra WideBand (UWB) antennas and microwave components in support of UWB systems [115]. An assiduous examination of recent research literature reveals that UWB applications have aroused considerable interest of academic researchers and RF and microwave industry since the Federal Communications Commission (FCC) authorized the frequency band from 3.1 to 10.6 GHz for commercial use [119]. This is very significant as UWB communications technology offers the potential for very high data rate (>500 Mbit/s) transmission at low transmit power levels making it suitable for emerging short-range technologies [120]. In this thesis, to achieve

UWB performance, a novel bowtie antenna with 3D structure is proposed. The proposed 3D antenna achieves broad operating bandwidth from 1.72 to 15.12 GHz. Simulation results of the propose antennas for reflection coefficient, VSWR, gain, directivity, efficiency, and group delay are demonstrated. In addition dipole and patch antenna configurations have been designed at 2.45 GHz and 5.8 GHz, respectively, to be fabricated using different AM technologies.

4.2 Design of Bowtie Antenna at the Center Frequency of 2.45 GHz

Figures 25 and 26 show the proposed bowtie antenna and its top view accompanied by corresponding physical parameters, respectively. The physical dimensions are given in Table 5. The antenna is designed and optimized at the center frequency of 2.54 GHz frequency as can be seen from Figure 27.

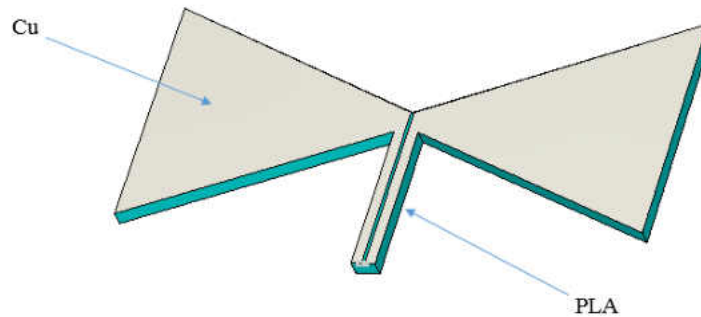


Figure 25. Configuration of the proposed antenna.

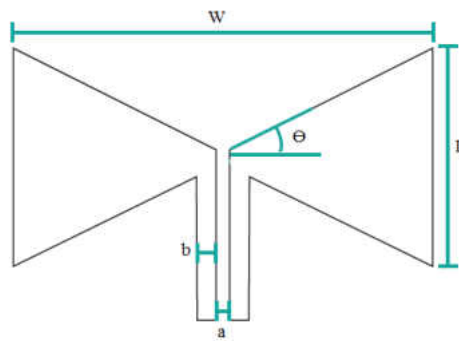


Figure 26. Top view of the proposed antenna with structural parameters.

Table 5: Physical dimension of the proposed bowtie antenna.

Parameter	Value
L	36 mm
W	72 mm
a	0.4 mm
b	1.4 mm
Θ	24 (degree)

It can also be observed that the proposed antenna supports another resonance frequency at 6.67 GHz with the optimized dimensions given in Table 5. The designed antenna provides reflection coefficient of around -20 dB at the operating frequency of 2.45 GHz. It should be noted that in this design the substrate and conductive parts of the antenna are considered as PLA and copper (Cu), respectively, for performing simulations.

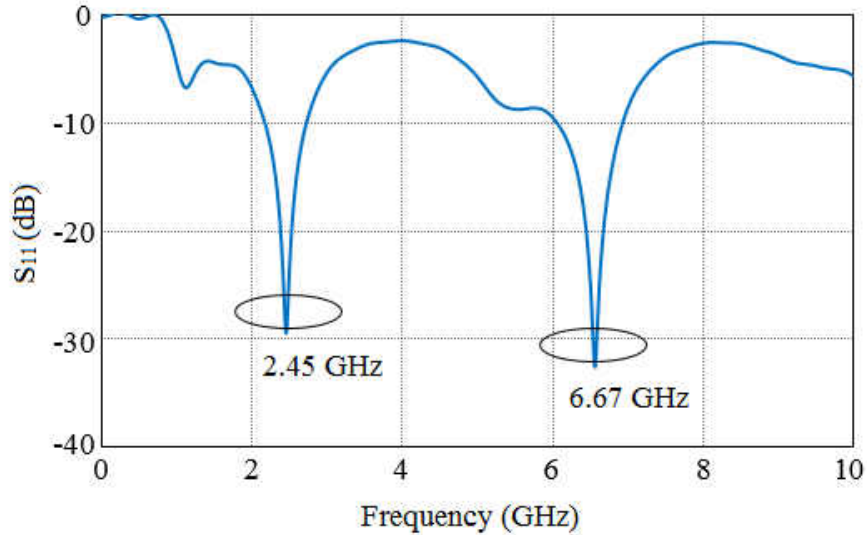


Figure 27. Reflection coefficient of the proposed antenna.

4.2.1 Parametric Study of the Proposed Bowtie Antenna

The effects of the individual structural parameters on the performance of the antenna have been studied and demonstrated. Figure 28 depicts the effect of thickness of the substrate (h) on the reflection coefficient of the proposed antenna. As can be observed

by increasing h , first the operating frequencies decrease, and then it remains almost constant.

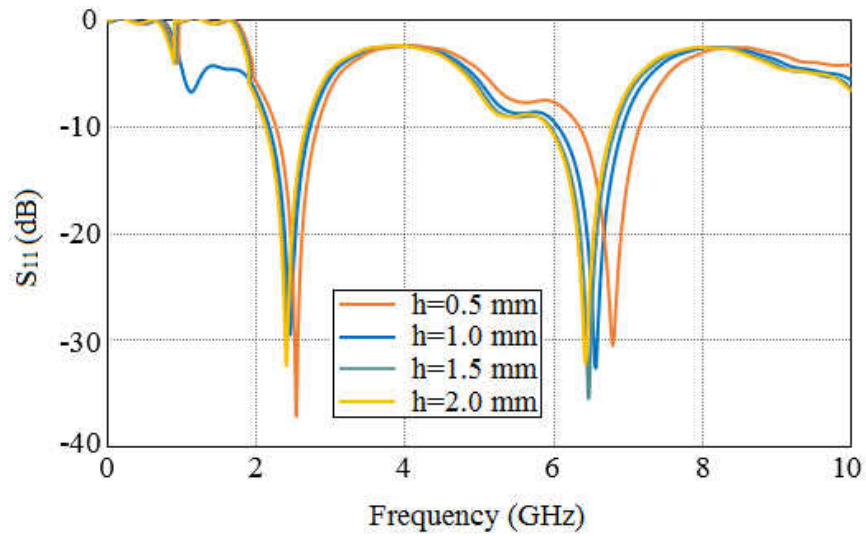


Figure 28. Reflection coefficient for varying h .

As can be seen from Figure 29, by increasing dielectric constant, the operating frequencies decrease, especially for the second resonance frequency of the designed antenna.

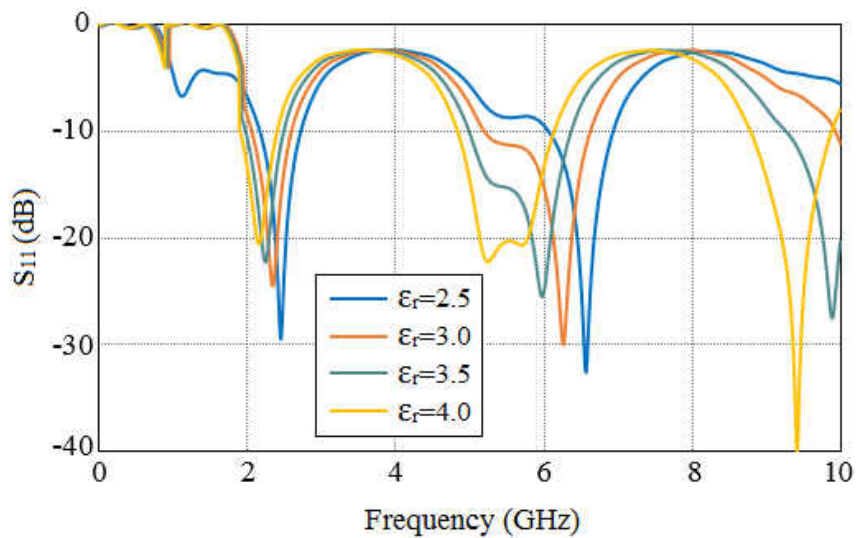


Figure 29. Reflection coefficient for varying dielectric constant.

Figures 30-33 show the effects of gap and width of feed lines, and width and length of bowtie on the reflection coefficient of the antenna, respectively.

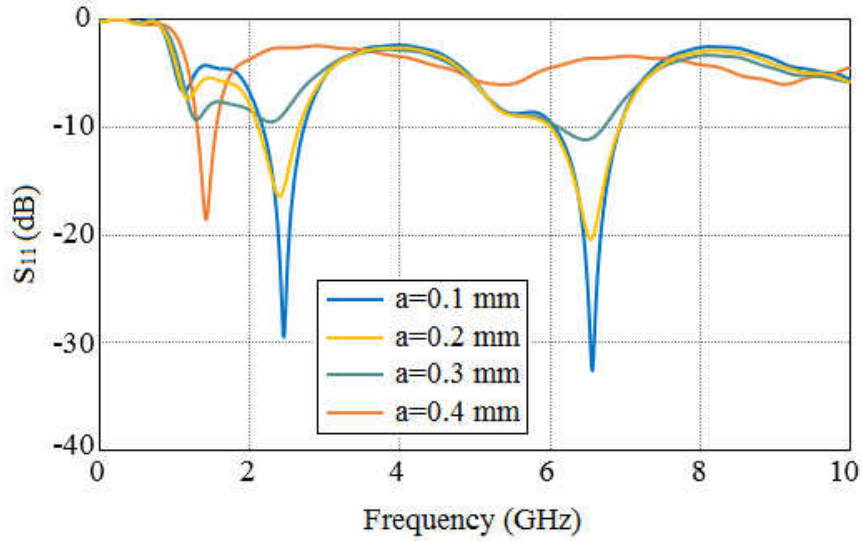


Figure 30. Reflection coefficient for varying feed lines gap a .

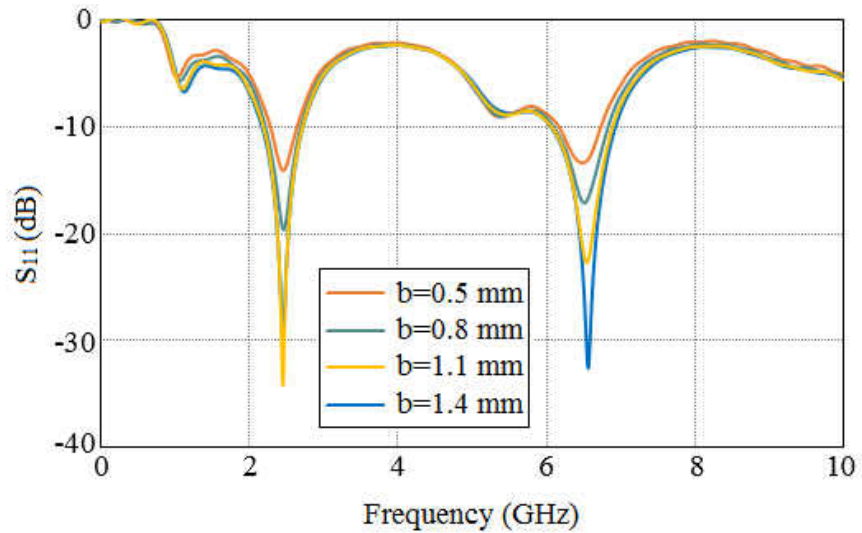


Figure 31. Reflection coefficient for varying feed lines width b .

As can be clearly observed from Figures 30 and 31, changing the gap between feed lines and the width of them has considerable effects on the reflection coefficient level at operating frequencies. The major reason for this behavior is that by changing the

width of feed lines and spacing between them the line impedance will change and this can decrease the impedance matching and affect the reflection coefficient consequently.

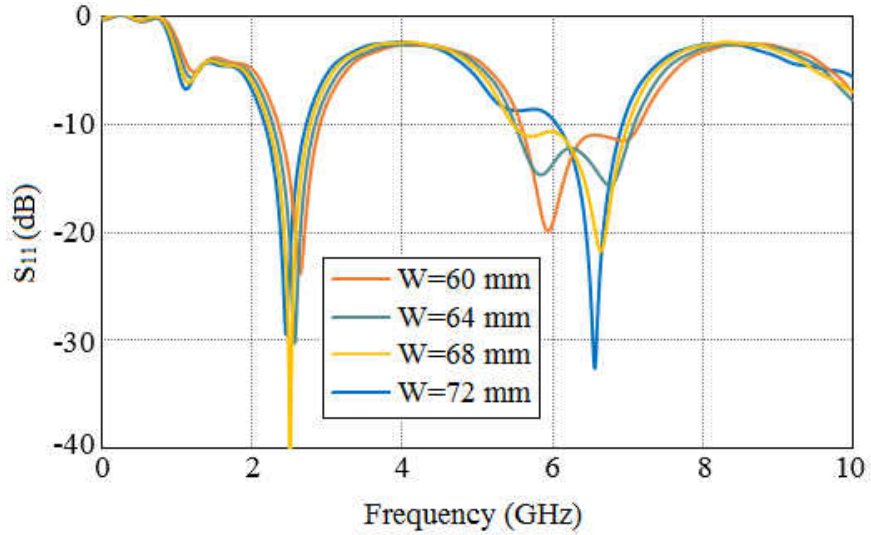


Figure 32. Reflection coefficient for varying bowtie width W .

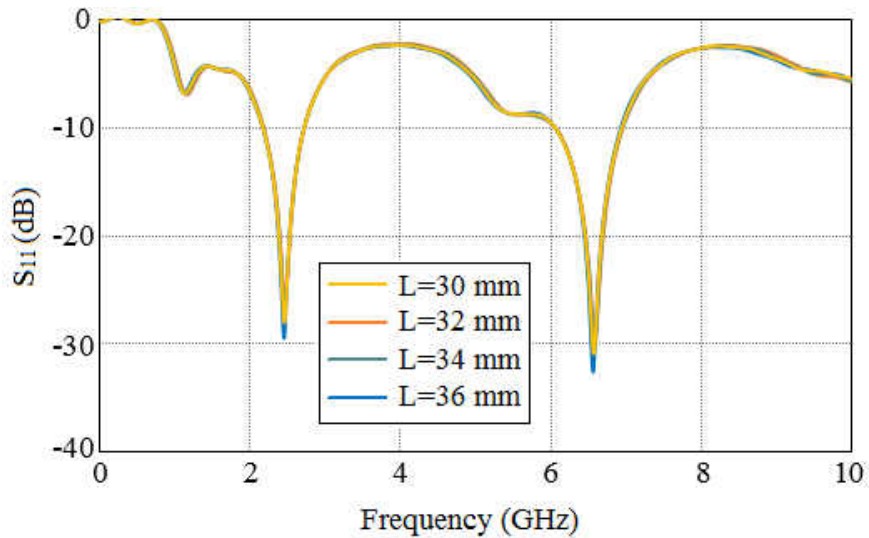


Figure 33. Reflection coefficient for varying bowtie length L .

As Figure 32 demonstrates varying the width of bowtie not only changes the level of reflection coefficient but it also changes the bandwidth of the second operating frequency band of the antenna considerably. From Figure 33, it can be observed that

increasing the length of bowtie from 28 to 34 mm, does not cause any considerable effects on the reflection coefficient of the antenna.

4.2.2 Far-field Study of the Proposed Antenna

The radiation characteristic of the proposed antenna has been simulated by a commercial simulation software CST Microwave Studio [121]. The simulations were performed at the center frequency of 2.45 GHz. Figure 34 shows the radiation pattern of the antenna on the E-plane and H-plane. As can be seen the antenna has donut shape radiation pattern, being directive on E-plane, and omnidirectional on the H-plane. In addition, the antenna shows very low cross-polarization (x-pol). Figure 35 demonstrates the surface current distribution of the antenna at 2.45 GHz.

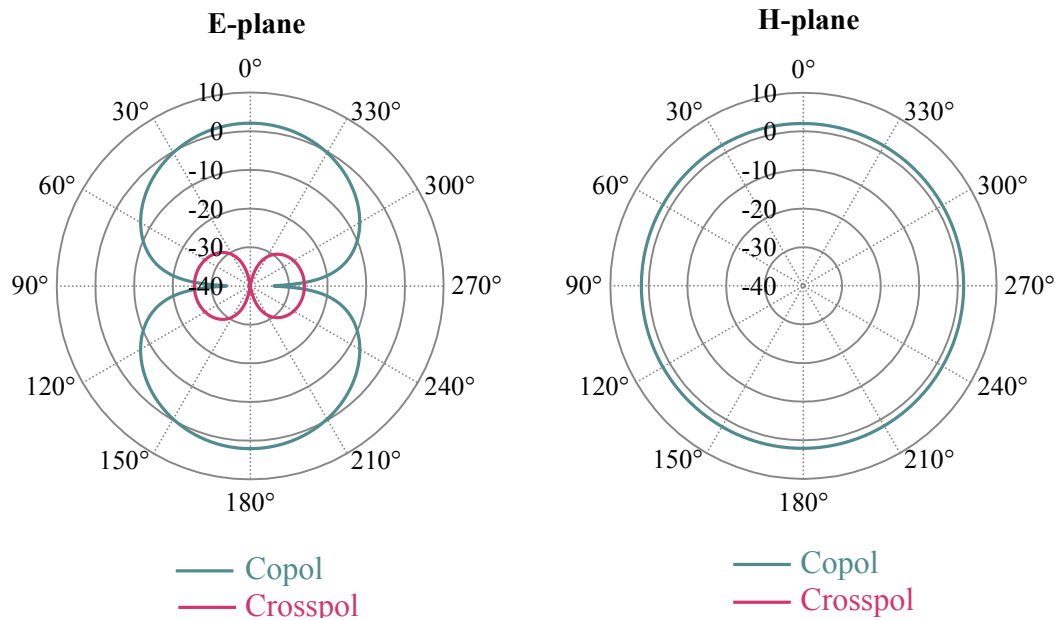


Figure 34. Simulated radiation pattern of the proposed bowtie antenna.

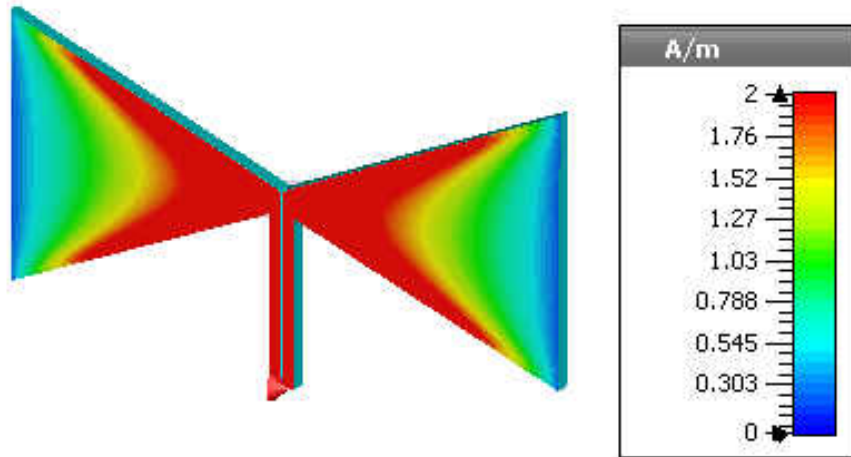


Figure 35. Simulated surface current of the designed bowtie antenna at 2.45 GHz.

4.2.3 Effects of Conductivity on the Performance

In this section the effects of the conductivity of the radiator part of the antenna on its performance is investigated. This can be useful since most of the available materials for 3D printing are made of lossy materials with low conductivity.

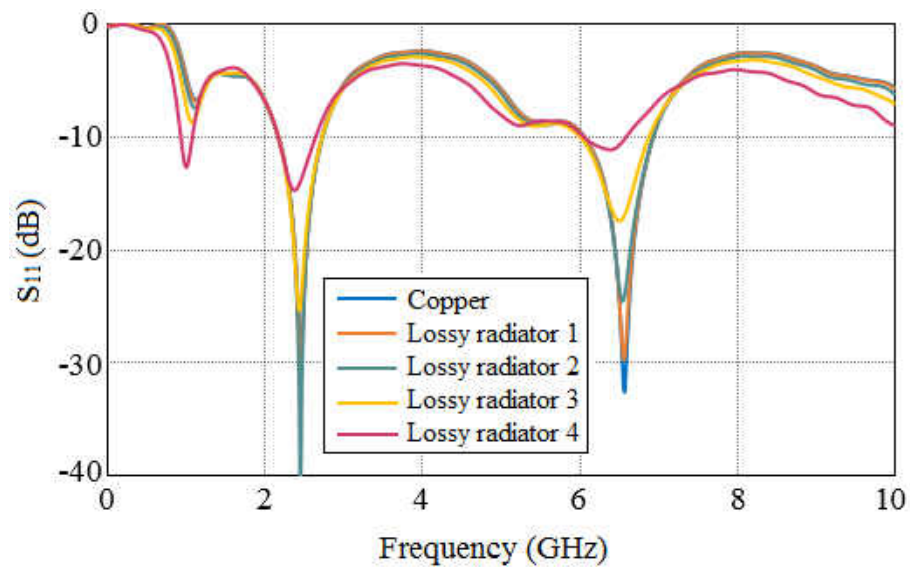


Figure 36. Effect of radiator conductivity on the reflection coefficient.

Figure 36 compares the reflection coefficient of the proposed antenna under five different conditions: i) radiator made from copper with conductivity of σ_{cu} , ii) radiator made of a material with conductivity of $0.1\sigma_{cu}$, iii) radiator made of a material with conductivity of $0.01\sigma_{cu}$, iv) radiator made of a material with conductivity of $0.001\sigma_{cu}$, and v) radiator made of a material with conductivity of $0.0001\sigma_{cu}$.

It should be noted the other antenna parameters remain the same. Table 6 also compares these five designs in terms of conductivity, directivity, and gain. In all cases radiation patterns on E- and H-plane are same.

Table 6: Effect of radiator conductivity on the directivity and gain.

Radiator	Conductivity	Directivity (dBi)	Realized Gain (dBi)
Copper	σ_{cu}^*	2.650	2.099
Lossy radiator 1	$0.1\sigma_{cu}$	2.649	2.056
Lossy radiator 2	$0.01\sigma_{cu}$	2.643	1.925
Lossy radiator 3	$0.001\sigma_{cu}$	2.633	1.540
Lossy radiator 4	$0.0001\sigma_{cu}$	2.629	0.596

Note: $\sigma_{cu}=5.9 \times 10^7$ s/m

As can be seen from Table 6, by varying conductivity, directivity remains almost constant, however the gain changes considerably. The major reason for this behavior is that by decreasing the conductivity, the ohmic resistance of the radiator will change, as predicted and this changes the efficiency, and consequently, the gain of antenna.

Table 7 gives a comparison between the surface currents for the above mentioned five conditions. As can be seen, by decreasing the conductivity, the surface current decreases as predicted.

Table 7: Effect of radiator conductivity on the surface current.

Radiator	Maximum surface current (A/m)
Copper	47.88
Lossy radiator 1	47.77
Lossy radiator 2	47.43
Lossy radiator 3	46.47
Lossy radiator 4	43.83

Figure 37 also illustrates the surface current distribution for the above-mentioned conditions. According to this figure they all have same current distribution at 2.45 GHz.

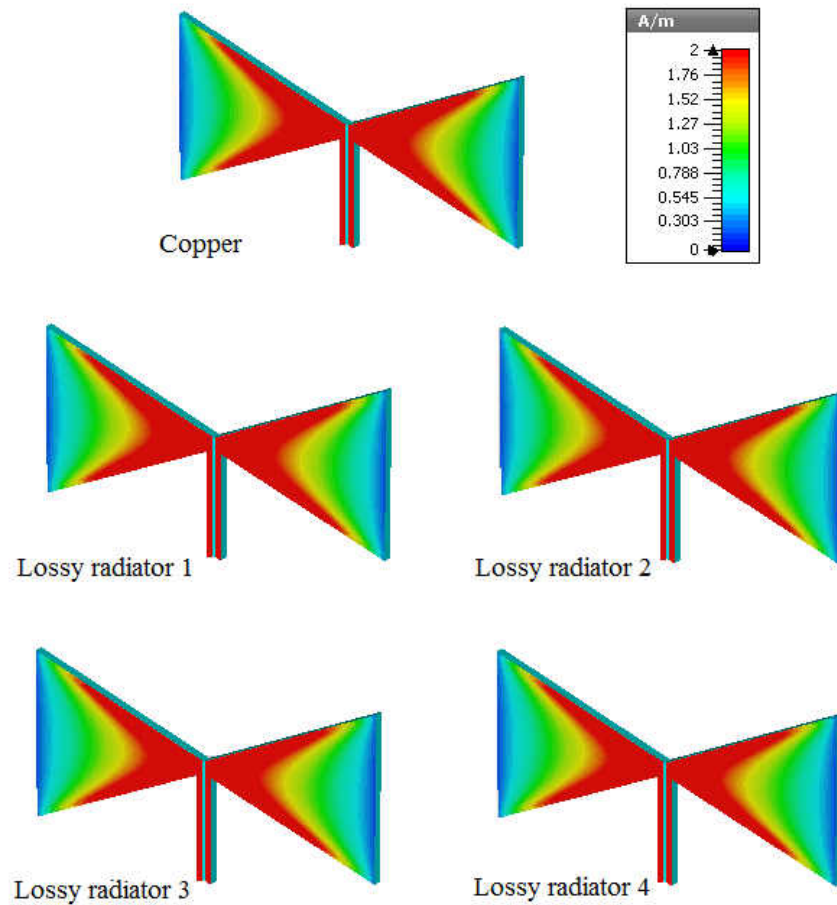


Figure 37. Surface current distribution for copper radiator and four lossy radiators with different conductivities in respect to copper at 2.45 GHz.

4.2.4 Effects of the Radiator Shape on the Performance of Bowtie Antenna

Since using AM technology makes it possible to create desired shapes for the substrate and radiator parts of the antenna, in this section the effects of the shape of radiator on the performance of the antenna is investigated. Figure 38 shows the proposed antenna with a staircase radiator shape configuration. The bowtie length and width are 30 mm and 56 mm, respectively. The other parameters (indicated in Table 5) are same as the flat surface bowtie antenna. The characteristics of flexible PLA have been considered for substrate part.

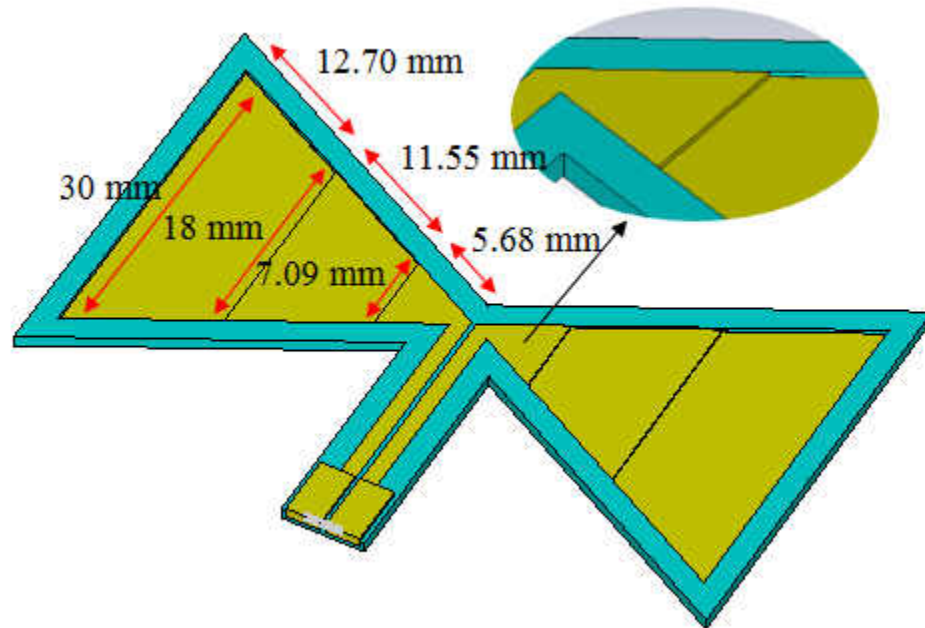


Figure 38. Proposed antenna with staircase shaped radiator.

Figures 39 and 40 show the current distribution for the antenna, and a close-up view of one of the radiator's edges, respectively. It should be noted that, a same antenna with flat radiator was simulated to see how radiator configuration can affect the current distribution. The simulated maximum current for this design was 89.28 A/m at 1.64 GHz,

however, for the planar design this value was 64.56 A/m. It should also be noted that a lossy radiator with conductivity of 59400 s/m for conductive parts of planar and 3D radiator antennas was utilized to perform simulations.

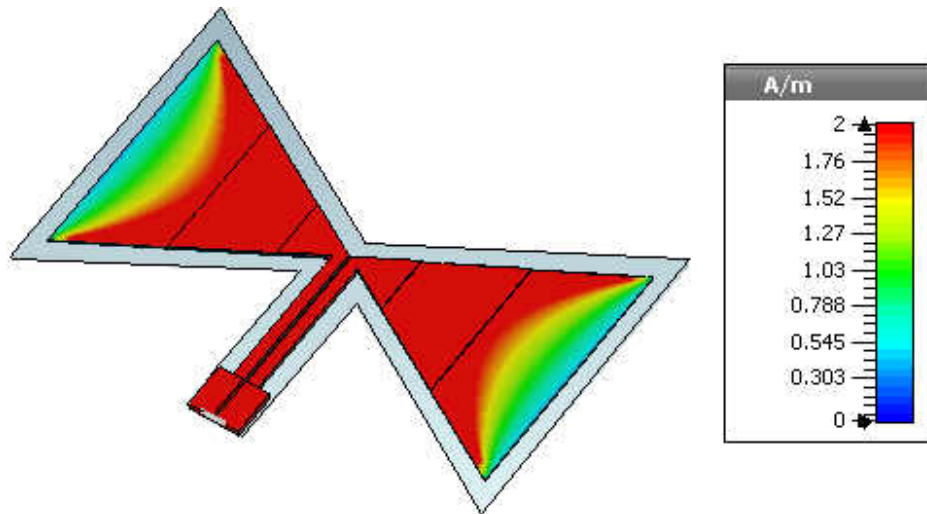


Figure 39. Surface current distribution of the proposed antenna with staircase radiator at 1.64 GHz.

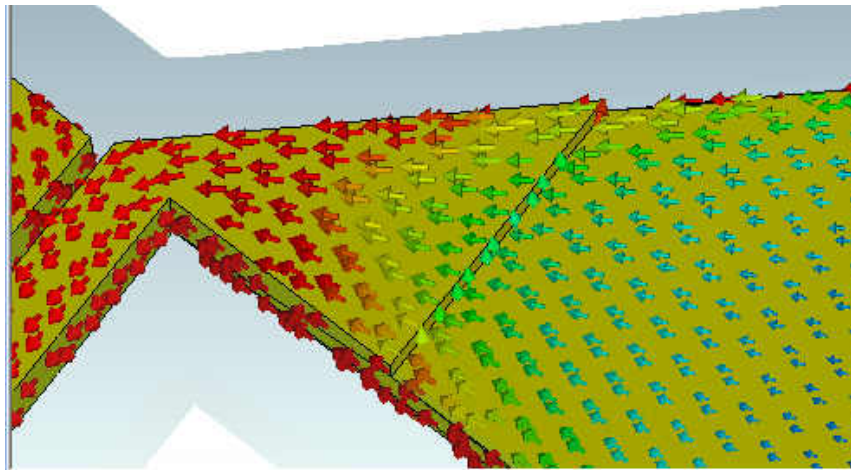


Figure 40. Surface current distribution of the proposed antenna at the radiator edges.

Figure 41 compares the simulated reflection coefficient of the bowtie antenna with planar and staircase radiator configurations. The designed antennas offer same

resonance frequency at around 1.64 GHz, however, at around 6.6 GHz, the antenna with staircase radiator shape shows better performance in terms of reflection coefficient.

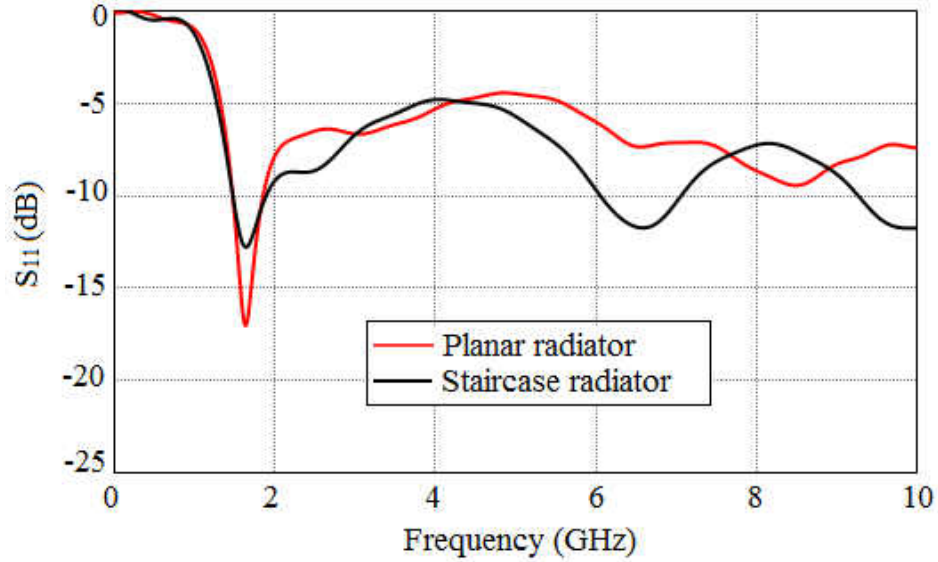


Figure 41. Simulated reflection coefficient of the staircase and planar radiator bowtie antenna.

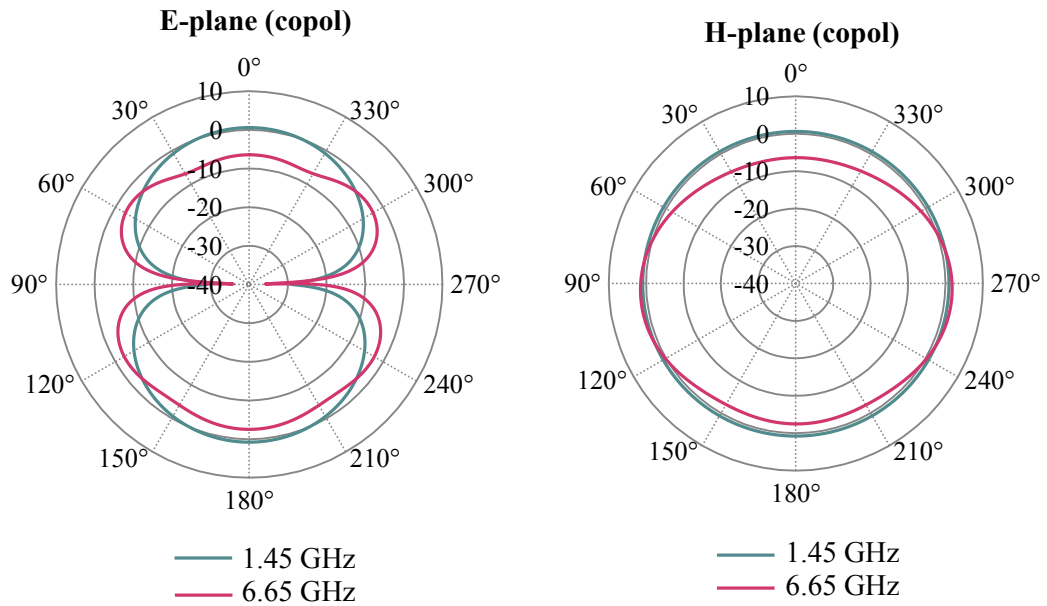


Figure 42. Simulated E- and H- plane of the proposed bowtie antenna with staircase radiator configuration.

The gain of the antenna with staircase radiator was around 0.93 dBi. This value was 1.24 dBi for planar one with exactly same dimensions. The radiation pattern of the staircase radiator antenna for E and H planes are illustrated in Figure 42.

4.3 Design of 3D Bowtie Antenna for UWB Applications

A new 3D broad band bowtie antenna is proposed in this section. Figure 43 shows the structure of the antenna with its optimized dimensions.

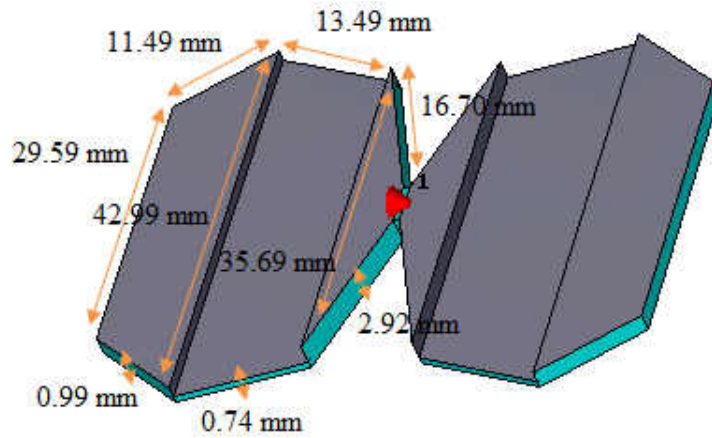


Figure 43. Configuration of the proposed 3D UWB bowtie antenna.

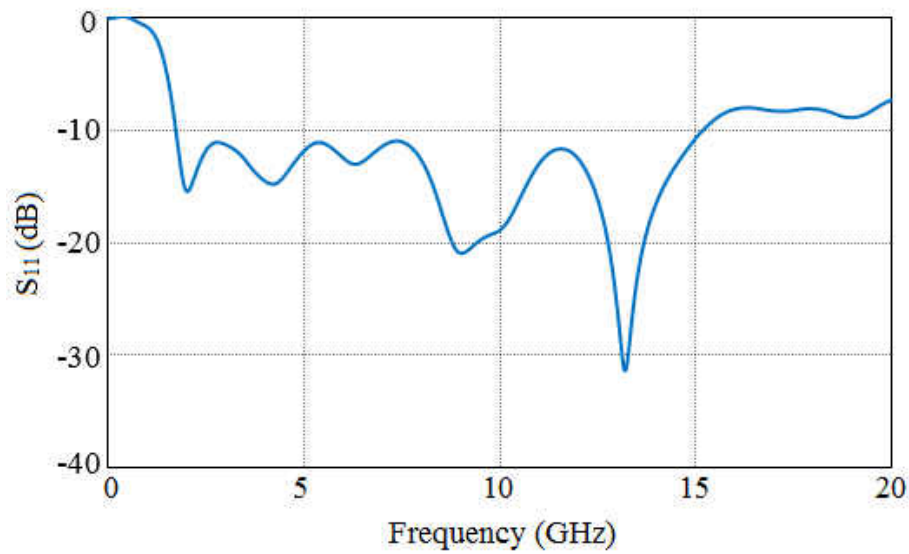


Figure 44. Reflection coefficient of the proposed 3D broad band antenna.

The characteristics of ABS and copper were considered in the simulations for the substrate and conductive parts of proposed UWB antenna, respectively. The difference between this design and the proposed one in section 4.2.4 is that the substrate of the proposed UWB bowtie antenna has 3D configuration.

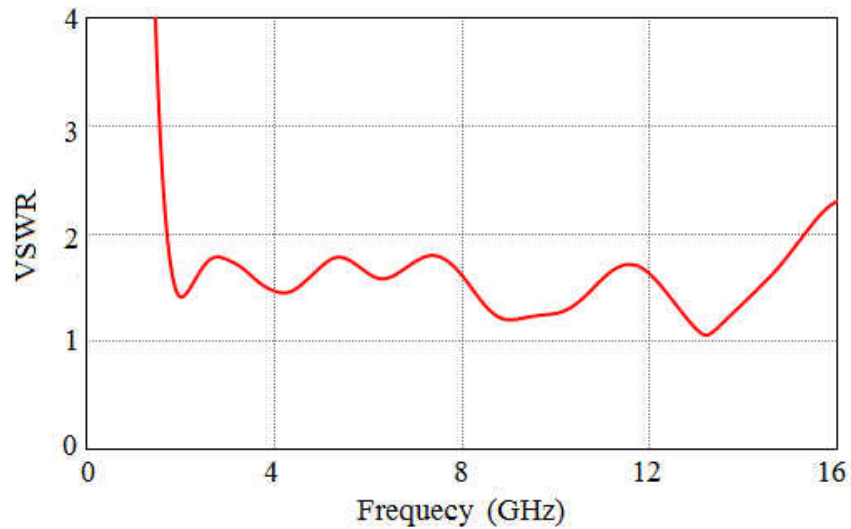


Figure 45. VSWR of the proposed UWB antenna.

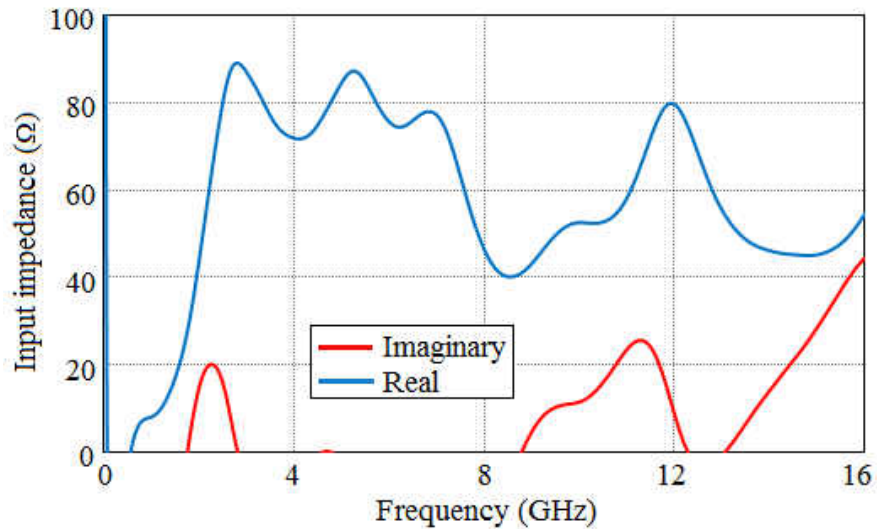


Figure 46. Input impedance of the proposed UWB antenna.

The simulated reflection coefficient of the antenna is depicted in Figure 44. As can be seen, the antenna offers UWB performance with 10-dB bandwidth of 13.4 GHz from 1.72 GHz to 15.12 GHz. Figure 45 shows the VSWR of the proposed antenna which is less than 2 for the operating frequency band.

Figure 46 shows the real and imaginary parts of the input impedance of the antenna. As can be seen the imaginary part is close to zero. It can also be observed that the input resistance is a little high, but in this situation the distance between the resonance frequencies of the antenna is small which make the design of UWB antenna a possible task.

The other important factor in the design of UWB component is the group delay which is depicted in Figure 47 for the proposed UWB 3D antenna. As can be seen, the proposed antenna offers relatively flat group delay with maximum variation less than 0.49 ns, except at around 2 GHz and 13 GHz.

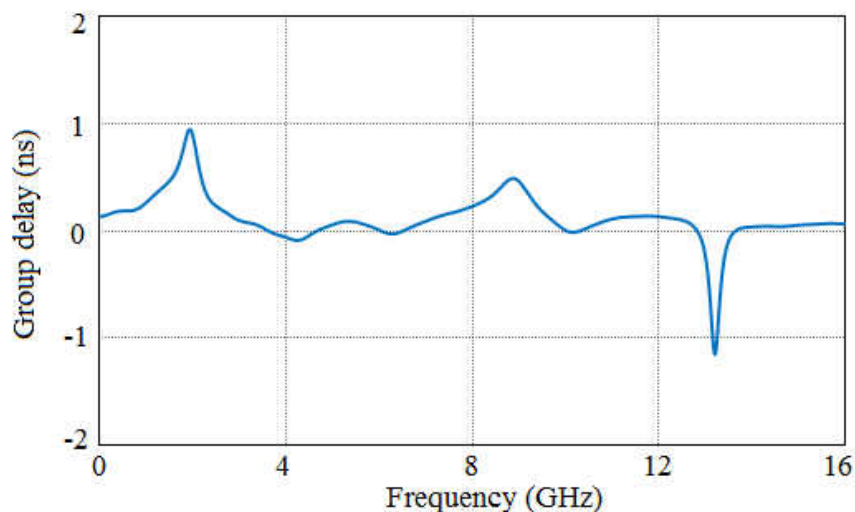


Figure 47. Group delay of the UWB antenna.

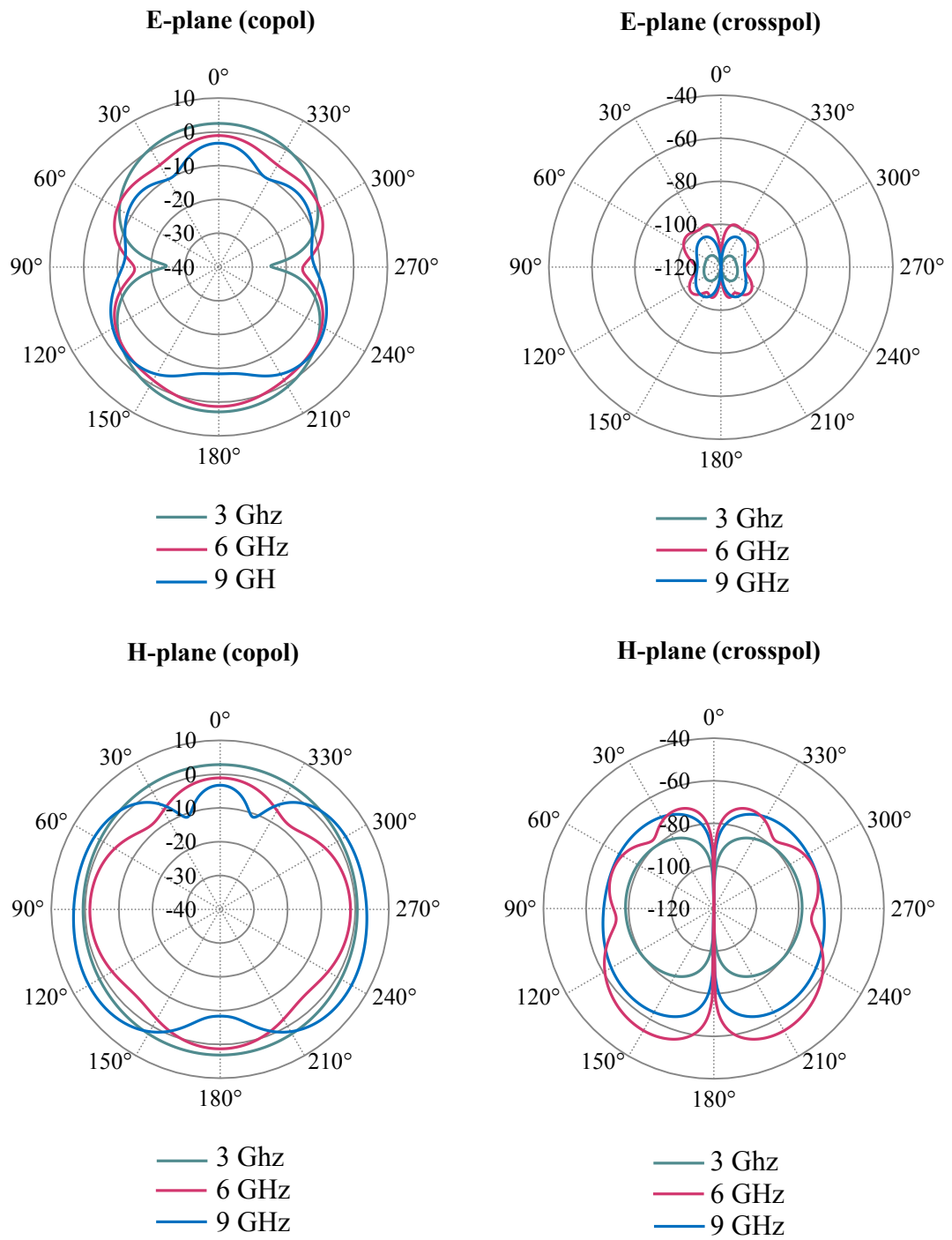


Figure 48. Radiation patterns of the UWB antenna at 3 GHz, 6 GHz, and 9 GHz.

The radiation patterns of the proposed antenna is given in Figure 48, at 3.6 GHz and 9 GHz. As can be observed, the antenna has similar radiation patterns in comparison

with bowtie antennas designed in previous sections. Figure 49 shows the current distribution for the proposed antenna at 3 GHz, 6 GHz, and 9 GHz.

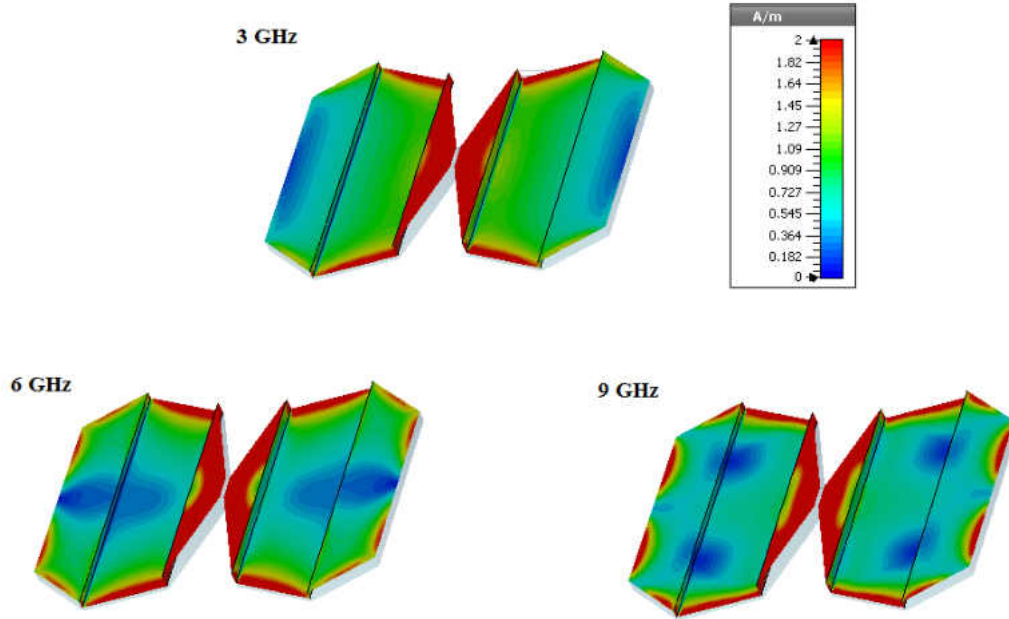


Figure 49. Current distribution of the UWB antenna at 3 GHz, 6 GHz, and 9 GHz.

Figure 50 depicts the efficiency of the proposed UWB antenna. As can be observed, it features more than 80% efficiency for the supported 10-dB UWB bandwidth.

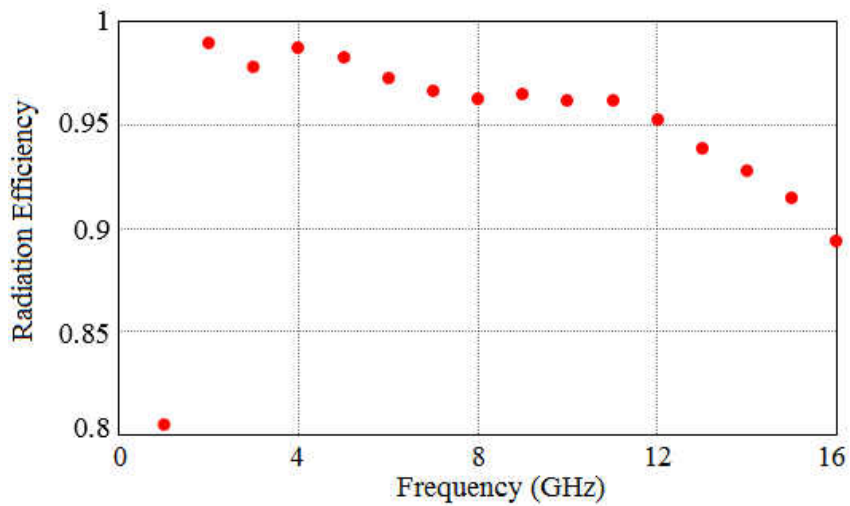


Figure 50. Efficiency of the proposed UWB antenna.

Table 8. Realized and IEEE gains of the antenna at different frequencies.

Gain \ Frequency	3 GHz	6 GHz	9 GHz
Realized Gain (dBi)	2.80	2.416	3.875
IEEE Gain (dBi)	3.138	2.673	3.910

Table 8 summarizes the realized and IEEE gains of the proposed UWB antenna. In comparison with the amount of gain in Table 6, it can be concluded that the antenna designed for UWB applications offers higher gain.

4.3.1 Comparison of the UWB Bowtie Antennas

To compare the antenna with its planar version in terms of performance, a planar antenna with exactly same dimensions with the proposed UWB 3D antenna was simulated. It was observed that the proposed 3D antenna offers higher gain in comparison with the planar one.

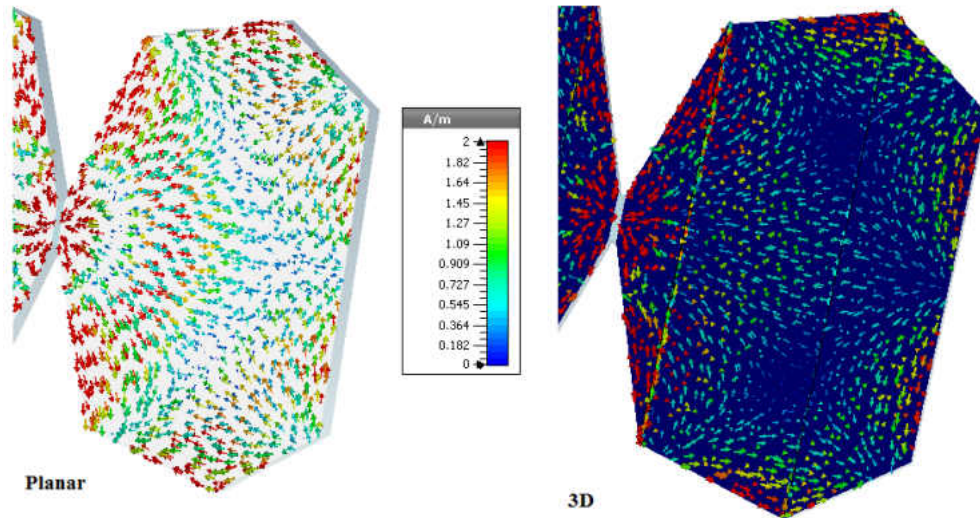


Figure 51. Surface current distribution for the UWB planar and 3D antennas.

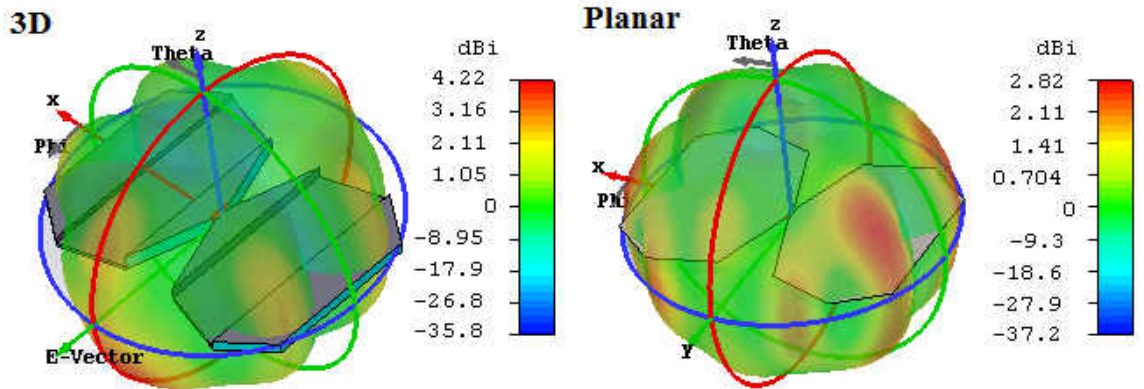


Figure 52. Radiation pattern for the planar and 3D antennas at 9 GHz.

Table 9: Comparison of planar and 3D antennas at 9 GHz.

Antenna	Maximum surface current (A/m)	10-dB Bandwidth (GHz)	Directivity (dBi)	Gain (dBi)
Planar design	93.94	1.72 to 10.62	2.815	2.251
3D design	58.51	1.72 to 15.12	4.219	3.875

Figure 51 compares the surface current distribution for the 3D and planar antennas. As can be seen, the proposed UWB antenna has more uniform current distribution which can contribute to the gain enhancement of the proposed 3D antenna.

The far-field radiation patterns of the UWB antennas are depicted in Figure 52. Table 9 summarizes the specification of the 3D and planar visions in terms of directivity, surface current, gain, and 10-dB bandwidth. As can be observed from the results, the 3D proposed antenna not only offers higher directivity and gain but it also offers larger bandwidth.

4.3.2 Optimizing Proposed Antenna for UWB Spectrum (3.1 to 10.6 GHz)

As indicated in Table 9, the proposed 3D antenna has broad 10-dB bandwidth from 1.72 to 15.12 GHz. In this section the proposed 3D antenna is optimized for operating across UWB spectrum from 3.1 GHz to 10.6 GHz. Figures 53 and 54 depict the configuration and simulated reflection coefficient of the antenna, respectively. The 10-dB bandwidth of the optimize antenna is from 2.78 GHz to 10.62 GHz.

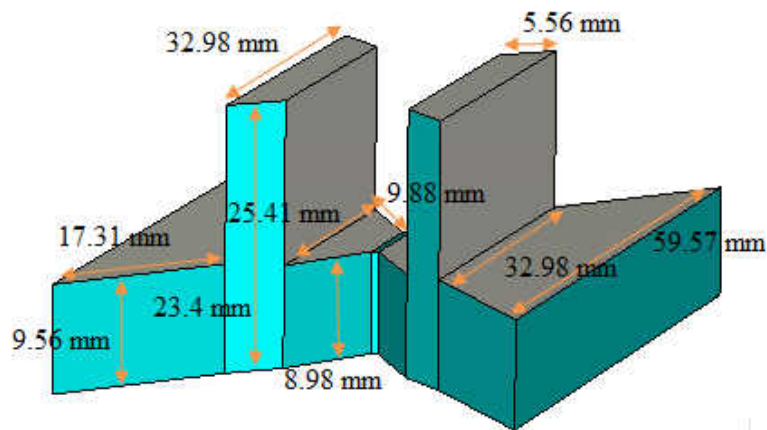


Figure 53. Configuration of the proposed antenna for UWB spectrum with optimized dimensions.

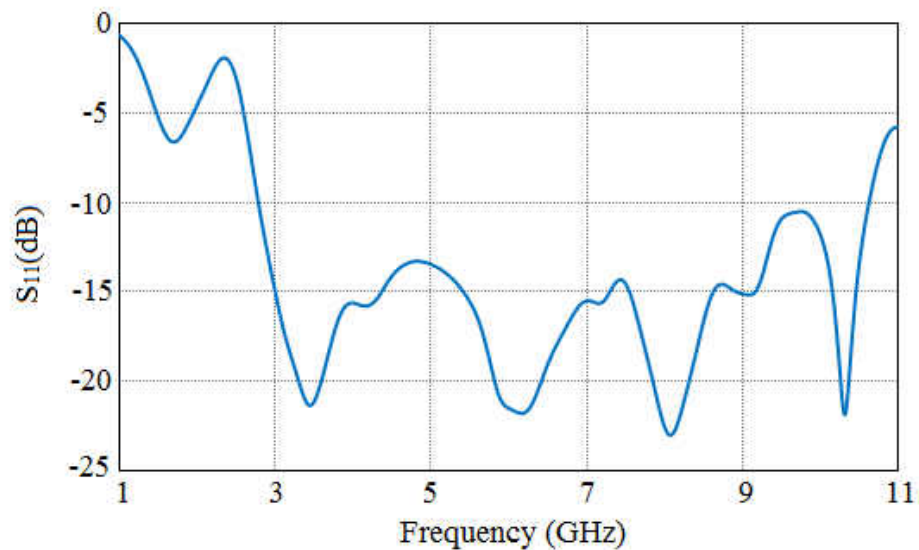


Figure 54. Reflection coefficient of the antenna.

The simulated radiation patterns of the antenna at 3 GHz, 6 GHz, and 9 GHz are illustrated in Figure 55.

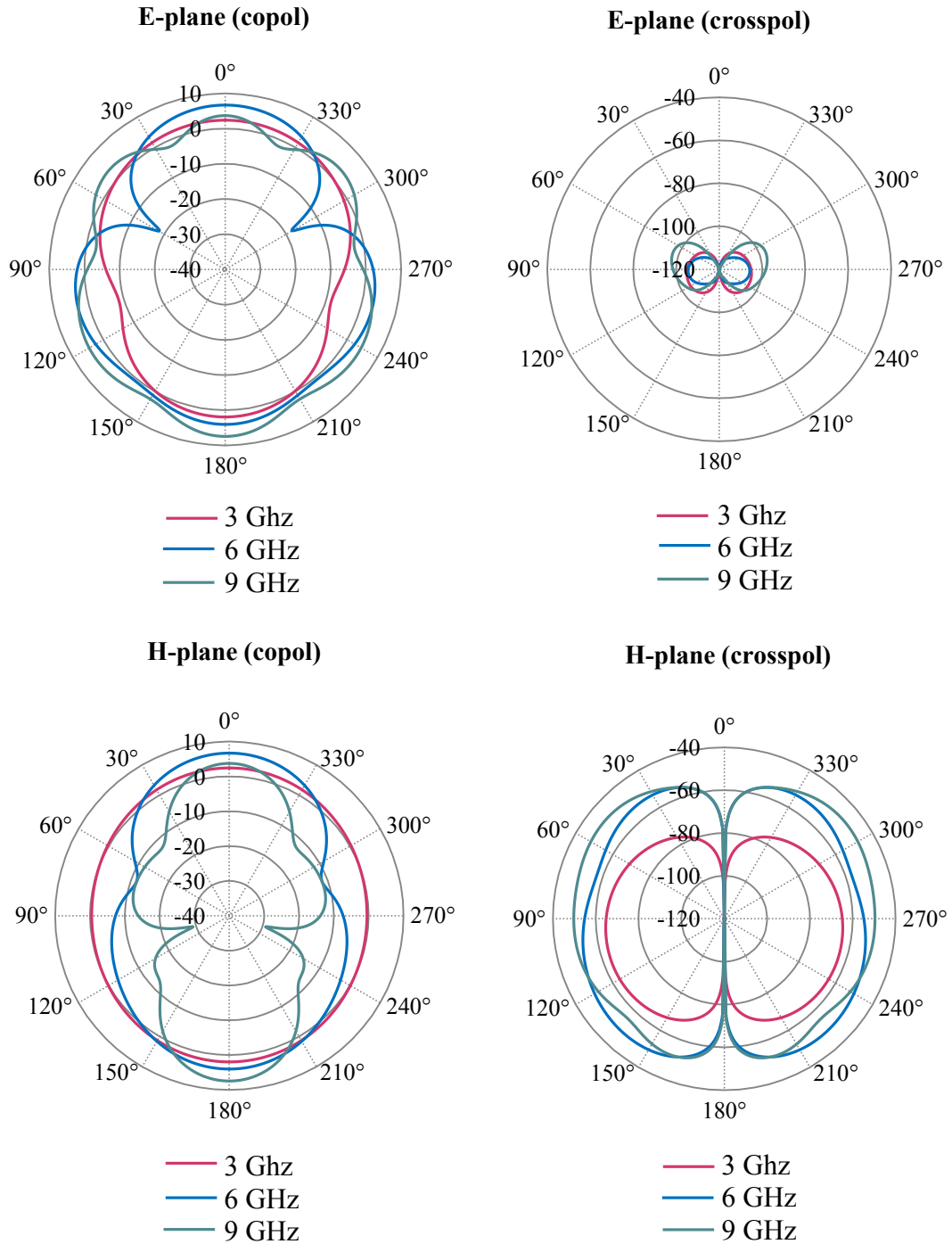


Figure 55. Radiation patterns of the UWB antenna.

Table 10 summarizes the realized and IEEE gains of the UWB antenna. In comparison with the amount of gain in Table 8, it can be concluded that the antenna optimized for UWB spectrum offers larger gain in higher frequencies in comparison with the UWB antenna presented in 4.3.

Table 10: Realized and IEEE gains of the antenna at different frequencies.

Gain \ Frequency	3 GHz	6 GHz	9 GHz
Realized Gain (dBi)	2.29	6.681	7.284
IEEE Gain (dBi)	2.423	6.711	7.419

Figures 56 and 57 show the input impedance and group delay of the antenna, respectively. In this design, a good separation between resonance frequencies has been achieved with relatively low input impedance so that a UWB band has been created.

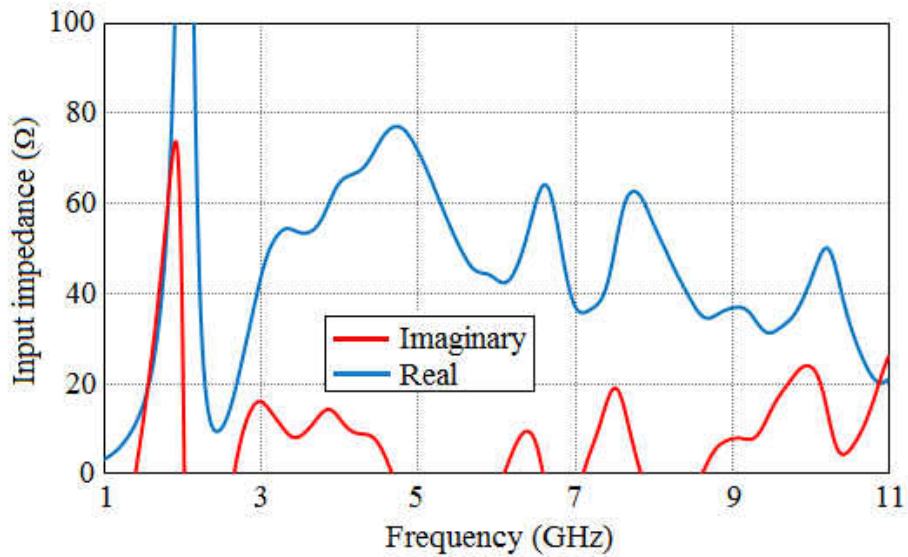


Figure 56. Input impedance of the UWB antenna.

In addition, the proposed UWB antenna offers a flat group delay with maximum variation less than 1.13 ns over the UWB spectrum as can be seen from Figure 57.

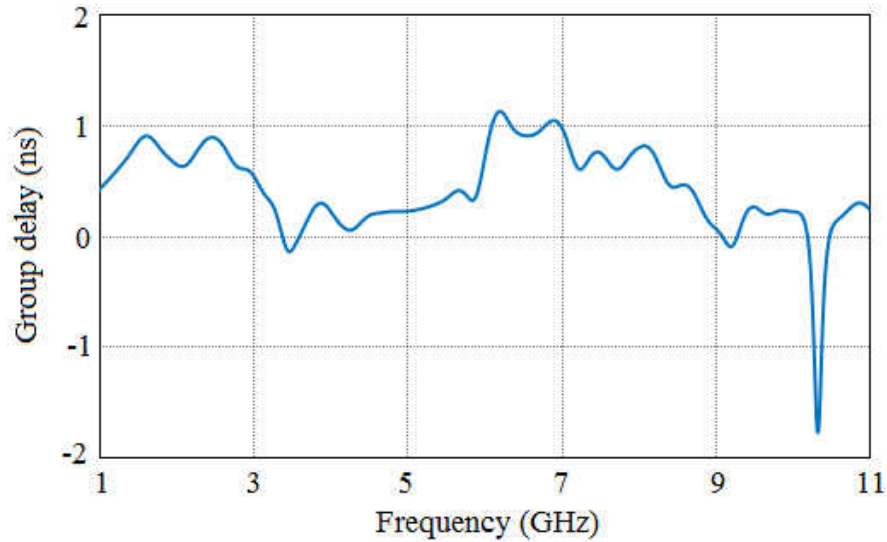


Figure 57. Group delay of the UWB antenna.

4.4 Design of Embedded 3D Dipole Antenna

To study the feasibility of embedding radiator inside 3D printed substrate structure, a dipole antenna with such configuration has been designed and simulated. Figures 58 and 59 show the configuration of the designed dipole antenna without and with radiator parts, respectively. In the simulation software the dielectric characteristic of the PLA has been considered for the substrate part of the proposed antenna.

For conductor part copper has been utilized. The antenna design was optimized for operating at 3 GHz. Figure 60 shows the simulated reflection coefficient of the proposed antenna. As can be seen the proposed antenna offers reflection coefficient better than -20 dB at 3 GHz.

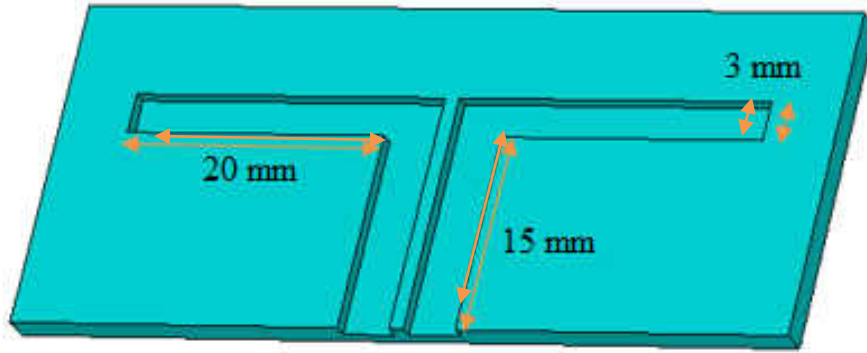


Figure 58. Proposed substrate for dipole antenna.

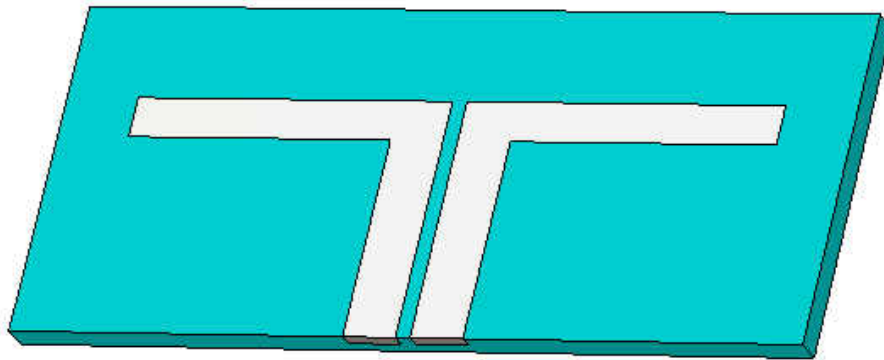


Figure 59. Proposed dipole antenna.

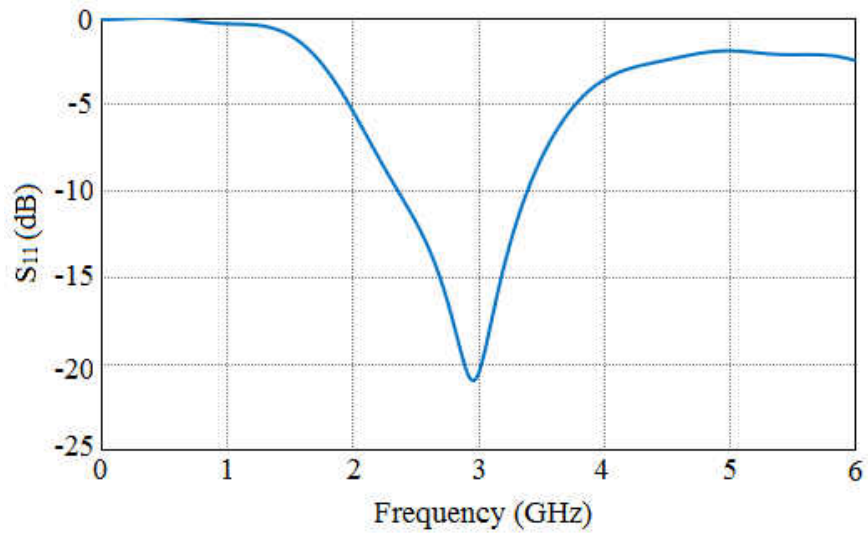


Figure 60. Reflection coefficient of the proposed dipole antenna.

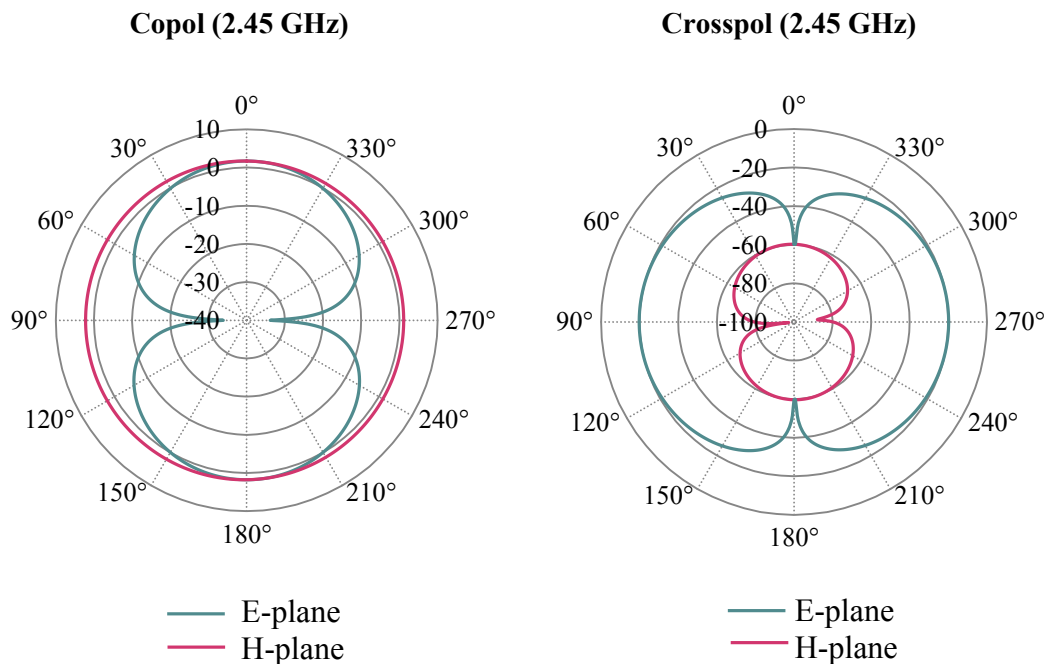


Figure 61. Radiation patterns of the designed antenna on E- and H-plane.

Figure 61 depicts the radiation pattern of the proposed antenna at 3 GHz for both E- and H- planes. It is clear that the antennas has omnidirectional radiation pattern with donut shape radiation in E-plane. It can also be seen that the proposed dipole antenna has more crosspol in E-plane.

The proposed dipole antenna has 2.396 dBi gain at 3 GHz. To improve the performance of the antenna in terms of directivity and gain, a Yagi-Uda configuration was proposed. Figure 62 shows the configuration of the designed Yagi-Uda antenna. It should be noted that this design has larger size in comparison with the proposed dipole antenna, however, it offers higher directivity and gain.

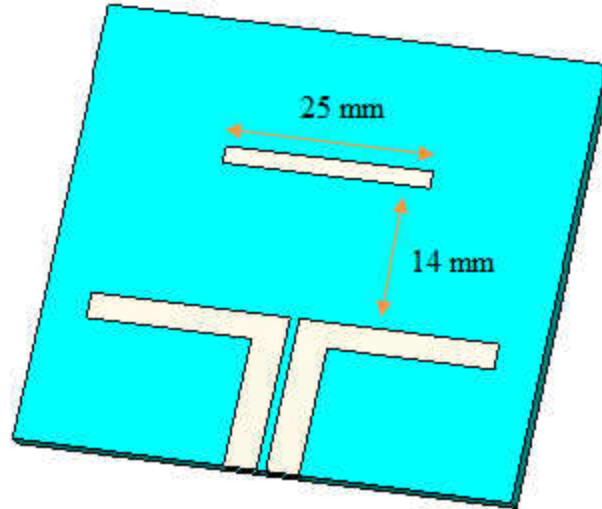


Figure 62. Configuration of the proposed Yagi-Uda antenna.

Figures 63 and 64 depict the reflection coefficient and radiation pattern of the designed Yagi-Uda antenna, respectively. This antenna has a resonance frequency at around 3 GHz as can be observed from Figure 63 and it offers more directive pattern in H-plane in comparison with the proposed dipole antenna.

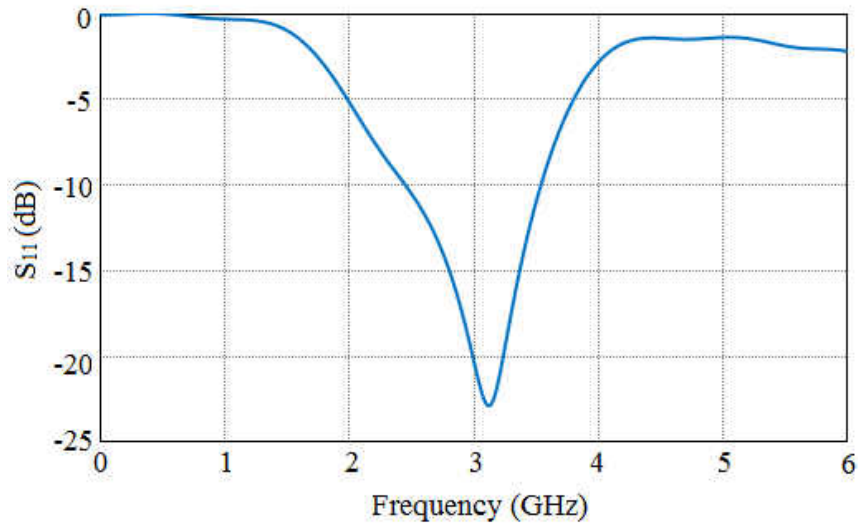


Figure 63. Reflection coefficient of the proposed Yagi-Uda antenna.

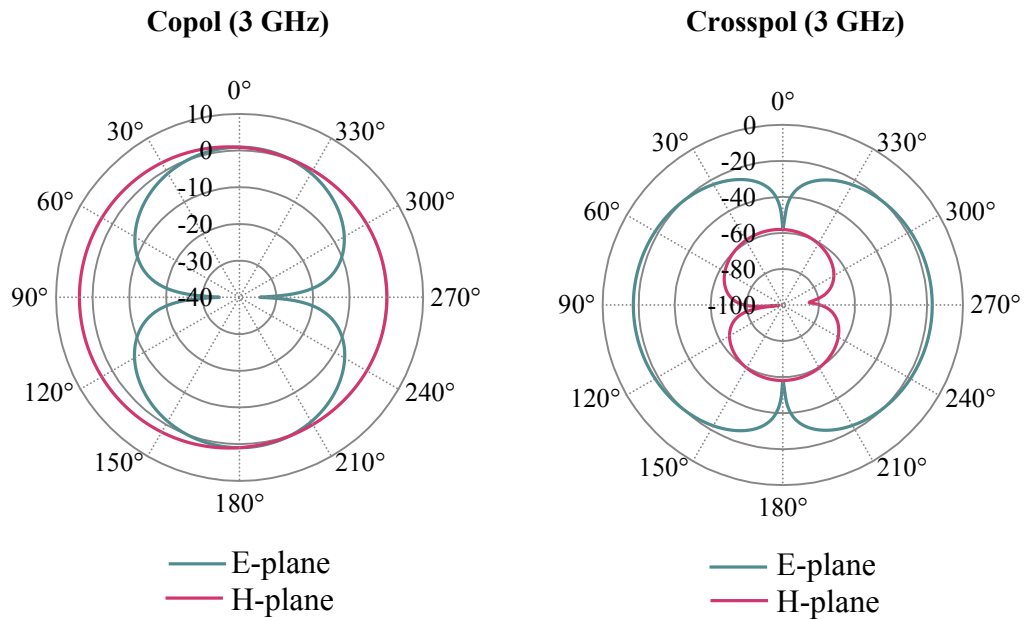


Figure 64. Radiation patterns of the designed Yagi-Uda antenna on E- and H-plane.

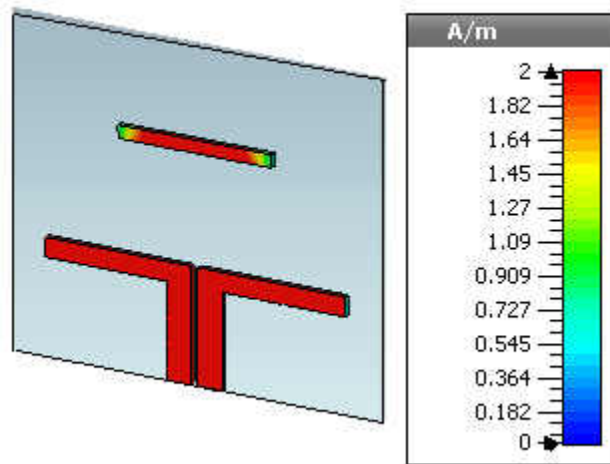


Figure 65. Current distribution on the surface of the Yagi-Uda antenna at 3 GHz

The surface current distribution of the Yagi-Uda is given in Figure 65. Figure 66 and 67 compares the 3D radiation patterns and H-plane of the 3D dipole and Yagi-Uda antenna, respectively.

Table 11 summarizes the specification of the two antennas in terms of size, bandwidth, directivity, and gain.

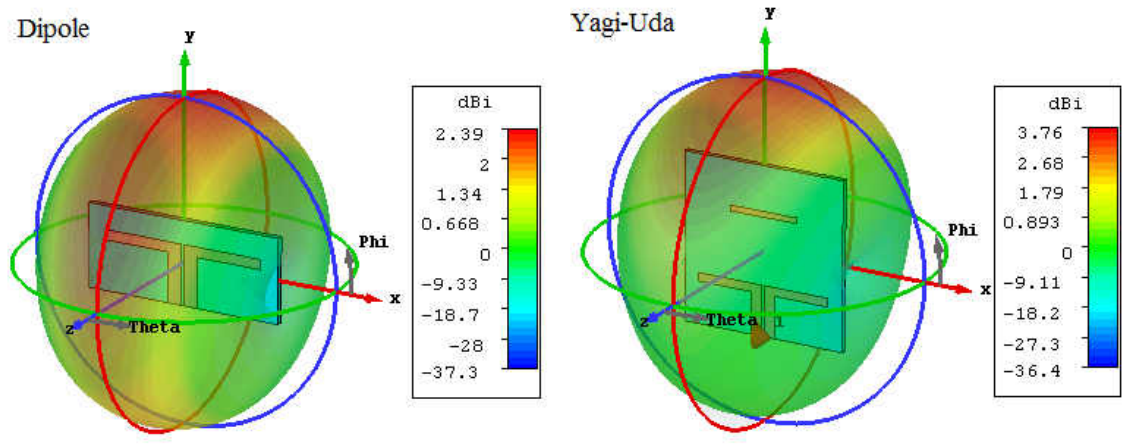


Figure 66. 3D Radiation patterns of the 3D dipole and 3D Yagi-Uda antenna at 3 GHz.

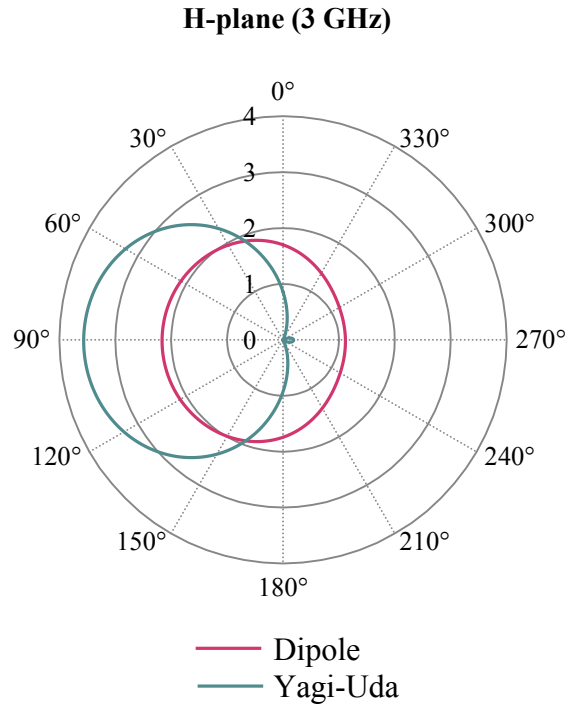


Figure 67. Comparison of the 3D dipole and 3D Yagi-Uda H-planes.

Table 11: Comparison of 3D dipole and 3D Yagi-Uda antenna.

Antenna	Size (cm ²)	10-dB Bandwidth (GHz)	Directivity (dBi)	Gain (dBi)
3D Dipole	15	1.02	3.045	2.390
3D Yagi-Uda	24	1.07	4.430	3.765

4.5 Design of 3D Microstrip Patch Antenna

In this section the design of pin-fed microstrip patch antenna at 5.8 GHz is studied. Figures 68 and 69 show the configuration of the antenna and its structural parameters, respectively. Table 12 gives the structural parameters of the antenna with their corresponding values. For performing simulations on the performance of the antenna, a substrate with dielectric properties of ABS thermoplastic has been considered. For the radiator part, a lossy metal with conductivity similar to platinum has been utilized.

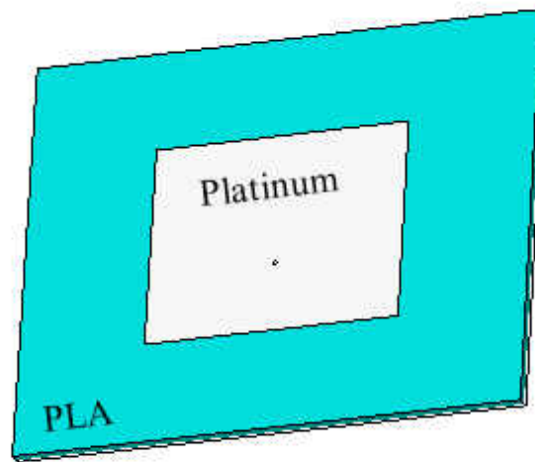


Figure 68. Configuration of the pin-fed patch antenna.

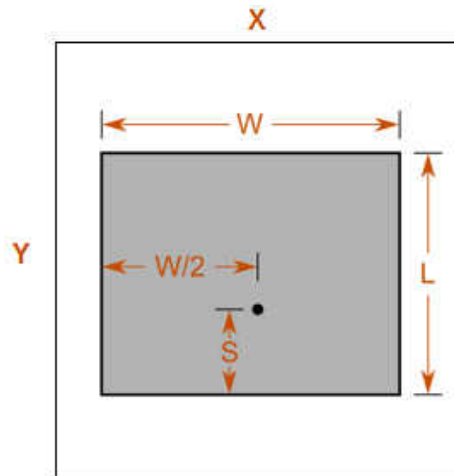


Figure 69. Top view of the patch antenna.

Table 12: Structural parameter of the patch antenna.

Name	Description	Value (mm)
L	Patch length	13.93
W	Patch width	17.83
S	Pin inset	4.81
Substrate thickness	Thickness of substrate	1.00
X	Ground plane width	35.67
Y	Ground plane length	25.87

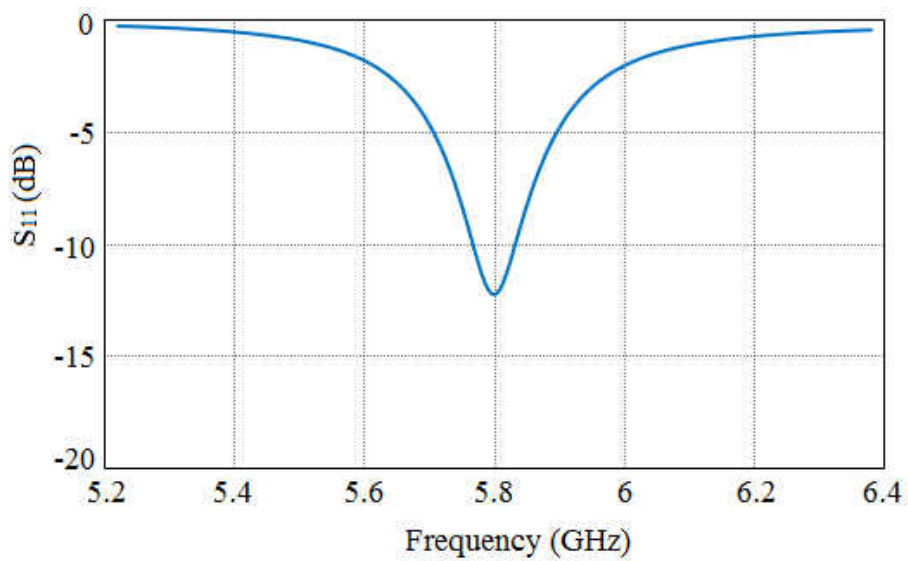


Figure 70. Reflection coefficient of the patch antenna.

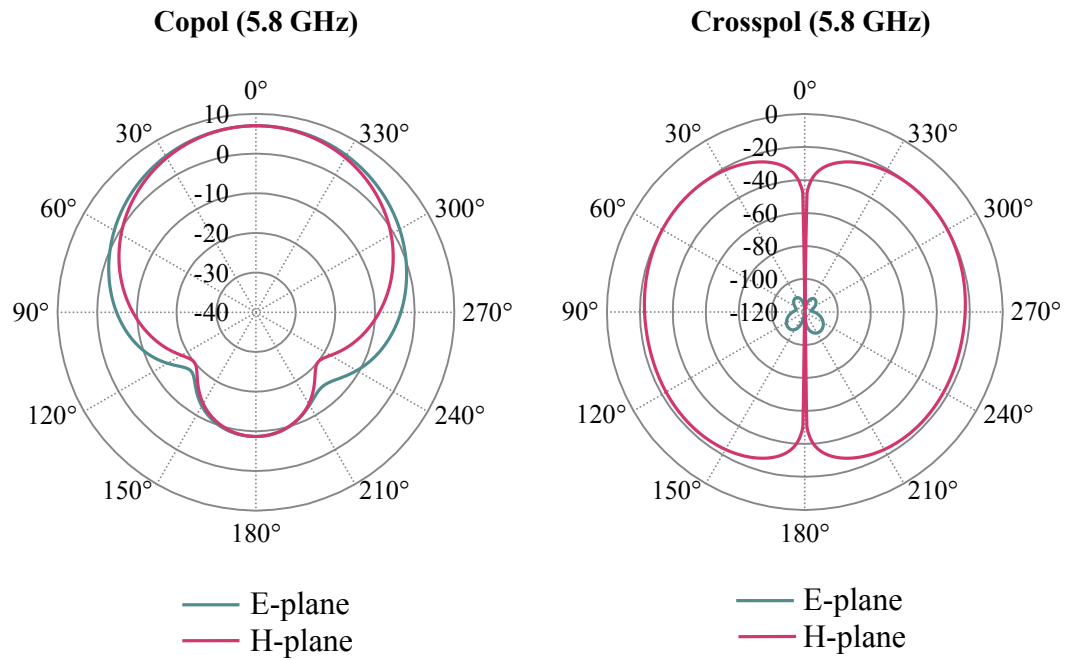


Figure 71. Radiation patterns of the patch antenna on E- and H-plane.

Figure 70 illustrates the reflection coefficient the antenna optimized at center frequency of 5.8 GHz. The simulated patch antenna features high directivity of 7.94 dBi and gain of 7.03 dBi.

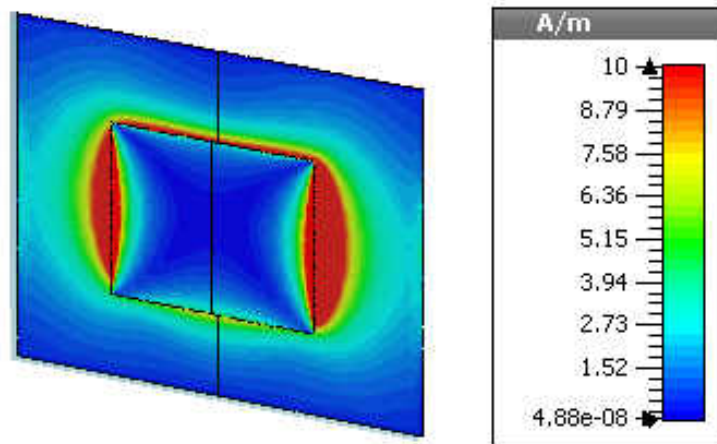


Figure 72. Surface current distribution of the patch antenna at 5.8 GHz.

The simulated radiation patterns of the antenna on E- and H-plane are showed in Figure 71. As can be seen from Figure 71, the patch antenna offers a directive pattern in both E and H planes. Figure 72 and 73 show the surface current and 3D radiation pattern of the patch antenna at 5.8 GHz, respectively.

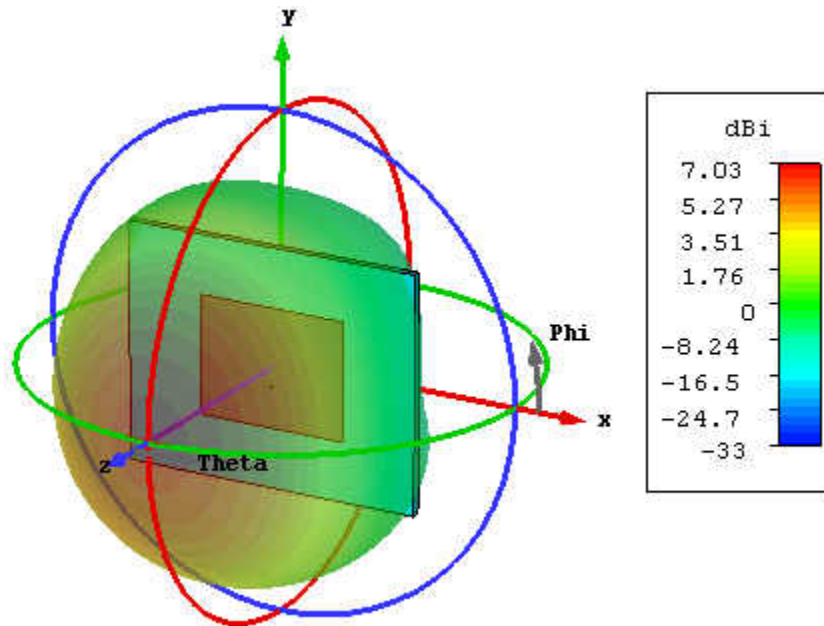


Figure 73. 3D radiation patterns of the patch antenna at 5.8 GHz.

Several antenna configurations for fabrication using advanced AM technology were studied in this chapter. The performance of the proposed antennas in terms of reflection coefficient, VSWR, gain, directivity, efficiency, group delay were simulated. In addition, the radiation patterns of the designed antennas were presented. The fabrication process of the proposed antennas will be presented in next chapter.

CHAPTER 5

FABRICATION PROCESS AND MEASUREMENT RESULTS

Several antenna configurations for fabrication using advanced AM technology were presented in Chapter 4. Their performance under different conditions were studied and the optimized dimensions were given. In this chapter the antenna fabrication process using different technologies and materials is introduced and the results of measurements are demonstrated.

5.1 Fabrication of Bowtie Antenna using PLA and ABS Materials

After the preliminary design of antennas was optimized in CST Microwave Studio [121], a 3D model of the antenna was created in SolidWorks [122] (Figure 74), a 3D CAD system available through Daussault Systemes. Since the precision of the 3D printer for printing the antenna was 0.011mm, the optimized dimensions were rounded off to the second decimal point. Once the 3D model was ready, it was then converted to an STL file which is the standard file format used in the 3D printing industry.

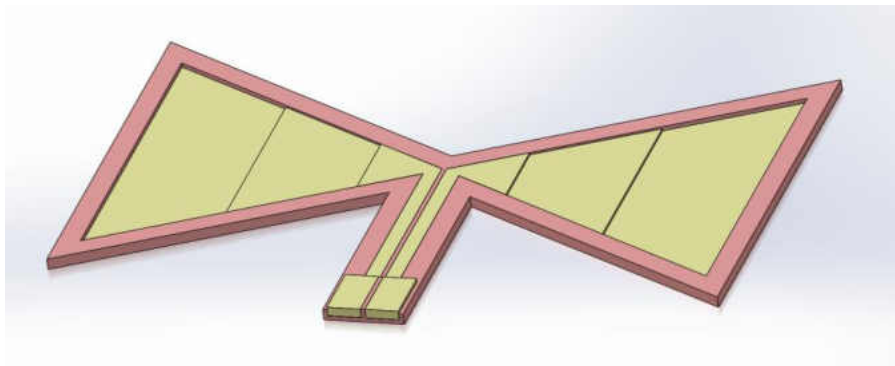


Figure 74. The 3D model of the antenna created in SolidWorks.

If the antenna model consisted of two components (represented in different colors in Figure 74), SolidWorks converts the assembly of two components into two separated files. The antennas were built in MakerBot Dual, a 3D printer commercially available through MakerBot Industries, LLC. Based on the FDM technology, this printer was equipped with two extruder heads, as shown in Figure 75, and could print up to two different materials simultaneously.

The printer was driven by the software, MakerBot Desktop, where a tessellated 3D model in the STL format was sliced into layers along the Z-axis, and a set of G codes was generated for each layer to move the extruder heads to specific X-Y positions for depositing the melted filament.

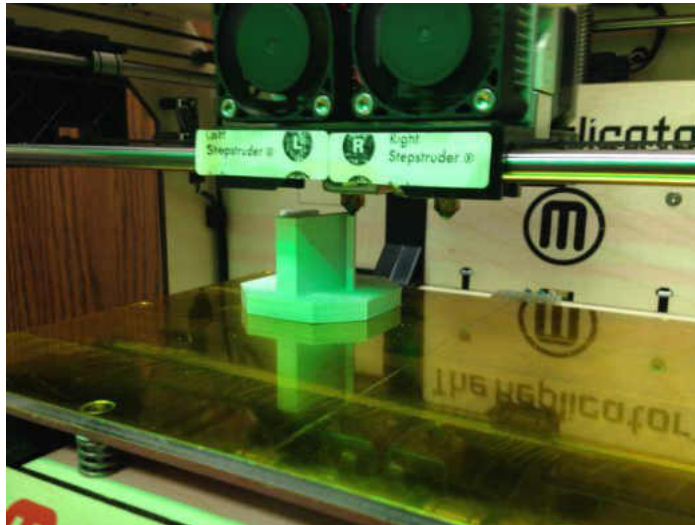


Figure 75. A printed part between the extruder heads of MakerBot Dual and the heated build plate.

To create 3D parts through the FDM technology, the filament needed to be heated up in the extruder head so the extrusion process from the filament of 1.75mm diameter could go through the extruder nozzle of a size of 0.4mm smoothly. The build plate that carried the built part also needed to be heated to ensure better bounding between layers.

The temperature of the extruder heads and the build plate was given in the MakerBot Desktop software. While there were suggested temperature ranges for different materials, a trial-and-error step was usually required to figure out the best combination of temperature for extruder heads and the build plate. If the extruder head is too hot, the material drips from the nozzle and the deposition location becomes unpredictable. If the build plate is too cold, the bonding between layers, especially layers of different materials, will not be ideal and eventually it becomes the spot of peeling off.

Tables 13 and 14 show the construction parameters of two bowtie antennas, including the material used, building temperature of the extruder heads and the build plate, the speed of the extruders, and the amount of time used to complete the construction. Note that for the planar antenna, only the substrate was built through the 3D printing process; the copper foil was cut separately and placed upon the antenna after the printing process was finished.

Table 13: Material and temperature for different antennas.

Antenna	Antenna material	Substrate material	Extruder head temperature (°C)
Planar Antenna	Copper foil	Clear PLA	230
3D Antenna	Conductive ABS (carbon-based)	Flexible PLA	230

Table 14: MakerBot Dual construction conditions for different antennas.

Antenna	Build plate temperature (°C)	Extruder speed (mm/s)	Build time (min)
Planar Antenna	112	40	10
3D Antenna	100	30	13

Figure 76 shows a photograph of the fabricated antenna using clear PLA and copper for substrate and radiator parts, respectively. The measured reflection coefficient of the fabricated antenna is shown in Figure 77. Agilent E5071C network analyzer was used for the reflection coefficient measurements.

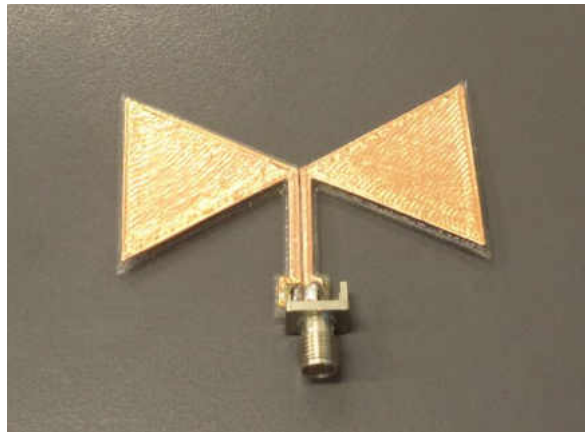


Figure 76. Fabricated bowtie antenna.

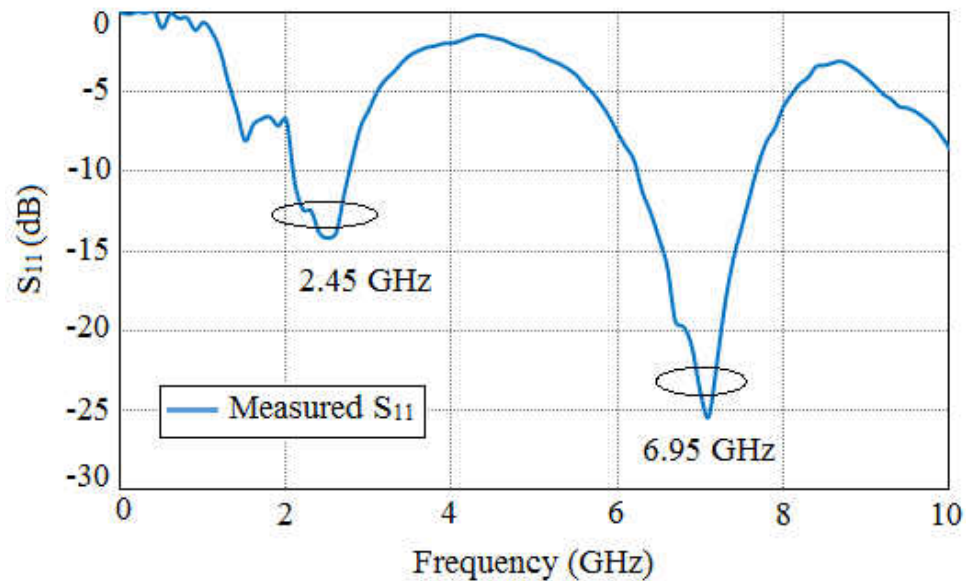


Figure 77. Measured reflection coefficient of the bowtie antenna.

The measured bowtie antenna offers two operating frequency bands centered at 2.45 GHz and 6.95 GHz which are in good agreement with the reflection coefficient of

the designed bowtie antenna (simulated with PLA for substrate and copper for radiator) presented in section 4.2. The corresponding simulated center frequencies were 2.45 GHz and 6.67 GHz for the first and second band, respectively.



Figure 78. Fabricated antenna under test.

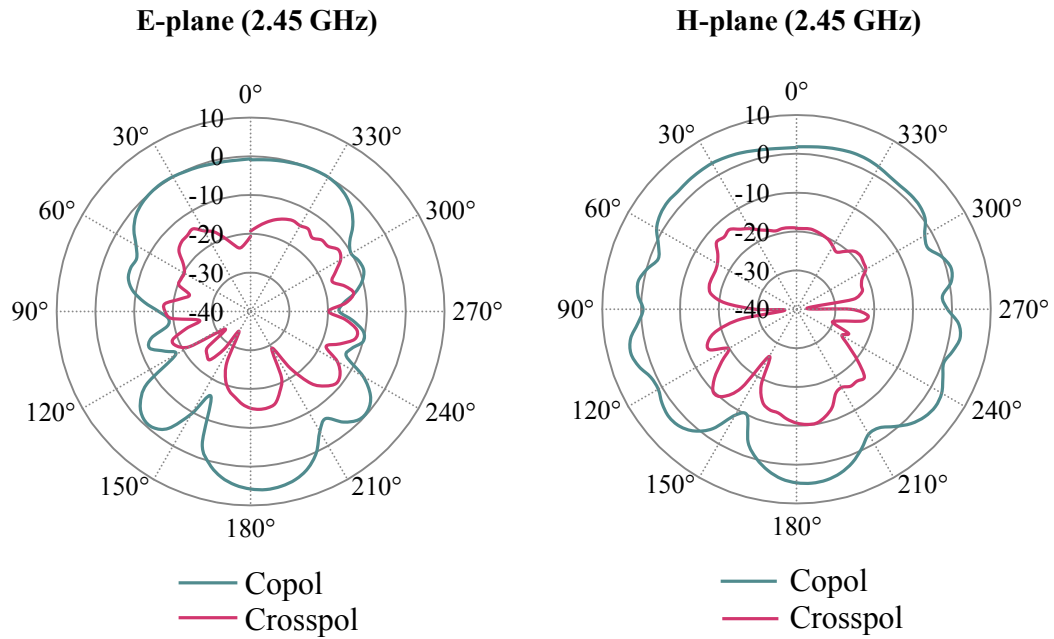


Figure 79. Measured E- and H-plane of the fabricated bowtie antenna.

The 10-dB bandwidth for the first operating band of the measured antenna was from 2.1 GHz to 2.8 GHz and the second one was measured from 6.2 GHz to 7.7 GHz. Figure 78 shows the antenna under test inside the anechoic chamber to perform radiation patterns measurements. Figure 79 illustrates the radiation patterns of E- and H-plane at 2.45 GHz. The measured directivity and gain were 7.40 dBi and 6.09 dBi for E-plane, respectively. These values were 3.24 dBi and 5.06 dBi for H-plane.

Figure 80 shows a photograph of the fabricated bowtie antenna with a staircase radiator configuration. It should be noted that the flexible PLA and conductive ABS has been utilized for the fabrication of the substrate and radiator parts, respectively.

The measured reflection coefficient of the antenna is shown in Figure 81. As can be observed from Figure 81, the antenna offers wide 10-dB bandwidth from 6.37 GHz to 8.76 GHz.

There were several challenges in the fabrication process of this antenna. The first challenge was printing coplanar stripline part. The two lines of coplanar stripline have a very small separation (0.4 mm). Due to the resolution of the printer, the printed lines could not have the exact separation as was given by the simulations. The second challenge was connecting SMA connector to the fabricated antenna. It is very difficult to solder the SMA connector to ABS since the thermoplastic will be melted by high temperature. The alternative way was using carbon paste to connect the SMA connector to the antenna. The problem with this method was that it could not keep the SMA connector firm enough to perform measurement and we had to reconnect it several times

during measurements. In addition carbon paste is less conductive than typical soldering materials.

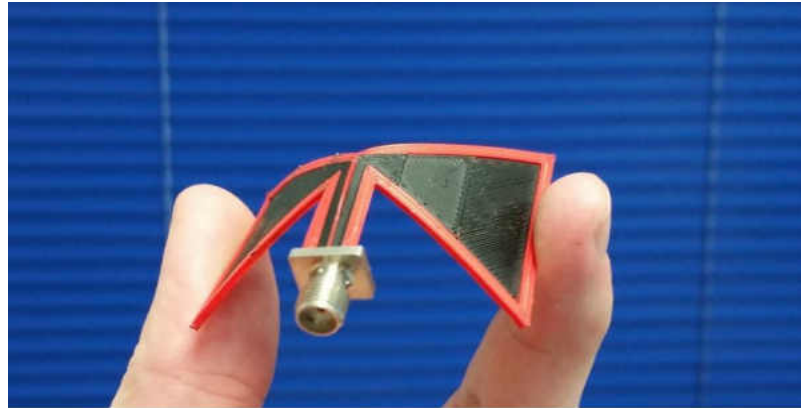


Figure 80. A photograph of fabricated bowtie with staircase radiator configuration.

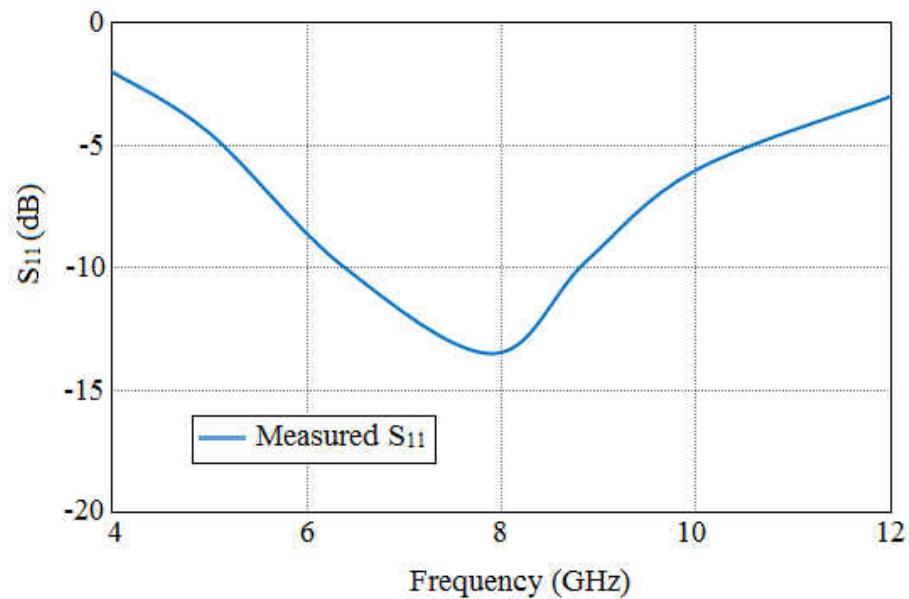


Figure 81. Reflection coefficient of the fabricated bowtie with staircase radiator configuration.

Figure 82 illustrates the radiation patterns on E- and H-plane for the fabricated antenna at 7.8 GHz. Due to the limitations of anechoic chamber, it was not possible to measure gain at this frequency. It should be noted that the maximum frequency for the

connecting cables in measurement setup was around 6 GHz which is less than the frequency that we performed measurements.

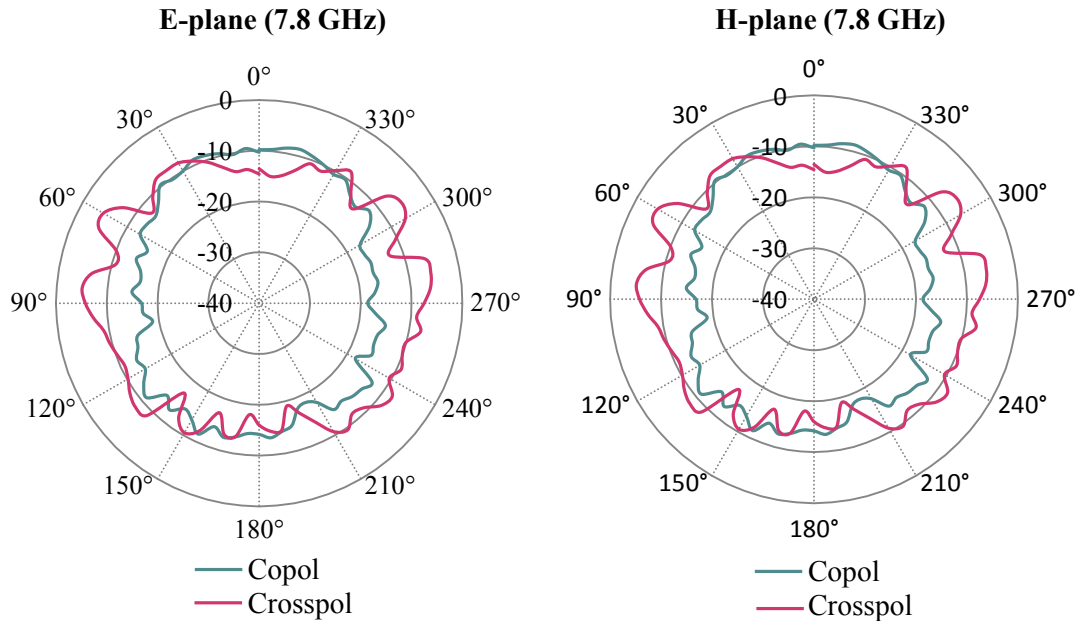


Figure 82. Radiation patterns of the fabricated bowtie antenna on E- and H-plane at 7.8 GHz.

Figure 83 shows the fabricated 3D bowtie antenna designed for UWB applications. For this antenna, substrate part was printed using uPrint SE printer. The copper paste were used for coating the antenna to implement the radiator part. The reflection coefficient of the fabricated antenna is depicted in Figure 84. The 10-dB bandwidth of the antenna is from 1.80 GHz to 6 GHz. The corresponding 10-dB bandwidth for simulated results were from 1.72 GHz to 15.12 GHz. Figure 85 shows the radiation patterns of the antenna on H- and E-plane at 3.5 GHz and 5.8 GHz.

Table 15 summarizes the specification of the fabricated antenna in terms of conductivity and gain at 3.5 GHz and 5.8 GHz.

Table 15: Comparison of the E- and H-plane of the 3D antenna.

Plane	Directivity(dBi) (3.5 GHz)	Gain(dBi) (3.5 GHz)	Directivity(dBi) (5.8 GHz)	Gain(dBi) (5.8 GHz)
E-plane	4.88	3.08	4.86	0.04
H-plane	3.40	3.33	3.95	-0.10

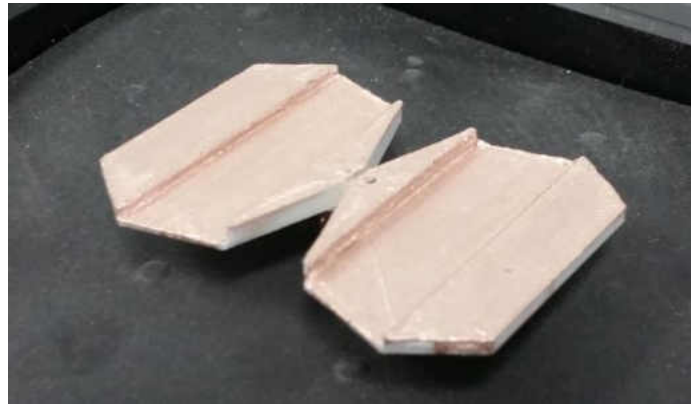


Figure 83. Fabricated 3D antenna.

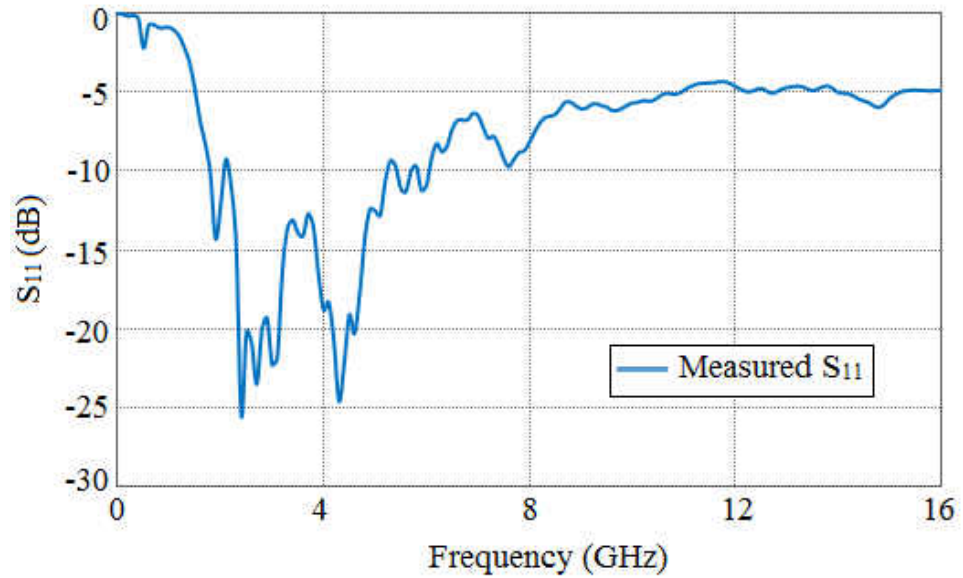


Figure 84. Reflection coefficient of the fabricated 3D antenna.

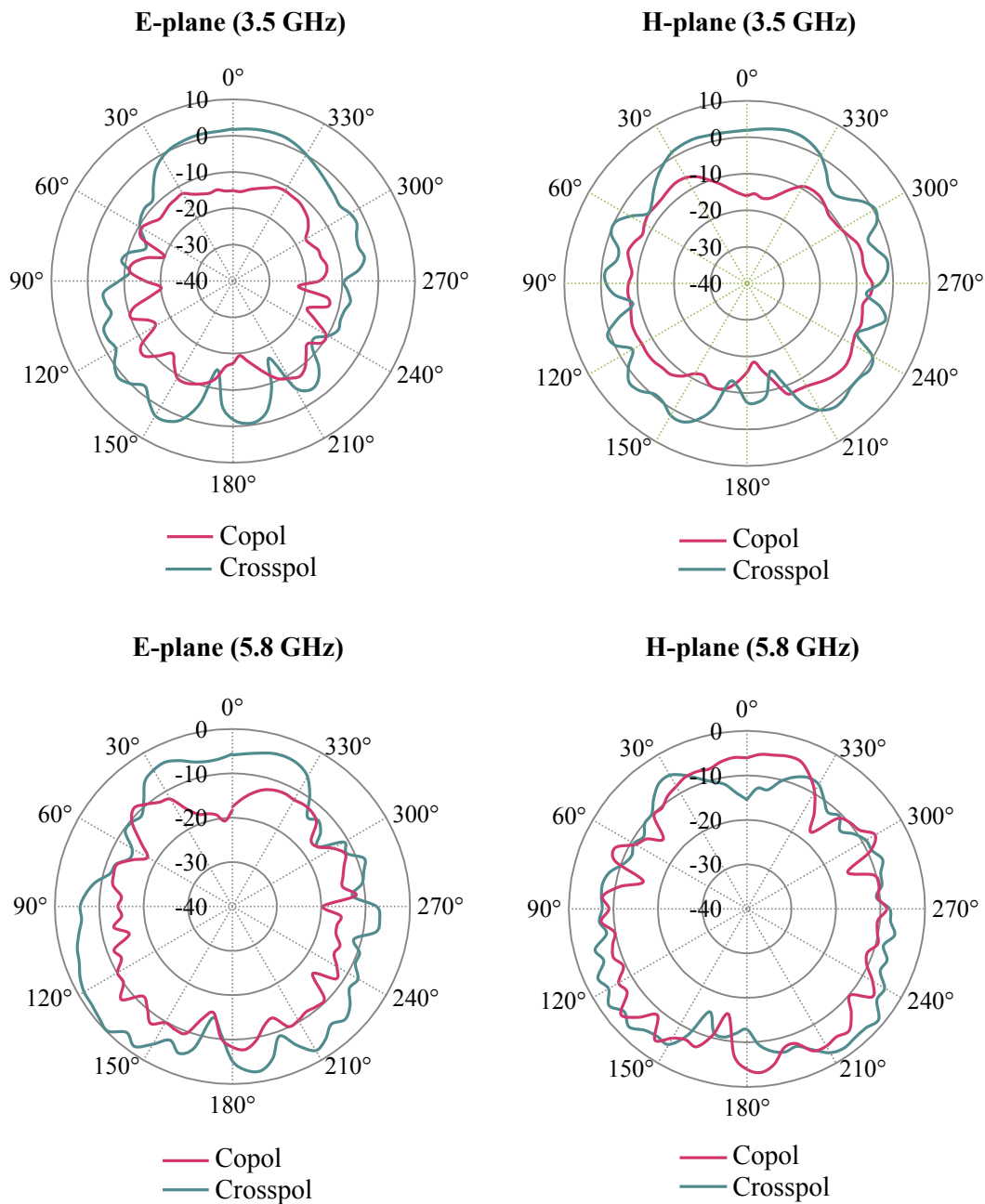


Figure 85. Radiation patterns of the fabricated UWB antenna on H- and E-plane at 3.5 GHz and 5.8 GHz.

5.2 Embedded Dipole Antenna Fabrication

This section presents the embedded dipole antennas fabrication process. For the dipole designs, the antennas substrates were fabricated using ROBO 3D printer, shown in Figure 86, using both PLA and ABS filaments. The diameter of the utilized filaments

were 1.75mm. To perform 3D printing process, the STL of the design was first loaded to the 3D printer software and the extruder and build plate were heated up to certain temperatures based on the type of utilized materials.



Figure 86. ROBO 3D printer.

Figures 87 and 88 show the fabricated dipole antennas using ABS and PLA, respectively. It should be noted that these antennas have the same structural parameters and conductive materials.

High temperature carbon paste which is a dispersion of carbon flakes in an inorganic silicate aqueous solution [122] was used for embedding conductor inside the 3D fabricated substrates. The measured reflection coefficients of the antennas are presented in Figure 89.

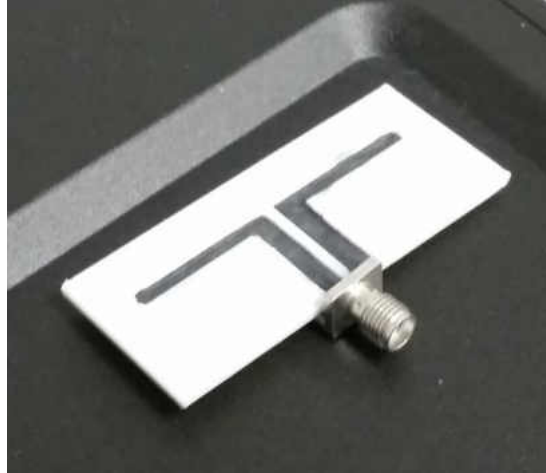


Figure 87. Fabricated dipole antenna with ABS and carbon paste.

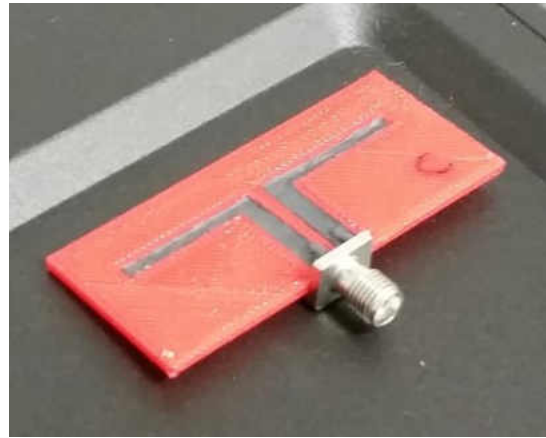


Figure 88. Fabricated dipole antenna with PLA and carbon paste.

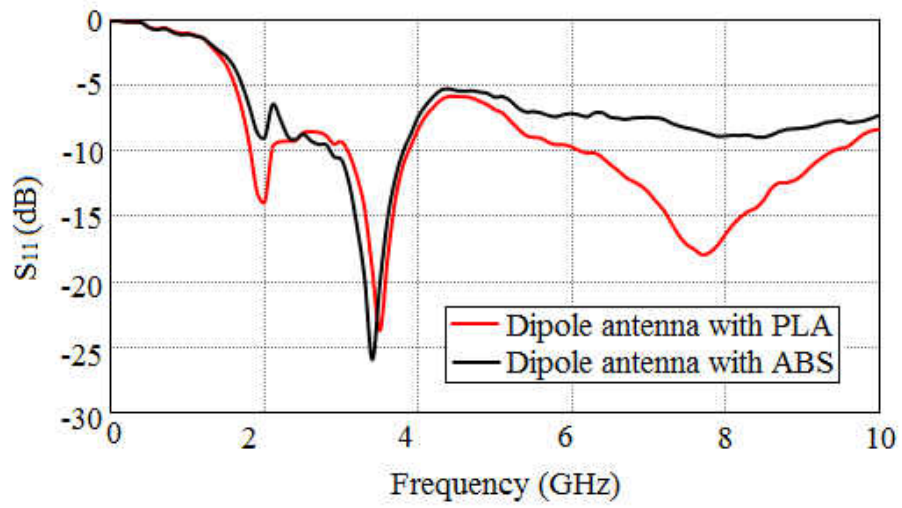


Figure 89. Measured reflection coefficient of the fabricated dipole antennas.

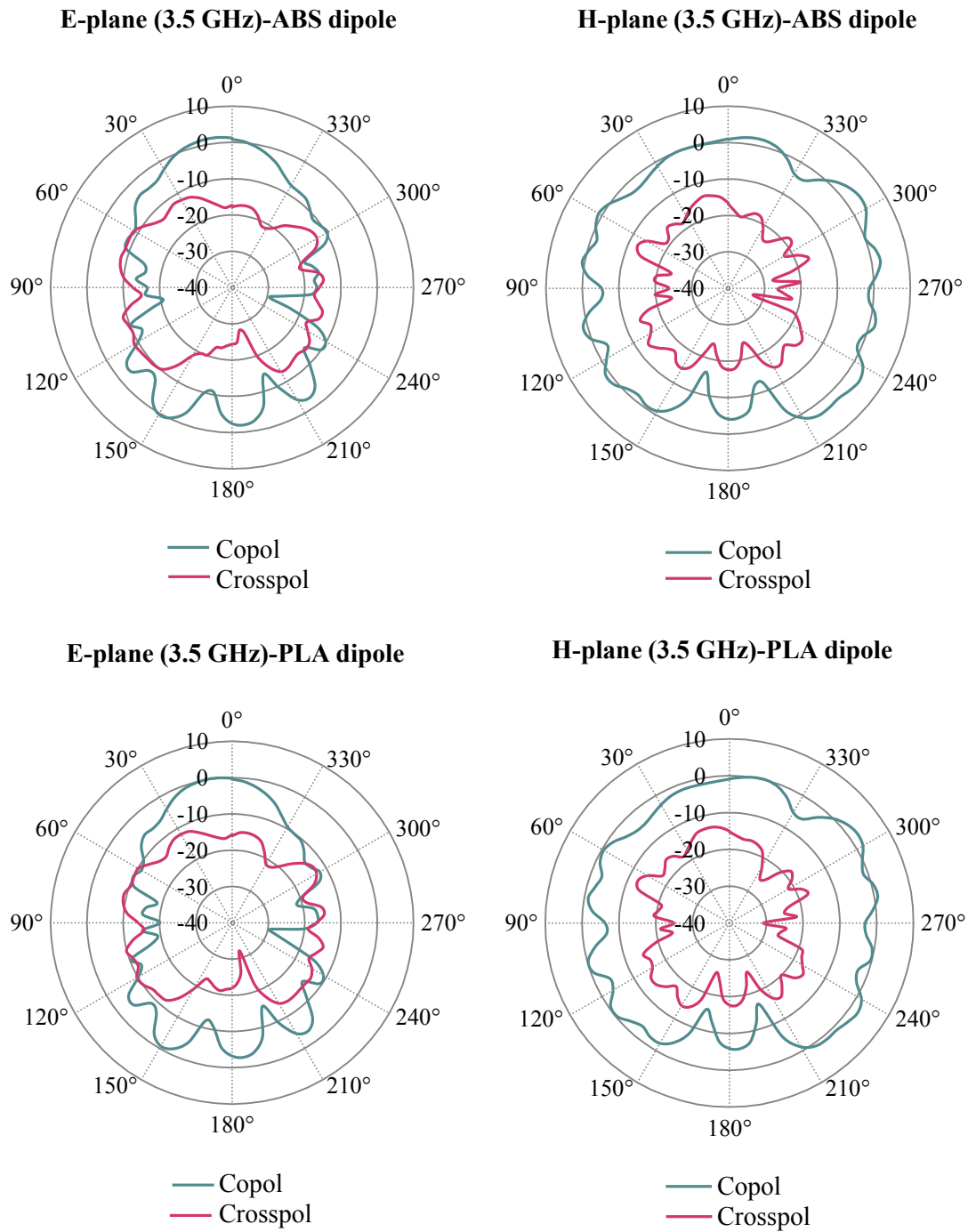


Figure 90. Measured reflection coefficient of the fabricated dipole antennas.

As can be observed from Figure 89, the fabricated antennas have the same resonance frequency at around 3.5 GHz, however, the antenna fabricated with PLA offers another wide operating band centered at around 8 GHz. Figure 90 illustrates the measured

radiation patterns of the fabricated antennas at 3.5 GHz. Table 15 summarizes the specification of the fabricated antennas in terms of directivity and gain on E-and H-plane at 3.5 GHz.

Table 16: Comparison of fabricated dipole antennas

Antenna	Directivity(dBi) E-plane (3.5 GHz)	Gain(dBi) E-plane (3.5 GHz)	Directivity(dBi) H-plane (3.5 GHz)	Gain(dBi) H-plane (3.5 GHz)
Dipole with PLA	5.69	0.17	4.06	2.57
Dipole with ABS	5.92	1.58	4.07	4.07

5.3 3D Printed Antennas Fabrication using Sputtering Technology

This section studies the feasibility of sputtering technology for the fabrication of radiator part of 3D printed antennas. A bowtie antenna was fabricated and measured using this method. The fabrication process of the proposed bowtie antenna and measured results are presented in this section.

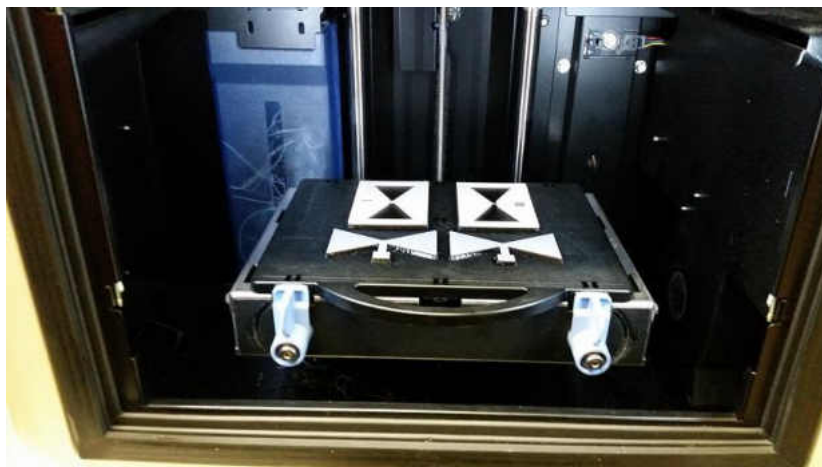


Figure 91. Fabricated bowtie substrate and its mask.

At the first step, the substrate of the bowtie antenna and its relevant mask were fabricated using uPrint SE printer. Figure 91 shows the 3D printed substrate of the bowtie antenna and the mask. It should be noted that the mask was placed on the top of the 3D printed substrate during sputtering process to create a gap between bowtie arms and coplanar stripline feed structure.

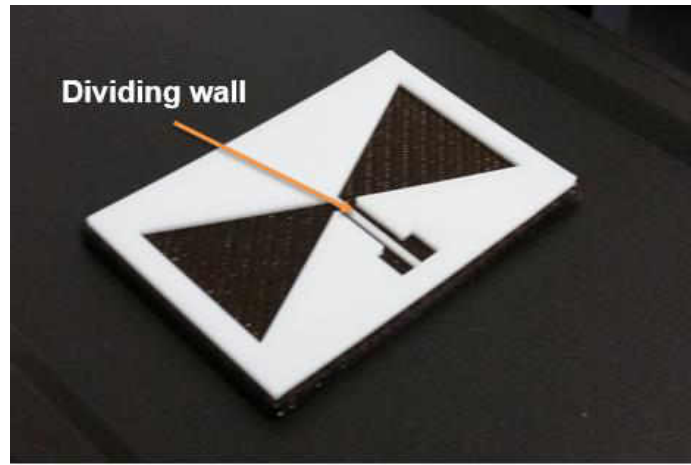


Figure 92. Fabricated mask for the bowtie antenna.

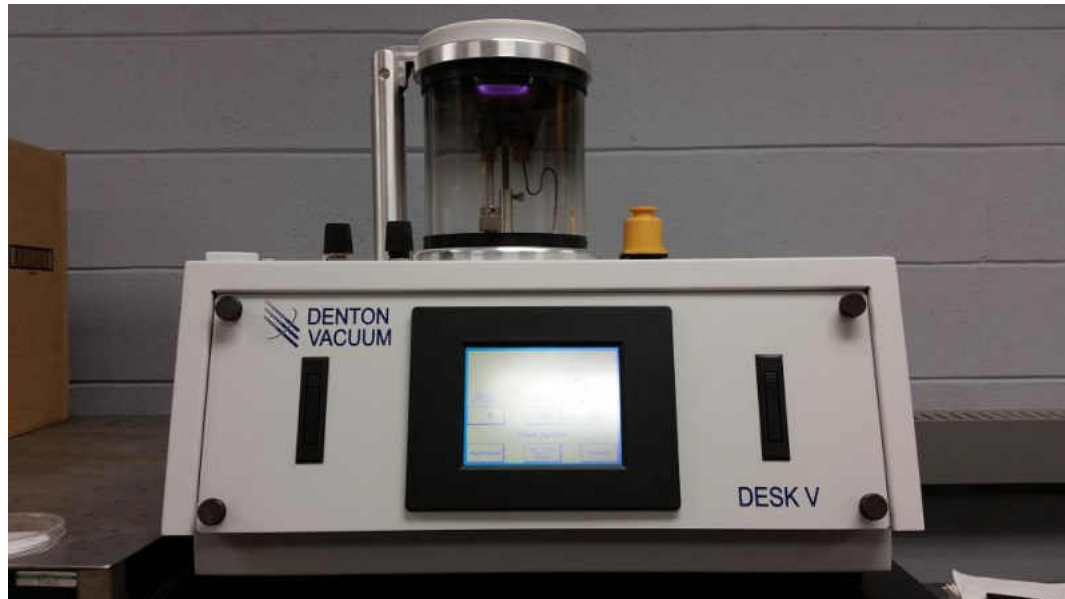


Figure 93. DESK V HP sputtering system.

The smallest width that we could produce using uPrint SE printer for the dividing wall, indicated in Figure 92, was 1mm which is 0.6 mm more than the gap between coplanar stripline in the simulated bowtie antenna presented in Chapter 4. The next step after producing bowtie and its relevant mask was coating the fabricated bowtie substrate with platinum using DESK V HP spurting system (Figure 93). The antenna was coated with platinum several times (each time 45 second) and the resistance of the antenna was checked after each time. Figure 94 shows the antenna under sputtering process. After getting a reasonable resistance, the SMA connector was then attached to the antenna using copper paste. Figure 95 shows the fabricated bowtie antenna with attached SMA connector.



Figure 94. Antenna under sputtering process.



Figure 95. A photograph of the fabricated antenna.

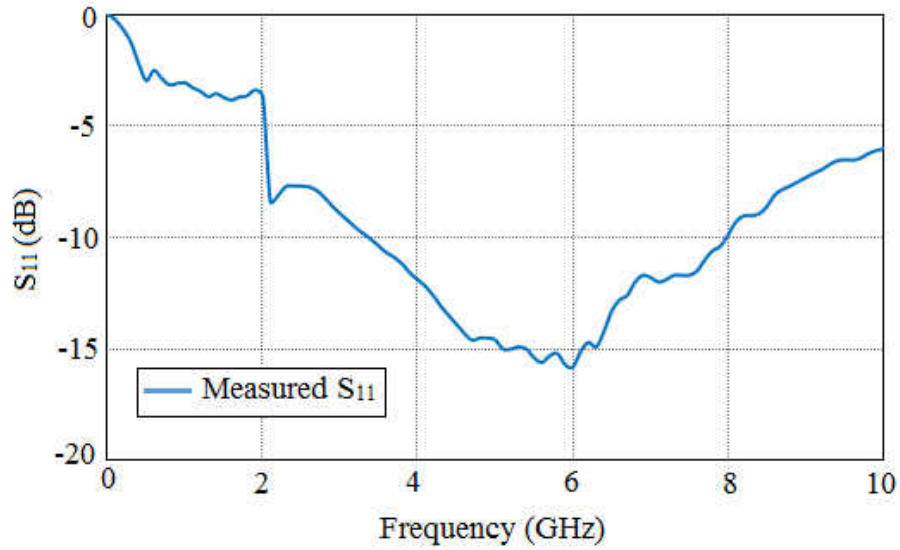


Figure 96. Measured reflection coefficient of fabricated bowtie antenna.

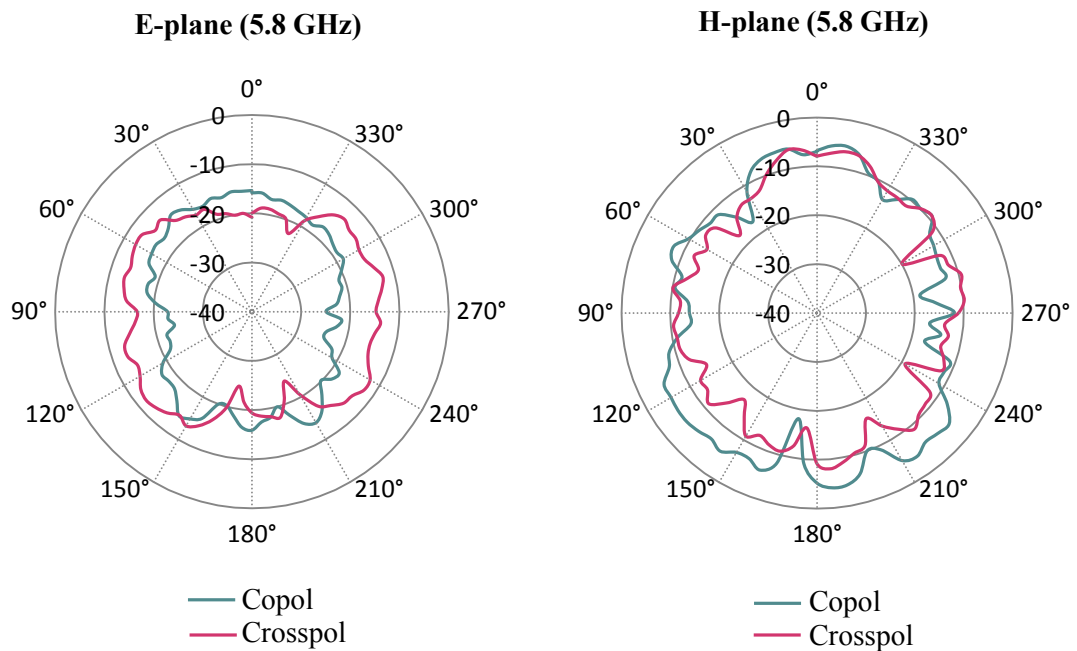


Figure 97. Measured radiation patterns of fabricated bowtie antenna on E- and H-plane.

After fabrication process, the reflection coefficient and radiation patterns of the antenna were measured. Figures 96 and 97 shows the measured reflection coefficient and radiation patterns of the antenna on E- and H-plane at selected frequency of 5.8 GHz,

respectively. The 10-dB bandwidth from 3.30 GHz to 8 GHz was achieved for the fabricated bowtie antenna. As can be observed from Figure 97, the antenna has omnidirectional radiation pattern with high x-pol on both E- and H-plane. The directivity and gain of the antenna in E-plane are 4.04 dBi and -4.22 dBi, respectively. The corresponding values for H-plane are 3.65 dBi and -2.62 dBi.

CHAPTER 6

FUTURE WORK AND CONCLUSION

This thesis proposes novel compact 3D antennas through advanced additive manufacturing technology for next generation of wireless communication systems. Different 3D antenna configurations including bowtie, dipole, Yagi-Uda, and microstrip patch have been designed, simulated, and fabricated. The effects of antenna structural parameters, radiator conductivity, and substrate type on the performance of the proposed antennas have been investigated. Additionally, the permittivity of the utilized materials were measured and the obtained results were demonstrated. This chapters will present the fabrication and measurement challenges and suggestions for the future works to overcome these challenges. In addition, conclusions based on the obtained results will be provided at the end.

6.1 High Frequency Materials Characterization

As the 3D printing using different materials for fabricating antennas and microwave components continues to expand, the broadband materials characterization are gaining importance. To perform the simulations of the antennas using commercial simulation tools, dielectric constant and loss tangent or conductivity of the materials are needed.

In this thesis, coaxial probe method has been utilized to measure the complex permittivity of the materials that have been utilized for antennas fabrication. This method

can be a good candidate for measuring the dielectric constant of liquids, semi-solids, and solids. The challenge with this method was that negative values for loss (imaginary part of permittivity) were obtained at under around 3 GHz for most of the cases. In addition we were unable to measure conductivity of conductive materials with this method. The other mentioned methods like transmission line, resonant cavity, and parallel plate could be good candidates for future studies to measure the complex permittivity and conductivity of the materials used in antennas fabrication.

Studying the influence of temperature on the complex permittivity and conductivity of the utilized materials in the fabrication of the antennas is also of interest to investigate the performance of the fabricated antennas under different conditions.

6.2 3D Antennas Fabrication

In this thesis 3 different desktop and commercial 3D printers were used to fabricate the proposed antennas. The commercial printer offered good accuracy in printing thin layers, however, we could use only ABS filament to print antennas using that. The challenge for the fabricating some of the antennas with thin layers was that the fabricated layers were not unite and they were made of parallel line with a little space between them. This caused considerable effects on the performance of the antenna especially in the case of bowtie antenna with conductive ABS. For the future works, using 3D printer with high accuracy in printing thin layers that can use conductive materials to print antennas is recommended.

6.3 Attaching SMA Connector

One of the major challenges in this thesis was attaching SMA connectors to the fabricated antennas to perform measurements. The fabricated substrates in this thesis are all made of thermoplastic which can be melt by high temperature. This makes the soldering process an impossible task to connect the SMA connectors to the fabricated antennas. In addition, all the fabricated antennas, except the bowtie made with copper foil, have a conductor part that is not suitable for soldering. This also makes soldering not a feasible option to connect SMA connectors to the antennas. We utilized carbon paste to attach the SMA connectors to the fabricated antennas. We had to reconnect the SMA connectors to some of the antennas several times during measurements.

Finding suitable curing process for the materials used as a radiator part of the antennas can be a good effort to find a way that helps for connecting SMA connector such that stay firm enough during measurement. In addition using new conductive materials with better mechanical and electrical performance is recommended for future works.

6.4 Antennas Measurements

An anechoic chamber was used to measure the far-field of the fabricated antennas. The maximum working frequency for the connecting cables in the measurement setup was 6 GHz which is close to 5.8 GHz and less than 7.8 GHz that we did some of the measurements at these frequencies in this thesis. As mentioned in Chapter 5, a high x-pol was observed for measurements in high frequencies. In addition, the measured gain values in this thesis are obtained with a single axis measurement. Equipping the

measurement setup with high frequency cables and dual axis measurements are recommended for future endeavors.

6.5 Conclusion

This thesis proposed novel 3D antennas utilizing advanced AM technology. Several antenna configurations were fabricated based on proposed novel methods. Different materials were utilized for the fabrication of the substrate and radiator parts of the proposed antennas. The complex permittivity of the materials were measured using coaxial probe method. Both desktop and commercial 3D printers were utilized for the fabrication of the proposed antennas. The reflection coefficient and the far-field of the fabricated antennas have been measured and demonstrated. The measured results attest to the fact that the proposed methods can be good candidates for the fabrication of 3D compact antennas for next generation of wireless communication systems.

REFERENCES

- [1] 3-D printing and custom manufacturing: from concept to classroom, Available: http://www.nsf.gov/discoveries/disc_summ.jsp?cntn_id=129774, visited June 2015.
- [2] Additive manufacturing: opportunities and constraints, Available: <http://www.raeng.org.uk/publications/reports/additive-manufacturing>, visited June 2015.
- [3] Wohler's Report (2013), Additive manufacturing and 3D printing state of the industry annual worldwide progress report, Wohler's Associates, Inc.
- [4] Application of additive manufacturing, Available: http://www.additive3d.com/rm_35.htm, visited June 2015.
- [5] Richard I Olivas, "Conformal electronics packaging through additive manufacturing and micro-dispensing," (January 1, 2011). ETD Collection for University of Texas, El Paso. Paper AAI1494367, Available: <http://digitalcommons.utep.edu/dissertations/AAI1494367>, visited June 2015.
- [6] Optomec developing production solution for 3D printed antennas additive manufacturing approach will offer cost, environmental and functional Benefits, Available: <http://www.optomec.com/optomec-developing-production-solution-for-3d-printed-antennas-additive-manufacturing-approach-will-offer-cost-environmental-and-functional-benefits/6-10-2015>, visited June 2015.
- [7] Optomec launches 5-axis platform for producing 3D printed antenna and sensors, Available: <http://www.optomec.com/optomec-launches-5-axis-platform-producing-3d-printed-antenna-sensors/>, visited June 2015.
- [8] T. J. Horn and O. L.A. Harrysson, "Overview of current additive manufacturing technologies and selected applications," *Science Progress*, vol. 95, no. 3, pp. 255-282, September 2012.
- [9] P. F. Jacob, *Rapid Prototyping and Manufacturing: Fundamentals of Sterolithography*, SME, 1992.
- [10] I. Gibson, D. W. Rosen, and B. Stucker, *Additive Manufacturing Technologies: Rapid Prototyping to Direct Digital Manufacturing*, Springer, New York, 2010

- [11] T. Wohlers, *Additive Manufacturing and 3D Printing State of the Industry Annual Worldwide Progress Report*, 2005.
- [12] 3D printed electronics: next phase of the additive manufacturing revolution?, Available: <http://www.advancedmanufacturinginsight.com/archived-articles/item/3d-printed-electronics-additive-manufacturing>, visited June 2015.
- [13] J. Hoerbera, J. Glasschroederb, M. Pfeffera, J. Schilpb, M. Zaehb, and J. Frankea, "Approaches for Additive Manufacturing of 3D Electronic Applications," *Variety Management in Manufacturing — Proceedings of the 47th CIRP Conference on Manufacturing Systems*, July 2014, pp. 806-811.
- [14] J. Thevenard, D. Lo Hine Tong, A. Louzir, C. Nicolas, C. Person, and J. P. Coupez, "3D multi-sector vivaldi antennas based on metallized plastic technology," *IEEE Antennas and Propagation Society International Symposium*, June 2007, pp. 5849-5852.
- [15] H. Wang, Y. Wang, Y. Liu, and W. Yu, "3D antenna for UHF RFID tags with near omni-direction," *IEEE 8th International Symposium on Antennas, Propagation and EM Theory (ISAPE)*, Nov. 2008, pp. 118-121.
- [16] S.-H. Chang and W.-J. Liao, "A compact 3D antenna with comprehensive LTE band coverage for use on notebook hinge," *IEEE Asia-Pacific Conference on Antennas and Propagation (APCAP)*, Aug. 2012, pp. 142-143.
- [17] P. Anacleto, P.M. Mendes, E. Gultepe, and D.H. Gracias, "3D small antenna for energy harvesting applications on implantable micro-devices," *Antennas and Propagation Conference (LAPC)*, Loughborough, Nov. 2012, pp. 1-4.
- [18] L. Tian, H. Guo, X. Liu, Y. Wang and X. Yang, "Novel 3D RFID antenna with low profile and low cost," *10th International Symposium on Antennas, Propagation & EM Theory (ISAPE)*, Oct. 2012 , pp. 69-72.
- [19] A. Enayati, S. Brebels, W. De Raedt, and G.A.E. Vandenbosch, "3D-antenna-in-package solution for microwave wireless sensor network nodes," *IEEE Trans. Antennas Propag.*, vol. 59, no. 10, pp. 3617-3623, Oct. 2011.
- [20] D. Kaddour, S. Tedjini, and A. Djamel, "3D antenna for UHF RFID tag on molded interconnect device," *IEEE Antennas and Propagation Society International Symposium (APSURSI)*, pp. 15020-1503, July 2013.
- [21] W. Mazhar, M. A. Tarar, F. A. Tahir, and W. Gulistan, "A low profile cross strip 3D monocone antenna for UWB applications," *Prog. Electromagn. Res. C*, vol. 46, pp. 51-61, 2014.
- [22] Y. Song, Z. Wu, J. C. Modro, and P. O'Riordan, "Modelling of miniaturised multiband 3D slot loop antennas," *Wideband and Multi-band Antennas and Arrays*, Sept. 2005. IEE (Ref. No. 2005/11059), pp. 153-157.

- [23] A. A. Serra, P. Nepa, G. Manara, and R. Massini, "A low-profile linearly polarized 3D PIFA for handheld GPS terminals," *IEEE Trans. Antennas Propag.*, vol. 58, no. 4, pp. 1060-1066, April 2010.
- [24] Antenna fabrication via direct print, Available: <http://www.sciperio.com/antenna/antenna-fabrication.asp>, visited July 2015.
- [25] I.T. Nassar and T.M. Weller, "An electrically-small, 3-D cube antenna fabricated with additive manufacturing," *IEEE Topical Conference on Power Amplifiers for Wireless and Radio Applications (PAWR)*, Jan. 2013, pp. 91-93.
- [26] I.T. Nassar, H. Tsang, K. Church, and T.M. Weller, "A high efficiency, electrically-small, 3-D machined-substrate antenna fabricated with fused deposition modeling and 3-D printing," *IEEE Radio and Wireless Symposium (RWS)*, Jan. 2014, pp. 67-69.
- [27] I. Nassar, H. Tsang, and T. Weller, "3D printed wideband harmonic transceiver for embedded passive wireless monitoring," *Electron. Lett.*, vol. 50, no. 22, pp. 1609-1611, Oct. 2014.
- [28] I. Nassar, "Long-range, passive wireless monitoring using energy-efficient, electrically-small sensor nodes and harmonic radar interrogator," PhD dissertation, University of South Florida, 2013
- [29] Design options abound with printed electronics, Available: <http://www.dupont.com/products-and-services/electronic-electrical-materials/printed-electronics.html>, visited June 2015.
- [30] P. Salonen, V. Kupiainen, and M. Tuohimaa, "Direct printing of a handset antenna on a 3D surface," *IEEE Antennas and Propagation Society International Symposium (APSURSI)*, July 2013, pp. 504-505.
- [31] M.F. Farooqui and A. Shamim, "An inkjet printed near isotropic 3-D antenna with embedded electronics for wireless sensor applications," *IEEE Antennas and Propagation Society International Symposium (APSURSI)*, July 2014, pp. 326-327.
- [32] Conformal Printed Antenna, Available: <http://www.optomec.com/additive-manufacturing/printed-electronics/aerosol-jet-core-applications/printed-antennas/>, visited June 2015.
- [33] J. A. Paulsen, M. Renn, K. Christenson, and R. Plourde, "Printing conformal electronics on 3D structures with Aerosol Jet technology," *Future of Instrumentation International Workshop (FIIW)*, Oct. 2012, pp. 1-4.
- [34] 3D printing method advances electrically small antenna design, Available: <https://engineering.illinois.edu/news/article/2011-03-15-3d-printing-method-advances-electrically-small-antenna-design>, visited June 2015.

- [35] J. J. Adams, E. B. Duoss, T. F. Malkowski, M. J. Motala, B. Y. Ahn, R. G. Nuzzo, J. T. Bernhard, and J. A. Lewis, "Conformal printing of electrically small antennas on three-dimensional surfaces," *Adv. Mater.*, vol. 23, pp. 1335-1340, March 2011.
- [36] J. J. Adams, S. C. Slimmer, T. F. Malkowski, E. B. Duoss, J. A. Lewis, and J.T. Bernhard, "Comparison of spherical antennas fabricated via conformal printing: helix, meanderline, and hybrid designs," *IEEE Antennas Wireless Propag. Lett.*, vol. 10, pp. 1425–1428, Dec. 2011.
- [37] S. Mufti, A. Tennant, and L. Seed, "3D electrically small dome antenna," *Antennas and Propagation Conference (LAPC)*, Loughborough, Nov. 2014, pp. 653-656.
- [38] SelectConnect technologies and LPKF USA announce joint laser direct structuring (LDS) webinar series, Available: <http://www.prweb.com/releases/2011/10/prweb8888850.htm>, visited June 2015.
- [39] A. Friedrich, B. Geck, O.Klemp, and H. Kellermann, "On the design of a 3D LTE antenna for automotive applications based on MID technology," *Proc. European Microwave Conf. (EuMC)*, Nuremberg, Germany, Oct. 2013, pp. 640–643.
- [40] C. Pfeiffer, X. Xu, S. R. Forrest, and A. Grbic, "Direct transfer patterning of electrically small antennas onto three-dimensionally contoured substrates," *Adv. Mater.*, vol. 24, no. 9, pp. 1166–1170, March 2012.
- [41] B.Y. Ahn, E. B. Duoss, M. J. Motala, X. Guo, S. -I. Park, Y. Xiong, J. Yoon, R. G. Nuzzo, J. A. Rogers, and J. A. Lewis, "Omnidirectional printing of flexible, stretchable, and spanning silver microelectrodes," *Science*, vol. 323, no. 5921, pp. 1590–1593, March 2009.
- [42] J. J. Adams, S. C. Slimmer, J. A. Lewis, and J. T. Bernhard, "3D-printed spherical dipole antenna integrated on small RF node," *Electron. Lett.*, vol. 51, no. 9, pp. 661-662, April 2015.
- [43] P. Nayeri, M. Liang, R. A. Sabory-Garcia, M. Tuo, F. Yang, M. Gehm, H. Xin, and A. Z. Elsherbeni, "3D printed dielectric reflectarrays: low-cost high-gain antennas at sub-millimeter waves," *IEEE Trans. Antennas Propag.*, vol. 62, no. 4, pp. 2000-2008, April 2014.
- [44] J. -M. Floch, B. El Jaafari, and A. El Sayed Ahmed, "New compact broadband GSM/UMTS/LTE Antenna Realise by 3D printing," *The 9th European Conference on Antennas and Propagation*, Lisbon, Portugal, April 2015.
- [45] A. Garcia Lopez, E. E. Lopez C., R. Chandra, and A. J. Johansson, "Optimization and fabrication by 3D printing of a volcano smoke antenna for UWB applications," *7th European Conference on Antennas and Propagation (EuCAP)*, April 2013, pp. 1471-1473.

- [46] O. S. Kim, "3D printing electrically small spherical antennas," *IEEE Antennas and Propagation Society International Symposium (APSURSI)*, July 2013, pp. 776-777.
- [47] I. T. Nassar, T. M. Weller, and H. Tsang, "3-D printed antenna arrays for harmonic radar applications," *IEEE 15th Annual Wireless and Microwave Technology Conference (WAMICON)*, June 2014, pp. 1-4.
- [48] B. Sanz-Izquierdo and E.A. Parker, "3D printed FSS arrays for long wavelength applications," *8th European Conference on Antennas and Propagation (EuCAP)*, April 2014, pp. 2382-2386.
- [49] E. E. Lopez Canelon, A. Garcia Loopez, R. Chandra, and A. J. Johansson, "3D printed miniaturized UWB antenna for wireless body area network," *8th European Conference on Antennas and Propagation (EuCAP)*, April 2014, pp. 3090-3093.
- [50] I. T. Nassar, T. M. Weller, and H. Tsang, "A 3-D printed miniaturized log-periodic dipole antenna," *IEEE Antennas and Propagation Society International Symposium (APSURSI)*, July 2014, pp. 11-12.
- [51] W. G. Whittow and A. Motevasselian, "Substrates with non-uniform 3D geometries for miniaturization of microstrip patch antennas and aesthetic design," *Radio Science Meeting (Joint with AP-S Symposium), USNC-URSI*, July 2014, pp. 11-12.
- [52] B. Sanz-Izquierdo and S. Jun, "WLAN antenna on 3D printed bracelet and wrist phantom," *Antennas and Propagation Conference (LAPC)*, Loughborough, Nov. 2014, pp. 372-375.
- [53] C. R. Garcia, R. C. Rumpf, H. H. Tsang, and J. H. Barton, "Effects of extreme surface roughness on 3D printed horn antenna," *Electron. Lett.*, vol. 49, no. 12, pp. 734-736, June 2013.
- [54] B. Sanz-Izquierdo and E.A. Parker, "3D printing technique for fabrication of frequency selective structures for built environment," *Electron. Lett.*, vol. 49, no. 18, pp. 1117-1118, Aug. 2013.
- [55] H. Lu, X. Sun, M. Bolding, C.J. Reddy, and S. Wang, "Fast prototyping of near-field antennas for magnetic resonance imaging by using MoM simulations and 3D printing technology," *IEEE Antennas Propag. Mag.*, vol. 57, no. 2, pp. 261-266, April 2015.
- [56] B. Sanz-Izquierdo and E.A. Parker, "3-D printing of elements in frequency Selective arrays," *IEEE Trans. Antennas Propag.*, vol. 62, no. 12, pp. 6060-6066, Dec. 2014.

- [57] J. -C. S. Chieh, B. Dick, S. Loui, and J.D. Rockway, "Development of a Ku-Band Corrugated Conical Horn Using 3-D Print Technology," *IEEE Antennas Wireless Propag. Lett.*, vol. 13, pp. 201,204, Feb. 2014.
- [58] M. Ahmadloo and P. Mousavi, "A novel integrated dielectric-and-conductive ink 3D printing technique for fabrication of microwave devices," *IEEE MTT-S International Microwave Symposium Digest (IMS)*, June 2013, pp. 1-3.
- [59] M. Ahmadloo, "Design and fabrication of geometrically complicated multiband microwave devices using a novel integrated 3D printing technique," *IEEE 22nd Conference on Electrical Performance of Electronic Packaging and Systems (EPEPS)*, Oct. 2013, pp. 29-32.
- [60] M. Ahmadloo and P. Mousavi, "Application of novel integrated dielectric and conductive ink 3D printing technique for fabrication of conical spiral antennas," *IEEE Antennas and Propagation Society International Symposium (APSURSI)*, July 2013, pp. 780-781.
- [61] M. Liang, C. Shemelya, E. MacDonald, R. Wicker, and H. Xin, "Fabrication of microwave patch antenna using additive manufacturing technique," *Radio Science Meeting (Joint with AP-S Symposium)*, USNC-URSI, July 2014, pp. 269-0269.
- [62] M. Liang, C. Shemelya, E. MacDonald, R. Wicker, and H. Xin, "3-D printed microwave patch antenna via fused deposition method and ultrasonic wire mesh embedding technique," *IEEE Antennas Wireless Propag. Lett.*, vol. 14, pp. 1346-1349, June 2015.
- [63] P. Kiddell, A basic overview of the pad printing process, Available: <http://www.epsvt.com/support/generalIssue.cfm?issID=15>, visited July 2015.
- [64] H. Kipphan, *Handbook of Print Media: Technologies and Production Methods*, 2001.
- [65] Z. Qu, Y. Xiong, Z. Li, Y. Fan, and Y. Yan, "The pad printing technology evaluation in mobile phone antenna manufacture," *9th International Symposium on Antennas Propagation and EM Theory (ISAPE)*, Nov.-Dec. 2010, pp. 15-18.
- [66] Y. Xiong and Z. Qu, "Antenna 3D pad printing solution evaluation," *IEEE International Symposium on Antennas and Propagation (APSURSI)*, July 2011, pp. 2773-2776.
- [67] P. I. Deffenbaugh, J. Goldfarb, X. Chen, and K. H. Church, "Fully 3D printed 2.4 GHz bluetooth/Wi-Fi antenna," *IMAPS, 46th International Symposium on Microelectronics*, Orlando, Florida, Sept.– Oct. 2013.
- [68] P. I. Deffenbaugh, 3D printed electromagnetic transmission and electronic structures fabricated on a single platform using advanced process integration

techniques, (January 1, 2014). ETD Collection for University of Texas, El Paso. Paper AAI3636252.

- [69] Printed impedance elements by micro-dispensing, Available: http://emlab.utep.edu/pdfs/Poster_3DZ.pdf, visited June 2.15.
- [70] N. Arnal, T. Ketterl, Y. Vega, J. Stratton, C. Perkowski, P. Deffenbaugh, K. Church, and T. Weller, "3D multi-layer additive manufacturing of a 2.45 GHz RF front end," *IEEE IMS*, 2015.
- [71] C. D. Saintsing, K. Yu, H. J. Qi, and M. Tentzeris, "Planar monopole antennas on substrates fabricated through an additive manufacturing process," *IEEE Radio and Wireless Symposium (RWS)*, Jan. 2015, pp. 159-161.
- [72] M. Mirzaee, S. Noghianian, L. Wiest, and I. Chang, "Developing Flexible 3D Printed Antenna Using Conductive ABS Materials," *IEEE International Symposium on Antenna and Propagation and North American Radio Science Meeting 2015*, Vancouver, Canada, July 2015.
- [73] A. Bisognin, D. Titz, C. Luxey, G. Jacquemod, F. Ferrero, D. Lugara, A. Bisognin, R. Pilard, F. Gianesello, D. Gloria, J. R. Costa, C. Laporte, H. Ezzeddine, E. B. Lima, and C. A. Fernandes, "A 120 GHz 3D-printed plastic elliptical lens antenna with an IPD patch antenna source," *IEEE International Conference on Ultra-WideBand (ICUWB)*, Sept. 2014, pp. 171-174.
- [74] H. Yi, S. -W. Qu, K. B. Ng, and C. H. Chan, "3-D printed discrete dielectric lens antenna with matching layer," *International Symposium on Antennas and Propagation (ISAP)*, Dec. 2014, pp. 115-116.
- [75] A. Bisognin, D. Titz, F. Ferrero, R. Pilard, C. A. Fernandes, J. R. Costa, C. Corre, P. Calascibetta, J. -M. Riviere, A. Poulain, C. Badard, F. Gianesello, C. Luxey, P. Busson, D. Gloria, and D. Belot, "3D printed plastic 60 GHz lens: Enabling innovative millimeter wave antenna solution and system," *IEEE MTT-S International Microwave Symposium (IMS)*, June 2014, pp. 1-4.
- [76] J. L. Volakis, *Antenna Engineering Handbook*. New York, 4th ed. NY: Mc GrawHill, 2007.
- [77] C. A. Balanis, *Antenna Theory: Analysis and Design*, 2nd ed. New York: Wiley, 2005.
- [78] J.D. Kraus and D.A. Fleisch, *Electromagnetics: with Application*, McGraw-Hill, New York, 1998.
- [79] L. H. Hemming, *Electromagnetic Anechoic Chambers*, Wiley-IEEE Press, 2002.

- [80] F. T. Ulaby, *Fundamentals of Applied Electromagnetics*, 1999 ed, Prentice-Hall, New York, 1998.
- [81] C. T. A. Johnk, *Engineering Electromagnetic Fields and Waves*, John Wiley and Sons, New York, 1975
- [82] C. A. Balanis, *Engineering Electromagnetics*, John Wiley and Sons, New York, 1989.
- [83] J. F. Aubin, "A brief tutorial on antenna measurement," *Microwave Journal*, Aug. 2005.
- [84] Antenna patterns and their meaning, Available: http://www.cisco.com/c/en/us/products/collateral/wireless/aironet-antennas-accessories/prod_white_paper0900aec806a1a3e.html, visited June 2015.
- [85] IEEE Std149-1979, Standard Test Procedure for Antennas.
- [86] Group delay, Available: <http://www.microwaves101.com/encyclopedias/group-delay>, visited June 2015.
- [87] Basics of measuring the dielectric properties of materials, Available: <http://cp.literature.agilent.com/litweb/pdf/5989-2589EN.pdf>, visited July 2015.
- [88] D. Doyle, T. Starr, and C. Christodoulou, "Dielectric characterization of 3D printed materials with a confocal Fabry Perot resonator for space utilization," *IEEE Antennas and Propagation Society International Symposium (APSURSI)*, July 2014, pp. 223-224.
- [89] M. Liang, X. Yu, C. Shemelya, D. Roberson, E. MacDonald, R. Wicker, and H. Xin, "Electromagnetic materials of artificially controlled properties for 3D printing applications," *IEEE Antennas and Propagation Society International Symposium (APSURSI)*, July 2014, pp. 227,228.
- [90] P. I. Deffenbaugh, R. C. Rumpf, and K. H. Church, "Broadband microwave frequency characterization of 3-D printed materials," *IEEE Trans. Comp., Packag., Manufact. Technol.*, vol. 3, no. 12, pp. 2147-2155, Dec. 2013.
- [91] Application Note 1369-1, solutions for measuring permittivity and permeability with LCR meters and impedance analyzers, Agilent Literature Number 5980-2862EN.
- [92] Application note 1287-1, Understanding the fundamental principles of vector network analysis, Agilent literature number 5965-7707E.
- [93] Application note 1287-2, Exploring the Architectures of Network Analyzers, Agilent literature number 5965-7708E

- [94] D. V. Blackham and R. D. Pollard, "An improved technique for permittivity measurements using a coaxial probe," *IEEE Trans. on Instr. Meas.*, vol. 46, no. 5, pp. 1093-1099, Oct. 1997.
- [95] ASTM, "Test methods for A-C loss characteristics and permittivity (dielectric constant) of solid electrical insulating materials," ASTM Standard D 150, American Society for Testing and Materials
- [96] S. M. Wentworth, *Fundamentals of Electromagnetics with Engineering Applications*, 1st ed, John Wiley & Sons, 2005, pp. 219-222.
- [97] H. Liu, H. Jiang, X. Guan, J. Lei, and S. Li, "Single-feed slotted bowtie antenna for triband applications," *IEEE Antennas Wireless Propag. Lett.*, vol. 12, pp. 1658-1661, Jan. 2013.
- [98] K. -L. Wong and W. -S. Chen, "Slot-loaded bow-tie microstrip antenna for dual-frequency operation," *Electron. Lett.*, vol. 34, no. 18, pp. 1713-1714, Sep. 1998.
- [99] C. -Y Huang, C. -C. Lin, and W. -F. Chen, "Multiple band-stop bow-tie slot antennas for multiband wireless systems," *IET Microw. Antennas Propag.*, vol. 2, no. 6, pp. 588-593, Sept. 2008.
- [100] H. Nakano, N. Oki, H. Iwaoka, H. Mimaki, and J. Yamauchi, "Slot bowtie antenna for dual-frequency operation," *Electron. Lett.* , vol. 43, no. 10, pp. 554-555, May 2007.
- [101] H. Wang, J. Liu, and G. Wang, "Asymmetric bow-tie antenna for GSM/CDMA and 3G/WLAN," *Electron. Lett.* , vol. 43, no. 23, pp. 1246 – 1247, Nov. 2007.
- [102] H. -W. Liu, F. Qin, J. -H. Lei, P. Wen, B. -P. Ren, and X. Xiao, "Dual-band microstrip-fed bow-tie antenna for GPS and WLAN application," *Microw. Opt. Technol. Lett.*, vol. 56, pp. 2088–2091, Sept. 2014.
- [103] H. Wong, K.-M. Mak, and K.-M. Luk, "Wideband shorted bowtie patch antenna with electric dipole," *IEEE Trans. Antennas Propag.*, vol. 56, no. 7, pp. 2098-2101, July 2008.
- [104] L. Xuyang, M. Jalilvand, Y. L. Sit, and T. Zwick, "A compact double-layer on-body matched bowtie antenna for medical diagnosis," *IEEE Trans. Antennas Propag.*, vol. 62, no. 4, pp. 1808-1816, April 2014.
- [105] K. W. Loi, S. Uysal, and M.S. Leong, "Design of a wideband microstrip bowtie patch antenna," *IET Microw. Antennas Propag.*, vol. 145, no. 2, pp. 137-140, Apr 1998.
- [106] C. J. Shannon, E. C. Fear, and M. Okoniewski, "Dielectric-filled slotline bowtie antenna for breast cancer detection," *Electron. Lett.*, vol. 41, no. 7, pp. 388-390, March 2005.

- [107] C. -Y. Huang and D. -Y. Lin, "CPW-fed bow-tie slot antenna for ultra-wideband communications," *Electron. Lett.*, vol. 42, no. 19, pp. 1073-1074, Sept. 2006.
- [108] Y. Ito, M. Ameya, M. Yamamoto, and T. Nojima, "Unidirectional UWB array antenna using leaf-shaped bowtie elements and flat reflector," *Electron. Lett.*, vol. 44, no. 1, pp. 9-11, Jan. 2008.
- [109] F. Sagnard and F. Rejiba, "Wide band coplanar waveguide-fed bowtie slot antenna for a large range of ground penetrating radar applications," *IET Microw. Antennas Propag.*, vol. 5, no. 6, pp. 734-739, April 2011.
- [110] Z. -Y. Zhang, S. -L. Zuo, and J. -Y. Zhao, "Wideband folded bowtie antenna With Γ -shaped strip feed and tuning stubs," *Microw. Opt. Technol. Lett.*, vol. 55, no. 9, pp. 2145-2149, Sept. 2013.
- [111] C. -F. Tseng and C. -C. Wan, "Small Sierpinski bowtie patch antenna with modified ground plane for improved bandwidth," *Microw. Opt. Technol. Lett.*, vol. 56, no. 6, pp. 1385-1387, July 2014.
- [112] R. C. Hadarig, M. E. de Cos, Y. Álv rez, and F. Las-Heras, "Novel bow-tie antenna on artificial magnetic conductor for 5.8 GHz radio frequency identification tags usable with metallic objects," *IET Microw. Antennas Propag.*, vol. 5, no. 9, pp. 1097-1102, June 2011.
- [113] G. E. Atteia, A. A. Shaalan, and K. F. A. Hussein, "Wideband partially-covered bowtie antenna for ground-penetrating-radars," *Prog. Electromagn. Res.*, vol. 71, pp. 211-226, 2007.
- [114] S. -W. Qu and K. B. Ng, "Wideband millimeter-wave cavity-backed bowtie antenna," *Prog. Electromagn. Res.*, vol. 133, pp. 477-493, 2013.
- [115] M. Mirzaee and B. S. Virdee, "UWB bandpass filter with notch-band based on transversal signal-interaction concepts," *Electron. Lett.*, vol. 49, no. 6, pp. 399-401, March 2013.
- [116] M. Mirzaee, "A novel small ultra-wideband bandpass filter including narrow notched band utilizing folded T-shaped stepped impedance resonator", *Prog. Electromagn. Res. C*, vol. 22, pp. 85-96, 2011.
- [117] M. Mirzaee, S. Noghianian, and B. S. Virdee, "High selectivity UWB bandpass filter with controllable bandwidth of dual notch bands," *Electron. Lett.*, vol. 50, no. 19, pp. 1358-1359, Sept. 2014.
- [118] M. Mirzaee, and B.S. Virdee, "Wide filter stopband aids UWB systems," *Microwaves & RF*, vol. 52, no. 1, Jan. 2013

- [119] Federal Communications Commission (FCC), Revision of part 15 of the commission's rules regarding ultra-wideband transmission systems, First Report and Order, FCC 02-48, 2002.
- [120] M. Mirzaee, B. S. Virdee, and S. Noghianian, "Compact ultra-wideband bandpass filter with variable notch characteristics based on transversal signal-interaction concepts," *Int. J RF and Microwave Comp. Aid. Eng.*, vol. 24, no. 5, pp. 549–559, Jan 2014.
- [121] CST Microwave Studio, www.cst.com, visited November 2013.
- [122] SolidWorks, www.solidworks.com , visited November 2013
- [123] PELCO® High Temperature Carbon Paste, Available: http://www.tedpella.com/technote_html/16057%20TN.pdf, visited July 2015.